Modelling of Layered Surface Acoustic Wave Resonators for Liquid Media Sensing Applications

A thesis submitted in fulfilment of the requirements
of the degree of Doctor of Philosophy

David A. Powell
BCSE (Hons)

School of Electrical and Computer Engineering
Science, Engineering and Technology Portfolio
RMIT University
May, 2006

[This page has intentionally been left blank.]

Declaration

I certify that except where due acknowledgement has been made, the work is that of the author alone; the work has not been submitted previously, in whole or in part, to qualify for any other academic award; the content of the thesis is the result of work which has been carried out since the official commencement date of the approved research program; and, any editorial work, paid or unpaid, carried out by a third party is acknowledged.

David Powell

Acknowledgement

I would like the thank the following people and organisations for their assistance in my research and in writing this thesis:

- My senior supervisor Prof. Wojtek Wlodarski for his advice, support and constructive feedback throughout my time at RMIT. His unique outlook was a source of much inspiration, and his understanding was most helpful to me.

- My second supervisor Dr Kourosh Kalantar-zadeh for giving me a practical introduction to the design and operation of SAW sensors and for his constant encouragement during my time as a student.

- My third supervisor Prof. Ali-Reza Baghai-Wadji for his sharing his insight into modelling techniques. I would particularly like to acknowledge his input into the development of the novel technique for electrodes buried in layered media, presented in Section 4.2.2.

- Dr Anthony Holland for lending his expertise on the use of the vacuum deposition facilities of the Microelectronics and Materials Technology Centre (MMTC).

- The technical staff within the MMTC and the School of Electrical and Computer Engineering for their assistance in fabrication technology, design of measurements systems and general technical advice.

- Current and former students within the Sensor Technology Group for providing feedback and friendship: Mr Samuel Ippolito, Dr Kosmas Galatsis, Dr Adrian Trinchi, Mr Glenn Matthews, Ms Lilin Li, Mr Alex Fechete, Mr Sasikaran Kandasamy, Mr Abu Sadek, Ms Joy Tan and Ms Rashidah Arsat.

- Special thanks are due to my parents Kerry and Ian and my brother Christopher, as well as all my other friends for their support and encouragement in undertaking a PhD.

- The Microtechnology CRC is thanked for supporting this project through funding of materials and mask fabrication, and for facilitating interaction with researchers from other disciplines. Funding was provided for my travel to present papers at Eurosensors XVII, 2003 IEEE Ultrasonics Symposium and to conduct collaborative research at the University of Perugia in between these conferences.

- The IEEE UFFC Society provided travel support to enable me to present a paper at the 2002 IEEE International Ultrasonics Symposium in Munich.

- I would like to thank Dr Luca Valentini and his group at University of Perugia for their generous invitation to conduct research with carbon nanotubes in their laboratory.

[This page has intentionally been left blank.]

Abstract

In this thesis a model is developed to characterise the behaviour of layered SAW 2-port resonator sensors operating in liquid media. In the critical review of literature, it is found that methods based on the periodic Green's function combined with the COM model are best suited to this task. However, an important deficiency of this approach is the lack of a good model for electrodes buried within layered media. This deficiency is resolved in this thesis by the formulation of a periodic matrix eigen-operator, using a phase-shifted Fourier series representation. This model is then utilised in the study of resonator behaviour as a function of guiding layer thickness, including the mass sensitivity.

Based on this modelling work, a SAW resonator structure is designed, and its frequency response is found to be in generally good agreement with theoretical predictions. The mass sensitivity of this device is then analysed using both theoretical and experimental means. In contrast to the sensitivity analyses found in the literature, sensitivity variation across the device surface is considered in this work. For the resonator structure it is found that sensitivity is greatest at the device centre, with the ends of the device making negligible contribution to the complete device response. The result is that the sensitive material may be deposited only in a small region in the centre of the device, with minimal reduction in device response.

Contents

List of Figures

List of Tables

Symbols and Abbreviations

Table 1: Symbols Used in this Thesis

Symbol	Meaning	SI Unit
A	MOM matrix	Vm/C
$B(\omega)$	susceptance	S
C	capacitance	F
D	matrix containing eigenvalues on the main diagonal	-
D	electrical flux	C/m^2
E	electric field	V/m
G	Green's function	mixed
$G(\omega)$	conductance	S
I	unit matrix	-
I	current	A
K	bulk modulus of liquid	N/m^2
K^2	electromechanical coupling	-
L	IDT length	m
L	algebraic equivalent of eigen-operator $\mathcal{L}$	mixed
M	combined material constants	mixed
N	direction vector for tensor variables in matrix form	-
P	P-matrix	mixed
P	Legendre function	-
P	Poynting vector	W/m^2
$\|P\|$	power flow per unit width	W/m

Symbol	Meaning	SI Unit
Q	characteristic wavenumber of array ($2\pi/p$)	m^{-1}
R	reflection matrix	mixed
R_s	sheet resistance	Ω
S_n	sign of n	-
S	strain	-
S_m	mass sensitivity	m^2/kg
T	stress	N/m^2
T	scattering transmission matrix	mixed
V	eigenvector matrix	mixed
V	terminal voltage	V
W	partial mode weighting referred to interface	-
W	aperture width	m
Y	admittance	S
Z	surface impedance matrix	mixed
a	surface area	m^2
a	electrode half width	m
c	stiffness	N/m^2
e	piezoelectric stress constant	C/m^2
f	frequency	Hz
h	layer thickness	m
h_e	electrode thickness	m
j	unit imaginary number	-
$\mathbf{k}$	spectral domain vector (wave vector)	m^{-1}
$\hat{\mathbf{k}}$	direction component of wave vector	-
l	electrode width	m
m	mass	kg
n_i	unit vector in direction i	-
p	period of electrode array	m
r	distributed resistance in electrode array	Ω
q	linear charge density	C/m

Symbol	Meaning	SI Unit
$\hat{q}$	COM normalised wavenumber	-
$\mathbf{s}$	slowness (normalised wave vector)	s/m
$\mathbf{u}$	particle displacement	m
Δv	velocity shift	m/s
$\mathbf{v}$	particle velocity	m/s
v_g	group velocity	m/s
v_p	phase velocity	m/s
w	half width of a pulse function	m
w	partial mode weighting	-
w_+/w_-	COM wave amplitude in positive/negative x_1 direction	$W^{1/2}$
w_i/w_r	P-matrix incident/reflected wave amplitudes	$W^{1/2}$
$\mathbf{x}$	Cartesian coordinate vector	m
Φ	transfer matrix in x_3 direction for layered media	mixed
Π	pulse function	-
α	attenuation	Nep/m
α	COM transduction parameter	$\Omega^{-1/2}\mathrm{m}^{-1}$
β	phase shift between periods of an electrode array	m^{-1}
γ	COM attenuation parameter	Nep/m
δ	normalised COM wavenumber	-
δ_{ij}	Kronecker delta function	-
$\delta(x)$	Dirac delta function	-
ε	dielectric tensor	F/m
η	viscosity	$\mathrm{Ns/m}^2$
κ	COM reflection	-
λ	wavelength	m
λ_0	period of electrode pair ($2p$)	m
ρ	mass density	$\mathrm{kg/m}^3$
$\underline{\underline{\rho}}$	extended density matrix	mixed
σ	conductivity	$\mathrm{S/m}^2$
σ_{sh}	sheet conductivity	S

Symbol	Meaning	SI Unit
$\boldsymbol{\tau}$	stresses on surface normal to Cartesian axis x_3	$\mathrm{N/m^2}$
ψ	variables which must be continuous in x_3 direction	mixed
φ	voltage field	V
ω	angular frequency	rad/s
$\mathcal{D}$	shorthand for D_3 to avoid subscript ambiguity	$\mathrm{C/m^2}$
$\mathcal{G}$	multi-spectral Green's function	mixed
$\mathcal{K}$	tensor divergence in wave vector form	$\mathrm{m^{-1}}$
$\mathcal{L}$	eigenvalue operator	mixed
$\mathcal{M}$	material component of eigenvalue operator	mixed
$\mathcal{P}$	partial mode transmission matrix	-
$\mathcal{Z}$	multi-spectral impedance	mixed
∇	gradient of a scalar field	$\mathrm{m^{-1}}$
$\nabla\cdot$	divergence of a vector field	$\mathrm{m^{-1}}$
$\underline{\underline{\nabla}}$	tensor divergence operator in matrix form	$\mathrm{m^{-1}}$

Table 2: Abbreviations Used in this Thesis

Abbreviation	Meaning
BAW	Bulk Acoustic Wave
BEM	Boundary Element Method
BG	Bleustein Gulyaev (Wave)
COM	Coupling of Modes
CVD	Chemical-Vapour Deposition
FBAR	Film Bulk Acoustic Resonator
FDTD	Finite Difference Time Domain
FEM	Finite Element Method
IDT	Inter-Digital Transducer
LSAW	Leaky Surface Acoustic Wave
MOM	Method of Moments
PSAW	Pseudo Surface Acoustic Wave
QCM	Quartz Crystal Microbalance
QCR	Quartz Crystal Resonator
RF	Radio Frequency
SAW	Surface Acoustic Wave
SBAW	Shallow Bulk Acoustic Wave
SDA	Spectral Domain Analysis
SH	Shear Horizontal
SMR	Solidly-Mounted Resonator
SSBW	Surface-Skimming Bulk Wave
STW	Surface Transverse Wave
TCD	Temperature Coefficient of Delay
TSM	Thickness Shear Mode

[This page has intentionally been left blank.]

Chapter 1

Introduction

This thesis is devoted to the design and optimisation of layered Surface Acoustic Wave (SAW) resonator sensors for liquid media sensing applications. In this chapter the concept of acoustic wave sensors will be introduced, and the specific features of the layered SAW and resonator configurations will be outlined.

In Section 1.1, the simplest type of acoustic wave sensors based on bulk acoustic waves will be described. In Section 1.2 surface acoustic wave devices will be introduced, and the distinction between Rayleigh and shear-horizontal waves will be made. In Section 1.3, the advantages of a layered SAW sensor will be explained, and applications of these devices in liquid and gas media will be reviewed. The resonator structure will be described in Section 1.4, and it will be explained why this structure was chosen for this work. The problem of sensing in liquid media will be introduced in Section 1.5, whilst sensing in gas media will be discussed in Section 1.6. An outline of the author's achievements and publication record will be given in Section 1.7. Finally, in Section 1.8, the objectives of the thesis will be introduced, and an overview of its structure will be given.

For the purposes of this thesis, acoustic wave sensors are those which measure the presence of some analyte by the influence it has on the propagation of a mechanical wave. The term acoustic is commonly used in the literature, even when referring to frequencies which are well above audible range. The analyte perturbs some property of the acoustic wave, most commonly velocity. This causes a change in the frequency response, which is typically characterised by measuring the change in resonant fre-

quency, or in the phase response. This phase or frequency change serves as a measure of the analyte concentration.

1.1 Bulk Acoustic Wave Sensors

The first acoustic device commonly used for electronic applications was the Quartz Crystal Resonator (QCR). It consists of a disc of quartz (typically AT-cut), with electrodes patterned on each side to excite acoustic waves using the piezoelectric effect, as shown in Figure 1.1. It is typically used for oscillator applications due to its high quality (Q) factor, low temperature sensitivity and compact form.

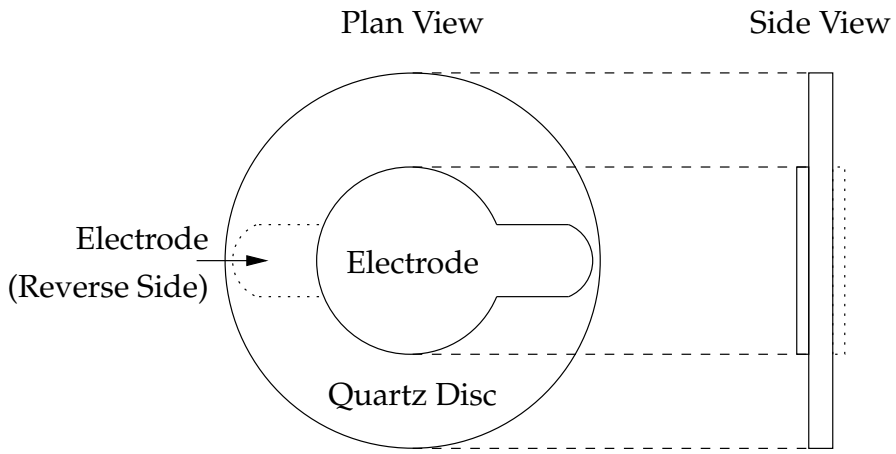

Figure 1.1: Quartz crystal resonator

The first reported use of this device for sensing application was made in 1959 by Sauerbrey [1]. When used as a sensor this device most commonly referred to as a quartz crystal microbalance (QCM), since its response is predominantly due to the mass of the analyte. For operation in gas media, it was shown that the fractional frequency change due to mass loading increases linearly with operating frequency. Since the device operates in thickness shear mode (TSM), it is also able to operate in liquid media with relatively little acoustic energy loss. It has been shown that in the liquid media case correction factors need to be included to take account of viscous effects on mass sensitivity [2].

1.2 Surface Acoustic Wave Sensors

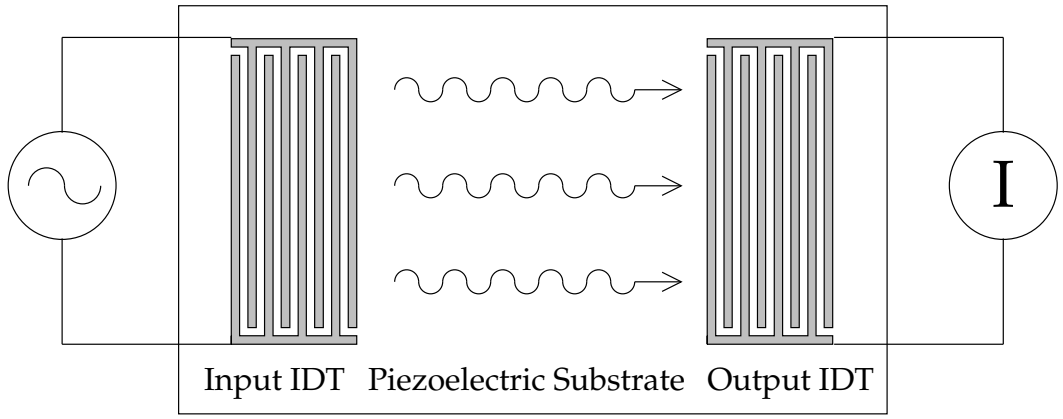

Figure 1.2: Delay line SAW device

Piezoelectric surface acoustic wave devices were first developed by White and Voltmer in 1965 [3]. In their most basic form, these devices consist of two interdigital transducers (IDTs) fabricated on a planar piezoelectric substrate and separated by a gap, as shown in Figure 1.2. An RF voltage applied across one interdigital transducer results in an alternating electric field, which launches acoustic waves due to the piezoelectric effect. The receiving transducer converts the acoustic signal back to electrical form. Due to the bidirectional nature of the IDT structure, the input and output IDTs can be interchanged. As the IDT structure only launches and detects acoustic waves with a wavelength similar to the period of the IDTs, a band-pass filtering effect occurs.

These devices were found to have a wide range of useful signal processing applications, due to the fact that acoustic wave velocities are at least 4 orders of magnitude lower than electromagnetic wave velocities [4]. This results in a corresponding reduction in wavelength, which allows for filter structures which had previously been impractical to construct.

Particularly in the initial years of their development, SAW devices mostly operated in Rayleigh mode, which has displacement components in the x_1 and x_3 directions, using the coordinate convention shown in Figure 1.3. Devices based on this mode were also the first to be used for sensing applications [5].

As with TSM resonators, the analyte perturbs the boundary conditions, and typically reduces the propagation velocity of the wave. These devices offer greater mass

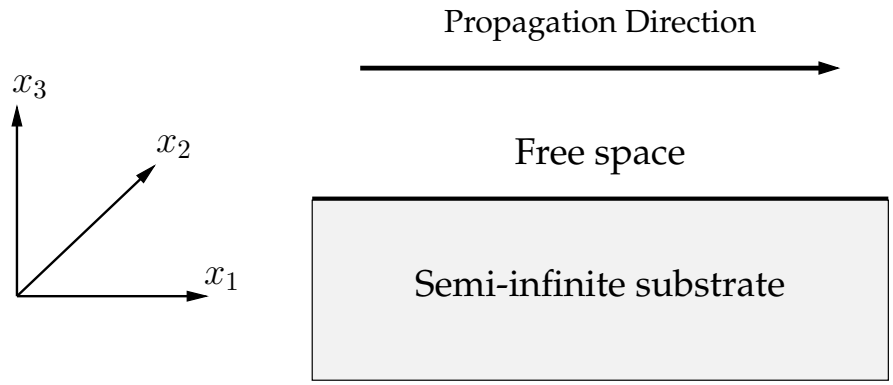

Figure 1.3: Coordinate system, where x_2 is the direction into the page

sensitivity than TSM sensors due to the their higher operating frequency, and because waves propagating near the device surface are more readily perturbed by changes in surface boundary conditions.

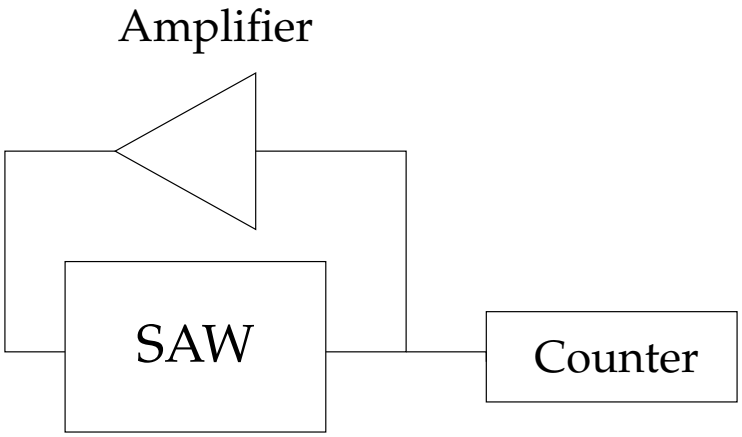

Figure 1.4: Feedback loop oscillator

To use the devices for sensing applications, they are most commonly employed in a feedback oscillator configuration, which is depicted in Figure 1.4. In this configuration, the circuit will oscillate at the resonant frequency of the SAW, and this will be measured by the counter.

In addition to the well known Rayleigh mode, there are a number of other acoustic modes which are able to propagate at or near the surface of solids. Most of these modes are either purely or predominantly polarised in the x_2 direction. They have certain advantages over Rayleigh modes in signal processing applications, such as higher velocity or stronger piezoelectric coupling. For sensing applications, they are of great interest because they are able to propagate while the device is in contact with a liquid

medium.

In the literature a number of different terms can be found to describe shear horizontal waves, which are listed here for clarity:

- Surface-Skimming Bulk Wave (SSBW) or Shallow Bulk Acoustic Wave (SBAW) - A bulk mode propagating at shallow angle to the surface.
- Leaky Surface Acoustic Wave (LSAW) or Pseudo Surface Acoustic Wave (PSAW) - A surface mode imperfectly confined by the surface, which ”leaks” energy into the substrate as it propagates.
- Bleustein-Gulyaev (BG) wave - A bulk mode confined to the surface by piezoelectricity in certain symmetry classes of material.
- Shear Horizontal Surface Acoustic Wave (SH-SAW), or Surface Transverse Wave (STW) - An SSBW mode which is confined to the device surface by an array of electrodes or a periodically grooved surface.
- Love Wave - An SSBW mode which is confined to the surface by a guiding layer of lower acoustic shear velocity than the substrate.

It should be noted that in some cases (particularly the PSAW), these modes may not be exactly shear-horizontally polarised, and are referred to as being “quasi-SH” modes. Additionally, some authors use the term SAW to include only modes which are perfectly guided by the surface, such as the Rayleigh wave. In this thesis, the term SAW will be used to denote any mode which is guided by the surface, even if this guiding is imperfect.

1.3 Layered SAW Sensors

A conventional SAW device consists of a piezoelectric substrate with metal inter-digital transducers (IDTs) patterned on the surface. Layered devices are fabricated by depositing a thin film onto the conventional SAW substrate. Any SAW chemical sensor will employ a sensitive layer which interacts with the analyte. However, in this thesis the term layered is used for devices where an intermediate layer has been added between

the substrate and sensitive layer because its acoustic, dielectric or protective properties will improve some aspect of device performance. This is illustrated in Figure 1.5, which also indicates the possible locations of the IDTs.

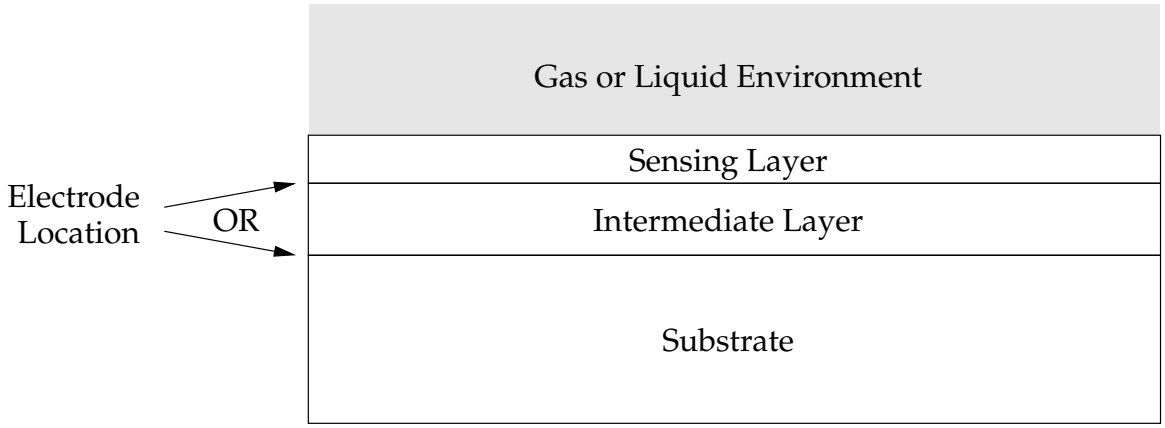

Figure 1.5: Layered SAW device configuration

Layered SAW sensors offer a number of advantages over conventional SAW devices without layers:

- By adding a layer with low density and low shear wave velocity, shear horizontal waves will be confined to the surface. This increases the mass sensitivity of the device and causes it to operate in a Love [6] mode. This is typically applied to substrates which support PSAW or SSBW modes.

- An intermediate layer over the IDTs which is protective or electrically shielding enables the whole sensor surface to be exposed to the analyte, thus increasing the response magnitude.

- A highly conductive sensitive layer or liquid environment may inhibit oscillation due to the high capacitive or conductive loading. Thus an intermediate layer can have a useful isolating effect which ensures that oscillation is reliable, and that the resulting signal is due to the acoustic response.

- A layer of passive material will protect the IDT electrodes from a harsh gas or liquid environment, which improves long term stability.

- Adding a piezoelectric or highly dielectric layer above the IDTs increases electromechanical coupling, allowing fabrication of devices with reduced insertion loss or smaller size.

- Temperature compensation can be achieved if the layer and substrate have temperature coefficients of opposite sign.

- A piezoelectric layer allows the generation of acoustic waves on non-piezoelectric substrates. This increases the design flexibility, and allows the SAW device to be fabricated on the same substrate as other components in the system.

- An intermediate layer can match the conductivity of a sensitive layer to the operating point of the SAW device, increasing the sensitivity for conductometric sensing applications.

1.4 SAW Resonator Structures

The delay line structure pictured in Figure 1.2 is commonly used in many sensing applications. However, an alternative SAW structure is the resonator. This may be either a 1-port or 2-port device, as illustrated in Figure 1.6. The reflective electrode gratings create a resonant cavity due to small reflections which add in phase at the resonant frequency.

Resonator structures are preferred for frequency stabilisation applications, since they can achieve high Q with a more compact layout than a delay line device. This is important because it reduces the instability due to noise, which can greatly improve the minimum detection limit of the device. Two port resonators are easier to work with than single port resonators, and are appropriate to use with the same feedback loop oscillator as is used for delay line structures [7].

Delay-line SAW sensors are well established in the literature, and a number of authors have used resonator structures for sensing applications [7–13]. However, there has been little work reported in the literature which gives great insight into how the behaviour of a resonator structure changes when a guiding layer is used, and when the device is loaded with liquid media. In addition, there are a number of deficiencies in

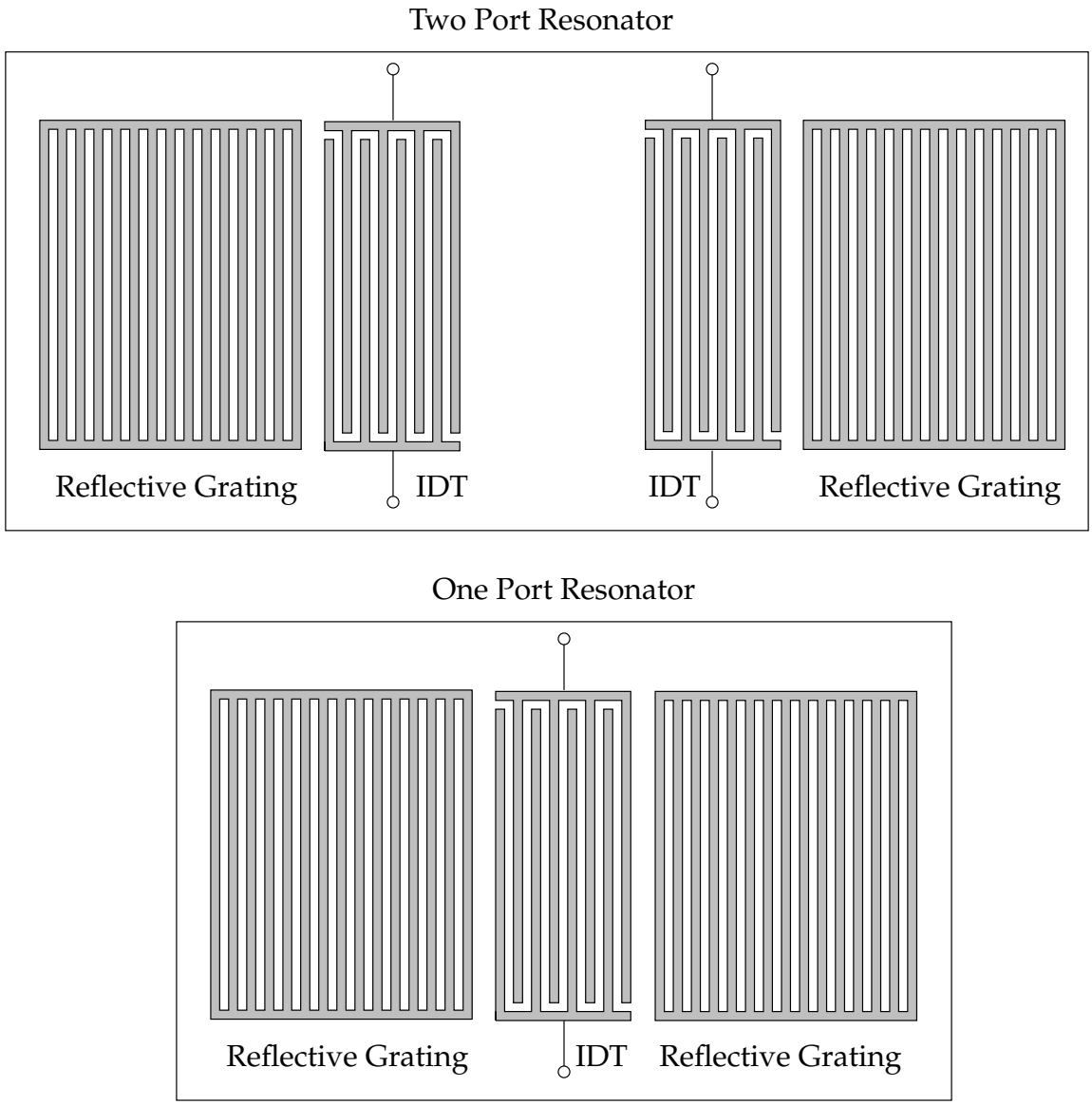

Figure 1.6: Basic one port and two port SAW resonator structures

the existing approaches to modelling these devices, which will be discussed in detail in Chapter 2. They are summarised briefly here, since addressing these deficiencies is a major goal of this thesis:

- A lack of insight into the interaction of acoustic waves with electrodes buried within layered media.
- No models for the behaviour of a periodic system of electrodes within layered media, and when subject to liquid loading.
- Poor understanding of the behaviour of resonator structures where the mass

loading does not occur evenly over the surface.

1.5 Sensing in Liquid Media

Layered SAW devices have received a great deal of attention for liquid media sensing applications. In liquid media, shear horizontal waves must generally be used, since a Rayleigh mode will radiate energy into the liquid and as a result will be severely attenuated. However, shear horizontal modes tend to be poorly trapped by the surface of a solid substrate, and thus have low mass sensitivity. For this reason a layered configuration is typically used to increase sensitivity.

1.5.1 Mass Sensing with Love Wave Devices

The theoretical work by Love [6] showed that a low velocity layer on a semi-infinite substrate will have a trapping effect upon shear waves. This trapping effect can be used to increase the mass sensitivity of a SAW sensor, since it makes the wave more sensitive to a change in surface boundary conditions. The first devices to take advantage of this phenomenon were reported by Gizeli et al. [14, 15]. A polymer (PMMA) guiding layer was deposited onto 90° rotated ST-cut quartz, and the device was applied as an immuno-sensor. In general, polymers have low density and low shear modulus, making them suitable candidates for use as the guiding layer (see Section 2.7.1). However, polymers have high acoustic losses in comparison with most other materials used for SAW devices. With a polymer guiding layer, the acoustic propagation loss increases strongly with increasing layer thickness [15]. Thus the optimum layer thickness for maximum sensitivity results in excessive insertion loss, which inhibits device operation. On the other hand, an attractive feature of polymer layers is that they can be deposited using relatively simple techniques such as spin coating.

Kovacs et al. introduced the SiO_2/90° rotated ST-cut quartz Love wave structure [16, 17]. The acoustic loss of SiO_2 is much lower than that of polymers; however for good sensitivity it is necessary to deposit a thick layer, resulting in long film deposition time for devices operating at low frequency. Ogilvy [18] and Du et al. [19, 20] carried out comprehensive studies of the SiO_2/90° ST quartz structure. They used RF mag-

netron sputtering for the deposition of SiO_2 films. They also conducted experimental analysis of the mass sensitivity as a function of layer thickness. This experimentally verified the predicted high mass sensitivity of the structure, but led to some anomalous results at high thickness that remain unexplained. Jakoby et al. [21, 22] utilised Chemical Vapour Deposition (CVD) for deposition of the SiO_2 guiding layer and theoretically modelled the sensitivity of such devices. Herrmann et al. [23] showed that the combination of 90° ST quartz and SiO_2 results in devices with poor temperature characteristics. They demonstrated that by selecting an appropriate orientation of quartz for the selected SiO_2 layer thicknesses, it is possible to achieve temperature compensation.

Another major step was taken by Du et al. with the introduction of a multi-layered structure [24]. Using a PMMA/SiO_2/quartz layered SAW higher sensitivity was obtained than with devices having only SiO_2 or PMMA layers. Harding [25] demonstrated that the acoustic properties of a SiO_2 thin film can be modified by introducing CF_4 gas during sputtering. This can be used to reduce the propagation velocity in the guiding layer, thus increasing mass sensitivity. In the same paper it was shown that the mass sensitivity can vary considerably across the surface of the device. This finding is quite significant because most existing models of the mass sensitivity of SAW devices assume that the device is uniformly loaded, which will be discussed further in Section 2.7.1.

By utilising ZnO as the guiding layer on a quartz substrate, Kalantar-zadeh et al. [26–28] showed that mass sensitivity is improved compared to SiO_2. As ZnO is a piezoelectric layer, it has the additional benefit of increasing the electromechanical coupling coefficient. Chu et al. [29] demonstrated that by controlling the thickness and deposition parameters, the temperature coefficient of ZnO/quartz devices can be reduced by an order of magnitude compared with non-layered devices. This is due to the opposite signs of the temperature coefficients for ZnO and 90° ST quartz, which results in a cancelling effect. In principal further compensation can be achieved but is limited by the precision with which the guiding layer deposition can be controlled.

When choosing a substrate and layer combination, a decision must be made to trade-off mass sensitivity, electromechanical coupling (which affects device size and insertion loss), and temperature stability. A good example comparing practical perfor-

mance of $LiTaO_3$ and quartz devices can be found in [30]. Since there is no material combination which out-performs all others in each of these areas, the best choice is dependant on the specific application.

1.5.2 Viscosity Influence

A difficulty arises from the presence of viscosity during mass sensing measurements, such as the viscous response during immuno-sensing [14], or during the measurement of liquid density. Using only velocity or frequency measurements, it is impossible to distinguish between the mass and viscosity components of the output signal. A common solution is to monitor both frequency and insertion loss of the device, since interaction with a viscous medium will attenuate the acoustic wave. This can be achieved by incorporating automatic gain control into the oscillator amplifier. Herrmann et al. [31] utilised a non-smooth surface by fabricating corrugated Love-mode devices. The showed that a dual configuration using conventional and corrugated devices was able to distinguish between viscosity and density of a liquid by measuring only frequency change.

1.6 Sensing in Gas Media

SAW devices have been investigated for sensing applications in gas media since 1979 [5]. Layered SAW devices have received much less attention for applications in gas media than for liquid media. An obvious advantage of using a layered structure is for protection of the IDTs. Many gaseous environments contain gasses which will damage or corrode the metal electrodes. This is detrimental to long-term stability, thus it is desirable to protect the metal patterns with an inert dielectric layer. For filter applications SAW devices are hermetically sealed, however this is not possible for sensing applications, thus a protective layer is preferred.

1.6.1 Mass Sensing

Because the acoustic radiation from a SAW device into gas is minimal, Rayleigh waves can be applied in gaseous media. Rayleigh waves are strongly guided by the surface

of the substrate, and an additional layer does not generally improve mass sensitivity. However, the mass sensitivity of Love wave sensors can be greater than that of Rayleigh wave devices, because the use of a guiding layer gives the sensor designer an additional degree of freedom to increase sensitivity. Thus, layered SAW sensors are advantageous for mass sensing applications such as sensing of organic vapours absorbed by a polymer layer. As an example of this, Jakoby et al. [22] applied a Love wave device to vapour sensing, applying the molecular imprinting technique to a polymer sensitive layer. Zimmermann et al. [32] successfully applied a Love wave device for the detection of organophosphorus vapours, and achieved approximately 10 times the sensitivity of a Rayleigh wave sensor operating at a similar frequency. A novel application of a layered SAW device was presented by Penza et al. [33], who used a SiO_2 layer on ST quartz for mass-based detection of organic vapours interacting with carbon nanotubes. In this case the SiO_2 layer prevents shorting of the IDTs by the conductive nanotubes, and protects the IDTs from exposure to the analyte.

1.6.2 Conductometric Sensing

In conductometric gas sensing applications, the interaction of the gas molecules with the sensitive layer perturbs the electrical boundary condition at the surface of the SAW device. As a result, the velocity and attenuation of the electro-mechanical waves are perturbed. Ricco and Martin [34] first reported SAW sensors based on the conductometric sensing mechanism, using a non-layered device. This conductometric sensitivity can be important even in cases where it is not desired, since it can lead to interference in the response.

1.7 Author's Achievements

This thesis describes the work undertaken by the author during his PhD program. The most significant achievements are:

- Development of a new model for mechanical interactions between acoustic wave and electrodes buried within layered media

- Use of the periodic Green's function and COM models to understand the behaviour of resonator structures fabricated using layered media, and the application to liquid loaded devices
- Development of a model for the behaviour of SAW resonator structures when subject to mass loading which varies across the device surface
- Design and fabrication of SAW resonator devices to experimentally verify the model

The following papers have been published based on the work undertaken in this thesis. Most of the material presented in these papers has been incorporated into this thesis.

- D. A. Powell, K. Kalantar-zadeh, W. Wlodarski, and S. J. Ippolito, "Layered surface acoustic wave chemical and bio-sensors," in *Encyclopedia of Sensors*, C. Grimes, E. Dickey, and M. V. Pishko, Eds. American Scientific, 2006, vol. 5, pp. 245–262.
- D. A. Powell, K. Kalantar-zadeh, and W. Wlodarski, "Spatial sensitivity distribution of surface acoustic wave resonator chemical and bio-sensors," *IEEE Sensors J.*, 2006, (accepted for publication).
- D. A. Powell, K. Kalantar-zadeh, and W. Wlodarski, "Numerical calculation of SAW sensitivity: Application to ZnO/$LiTaO_3$ transducers," *Sens. Act. A: Phys.*, vol. 115, pp. 456–461, 2004.
- D. A. Powell, K. Kalantar-zadeh, and W. Wlodarski, "Comprehensive analysis of SAW sensor performance in liquid media by Green's function method," in *Proc. IEEE Ultrason. Symp.*, Oct. 2003, pp. 146–149.
- D. A. Powell, K. Kalantar-zadeh, S. Ippolito, and W. Wlodarski, "A layered SAW device based on ZnO/$LiTaO_3$ for liquid media sensing applications," in *Proc. IEEE Ultrason. Symp.*, 2002, pp. 493–496.

A number of presentations have been given by the author at international conferences:

- 2002 IEEE International Ultrasonics Symposium, October 8-11, 2002, Munich, Germany
- Eurosensors XVII, September 21-24, 2003, Guimarães, Portugal
- 2003 IEEE International Ultrasonics Symposium, October 5-8, 2003, Honolulu, USA
- IEEE Sensors 2005, October 31-November 3, 2005, Irvine, USA

The research described in thesis was conducted within the scope of the Co-operative Research Centre (CRC) for Microtechnology Project 3.5 "BIO-SAW". This project aims to develop and commercialise a SAW biosensor system through a spin-off company "Bio-Senz". The author of this thesis was involved in collaborative work within the CRC with researchers from other fields, and has delivered a tutorial on the theory of surface acoustic wave devices.

In addition, the author has been involved in a number of other research activities, which were conducted in collaboration with other researchers:

- Development of a Langasite SAW device with a carbon nanotube functional layer for NO_2 and H_2 sensing applications.
- The study of layered SAW structures for gas sensing with conductometric sensitive materials, with an analysis of the effects of layered media.

These have resulted in the following publications:

- D. A. Powell, L. Valentini, I. Armentano, W. Wlodarski, K. Kalantar-zadeh, and J. M. Kenny, "Langasite SAW gas sensor with self-assembled carbon nanotube functional layer," in *Proc. Eurosensors XIX*, 2005.
- D. A. Powell, K. Kalantar-zadeh, S. Ippolito, and W. Wlodarski, "Comparison of conductometric gas sensitivity of surface acoustic wave modes in layered structures," *Sensor Letters*, vol. 3, no. 1, pp. 66–70, Mar. 2005.
- K. Kalantar-zadeh, D. A. Powell, S. Ippolito, and W. Wlodarski, "Study of layered SAW devices operating at different modes for gas sensing applications," in *Proc. IEEE Ultrason. Symp.*, 2004, pp. 191–194.

1.8 Thesis Objective and Structure

The objective of this thesis is to develop an improved model of layered SAW resonator sensors operating in liquid media. The remainder of this thesis is primarily devoted to this topic, and is divided as follows:

- Chapter 2 gives a review of modelling techniques and describes the limitations of existing work in the literature. In this chapter it will be shown that models based on the development of a periodic Green's function, combined with the extraction of parameters for a phenomenological model, are the best tool for analysing resonator structures. The limitations of existing models will be described, and the need for the author's novel model will be explained in detail.

- Chapter 3 introduces a simpler model based on the spectral domain Green's function. This will be used to provide the underlying mathematical framework for other techniques developed in this thesis. It will also be shown that this model can be used to find many useful parameters for SAW sensors

- Chapter 4 introduces the periodic Green's function model, and describes the extraction of parameters for phenomenological models. Most importantly *the author's novel developments will be presented, which make these techniques better suited to resonator structures fabricated in a layered configuration*. This is achieved by accounting for the mechanical influence of electrodes buried within layered media. Modelling results are presented for the behaviour of resonator structures in layered media subject to liquid loading.

- Chapter 5 utilises the developed modelling techniques to design a layered SAW resonator sensor. The design process is presented and the fabrication procedure is described. A comparison is made between the measured and calculated frequency response of the device, and discrepancies are discussed.

- Chapter 6 presents *a novel approach to characterising the sensitivity of SAW resonator sensors where the mass loading is not uniform over the surface*. This phenomenon has not been studied previously in the literature, and is much more predominant in the SAW resonator structure than the delay line structure. The theoretical work

developed to this point, including the author's novel technique, will be used to solve this problem.

- Chapter 7 concludes the thesis, and suggests likely advances in several emerging areas of research which are related to the work presented in this thesis.

Chapter 2

Review of Modelling Techniques

2.1 Introduction

In this chapter a critical literature review will be undertaken, with a view to developing a model for SAW sensors based on layered resonator structures. Particular attention will be paid to the complications which arise when operating such a device in liquid media. To the best of the author's knowledge, an adequate model for this application cannot be found in the publicly available literature. Layered resonator structures operating in liquid media have important applications in bio-sensing, liquid viscosity and density monitoring as well as liquid identification. A model for these devices is necessary in order to understand the operation of these transducers and to optimise their design.

There is an extensive body of knowledge regarding design and modelling of SAW devices [35]. They have the interesting property that their operating principal is simple to comprehend, yet the details of their operation can be quite complex. The physics of acoustic and piezoelectric wave propagation are well understood [36, 37], which facilitates the analysis of SAW devices. This analysis has two main purposes: understanding the properties of materials and their combination regarding propagation, generation and detection of acoustic waves, and analysing and designing structures such as transducers, reflectors and couplers to obtain a desired frequency response. While the latter purpose is the major concern in the design of communications and signal processing components, sensor design places much greater emphasis on the former.

A technique to model SAW devices should ideally give highly accurate results, be quick and easy to compute, and directly show the relationship between the parameters of a device and its performance. A wide variety of techniques have been developed to model SAW devices, each of which makes a compromise between these criteria. In this chapter, modelling techniques for SAW devices will be compared. The majority of these techniques were developed for signal processing applications, however this review is specifically concerned with techniques which may be applicable to SAW sensors. Particular emphasis will be placed on techniques which are suitable for layered resonator type SAW sensors, operating in liquid media.

In order to evaluate and compare models of SAW sensors, there are a number of parameters which are required and effects which need to be taken into account, which will be discussed in Section 2.2. There are two broad categories of SAW device model, phenomenological and numerical. The phenomenological models which calculate the device response based on that of a simple equivalent system will be presented in Section 2.3. In Section 2.4 numerical models will be discussed, which differ significantly from phenomenological models, since they solve the piezoelectric equations with varying degrees of approximation. Subsequently, the extension of both classes of model to the case of layered media will be discussed in Section 2.6. In Section 2.7 the application of these models to SAW sensors will be discussed, and they will be compared with the simpler models used exclusively for sensor applications.

2.2 Features Required of SAW Modelling Techniques

In this section the requirements which a model for SAW sensors must meet are discussed. This begins with the output parameters, and is followed by a discussion of the effects which must be taken into account to calculate these parameters.

2.2.1 Parameters Obtained from Model

Modelling techniques can be used to calculate various parameters of interest for SAW device design, the most important of which are given here. These are essential to the performance of any SAW device, regardless of whether it is used for sensing or sig-

nal processing applications. Parameters specific to SAW sensors are discussed subsequently.

- Phase velocity - The phase velocity v_p determines the operational frequency of the device. For sensing applications the change in propagation velocity is measured, typically via a change in oscillation frequency. It can also be measured via the phase change of a constant frequency signal [14], and in wireless sensing applications it is usually measured via a change in time-domain response [38]. Regardless of how the sensor response is measured, it is important to know how the device configuration and environmental parameters contribute to the phase velocity.

- Frequency response - For signal processing applications, the frequency response is usually the most important parameter in SAW device performance, although occasionally the time-domain response may be of interest instead. In sensing applications the frequency response is still very significant in determining device performance. The complete 4-parameter frequency response is typically expressed using a scattering matrix S or admittance matrix Y. An important component of the frequency response is the input admittance [4], as it determines the interaction between the SAW device and external circuit elements. Ignoring parasitic effects such as electrode resistance, it can be represented by a parallel radiation conductance G_a, radiation susceptance B_a and input capacitance C (see Figure 2.1). Alternatively a series equivalent representation may be used, giving the same information.

- Quality factor - An important parameter which can be determined from the frequency response of a resonator is its quality factor (Q). This is a measure of how strongly the SAW device determines the oscillation frequency, and rejects the influence of phase fluctuations due to other circuit elements. It is related to the slope of the phase response and the bandwidth of the resonant peak. In the case of a delay line structure the group delay plays a similar role.

- Electromechanical coupling coefficient - Electromechanical coupling parameter K^2 is an approximate measure of the strength of coupling between the electrical

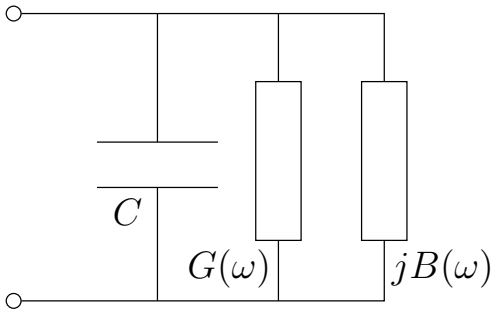

Figure 2.1: Parallel representation of SAW input admittance

and mechanical fields, and thus has a very strong bearing on reflection, generation and detection of acoustic waves. Unfortunately it does not have an unambiguous definition which is valid in all contexts. Informally, it may be described as a measure of the importance of the piezoelectric properties of the material relative to its dielectric properties.

It was shown by Campbell and Jones [39] that the electromechanical coupling could be estimated from the difference between phase velocity with a free surface boundary condition(v_f) and that with an infinitely thin, perfectly conducting layer on the surface of the SAW (v_m):

$$K^2 \approx 2\frac{v_f - v_m}{v_f}. \tag{2.1}$$

This estimate is most accurate in cases where the difference between free and metallised surface velocities is small, and where the wave is strongly guided. Equation (2.1) is often used as the definition of K^2, although it is not universally applicable. In some cases the coupling is different on free and metallised surfaces, or the SAW may only propagate on a metallised surface. In this thesis, more rigorously defined measures of piezoelectric coupling will be used when referring to the properties of an electrode array. However the parameter K^2 has some intuitive value, and equation (2.1) is sufficiently accurate for many requirements.

When considering SAW sensors the most important additional parameter is sensitivity. This will be a change in one of the parameters in the above list, most commonly the propagation velocity, due to some external interaction with the SAW device. The most important types of sensitivity are:

- Mass sensitivity - Mass sensitivity (sometimes termed gravimetric sensitivity) is defined as the velocity or frequency shift caused by the addition of a small layer of material onto the surface. It is strongly related to the surface confinement; i.e. the guiding of acoustic energy near the surface. This is the primary mechanism by which most SAW sensors operate. In practice, stiffness, viscosity and geometry of the material will affect the response, particularly if the layer thickness is a significant fraction of the acoustic wavelength.

- Sensitivity to liquid loading - The effect of liquid loading is particularly important for sensing applications in liquid media, since it can introduce losses through viscosity, conductivity and energy radiation mechanisms. The dielectric and conductive properties of a liquid can also influence the charge distribution on electrodes if the device is not shielded by a conductive layer.

- Conductometric sensitivity - Conductometric sensitivity is the change of velocity or frequency due to the addition of a thin layer on the surface with some finite conductivity. For sensing applications, this allows a conductometric response to be used, which is particularly useful in the case of strongly oxidising or reducing gasses.

The analytical expressions for these sensitivity parameters are given in Section 2.7. SAW devices are also sensitive to physical parameters such as pressure, electric field and torque, however these will not be considered in this thesis. From the appropriate sensitivity parameter, the sensitivity of the SAW device to the target analyte can be calculated. However, this requires some knowledge of the sensitive material and its interaction with the analyte. For example, the change in mass due to the interaction between antibodies and antigens, or the change in conductivity of a metal oxide due to an oxidising gas. The behaviour of the sensitive layer dominates many sensing parameters such as sensitivity, selectivity, response time and recovery time. These properties of the sensitive layer are beyond the scope of the models considered here.

2.2.2 Effects Influencing Device Response

Returning to the most general case of SAW device analysis, there are a number of effects which may need to be taken into account. The most important effects are:

- Wave type - The type of acoustic mode and corresponding polarisation have a large impact on the device response, since different modes can behave differently when propagating under an electrode structures. For sensing applications, the wave polarisation is extremely important. For example, Rayleigh waves with shear vertical and longitudinal components are well guided by a surface, and thus have high mass sensitivity. On the other hand, in liquid media shear horizontal waves must be used, since they minimise the energy dissipated into the liquid. However, shear horizontal waves have much more complicated behaviour, due to their interaction with bulk waves [40]. A surface wave in anisotropic media will in the most general case exhibit particle displacement components in all 3 directions.

- Propagation loss - Any acoustic wave will suffer from some finite attenuation as it propagates, which is usually undesirable. Slobodnik [41] attributes this attenuation to three mechanisms which are dominant in signal processing applications. The first is interaction of the acoustic wave with thermally excited phonons. The second is due to defects, impurities and scratches in the material as well as scattering from grain boundaries in polycrystalline materials. The third mechanism is due to coupling of acoustic energy into the surrounding air, and in the sensing case this can be generalised to include a surrounding liquid.

  These mechanisms are the most significant for single and poly-crystalline materials, however polymer layers are often used for SAW sensors. In these materials there is usually high energy loss due to viscoelastic behaviour caused by relaxation of the polymer chains [42]. Since these phenomena are quite complex, they must generally be treated by empirical parameters. As a further cause of wave attenuation, Pseudo-SAW and SSBW modes are not perfectly guided by a surface and will partially radiate energy into the substrate, where it cannot be usefully recovered. It should be noted that the attenuation can also be used as an output

signal of the sensor, since in some cases it will change significantly in the presence of an analyte [43].

- Electrode mechanical and electrical loading - The mass loading of an electrode and the local short circuit boundary condition which it imposes upon the wave cause mismatch of the wave under and between electrodes. This is analogous to a change of characteristic impedance in a transmission line, which causes wave reflections. For a periodic system of electrodes, these reflections will add in phase at the resonant frequency to form a Bragg reflector. For resonator applications these reflections are essential for device operation, but for delay lines they represent an undesired distortion. The electrode mass and electrical loading also causes a change in the effective propagation velocity of the wave through an electrode array.

- Bulk wave interference - Interference from undesired bulk wave modes can degrade the frequency response of a SAW device. In sensor applications this can cause the output signal to have a contribution from multiple modes, which means that the response will have an unpredictable mixture of sensitivities. This can also cause ripple in the passband response, creating uncertainty as to the start-up frequency of oscillation. The problem is particularly complex in shear horizontal waves, where the surface wave can interact with bulk waves. This can result in energy being to be lost to bulk waves, and energy storage effects changing the effective propagation velocity of the SAW in an electrode array.

- Velocity dispersion - Under an electrode grating, or in a layered device, the phase velocity can vary with frequency. This dispersion effect is most significant in wide-band devices, however the concept is an essential part of device operation in layered media and under electrodes, since propagation properties in such structures strongly depend on the wavelength. Further dispersion may be caused in electrode structures due to energy storage effects, or to materials with losses which vary strongly with frequency. It is possible to define a group velocity v_g at which a wave packet will travel, and in dispersive structures this will differ from the phase velocity v_p.

- Effect of layered media - For many sensing applications, thin films are placed on top of the substrate because of their wave-guiding, protective or sensitivity enhancing effect. These films affect all of the parameters of a SAW device to a greater or lesser extent. Layered media are also used for some signal processing applications, including piezoelectric layers used on non-piezoelectric substrates. Acoustic wave propagation in layered media exhibits velocity dispersion, thus complicating analysis.

- Triple-transit interference - When the acoustic wave reaches the output IDT, the resultant charge distribution will generate an acoustic wave returning to the input IDT. At the input IDT a charge distribution will be generated which will again cause another signal to travel to the output IDT. In principal this process will continue infinitely, but in practice the signal which travels the distance between input and output IDTs 3 times is the most significant, hence the name of this phenomenon. This will interfere with the desired signal in delay line devices, causing distortion of the amplitude and phase response. This is not a problem in resonator devices, where reflection is deliberately enhanced.

- Electromagnetic feed-through - Electromagnetic feed-through is the direct coupling between input and output IDTs due to the propagation of an electromagnetic wave. This degrades the frequency response of the SAW, and can cause interference in the output signal of a sensor.

- End effects - The change between an electrode array and a free or metallised surface may result in some energy being scattered into the bulk of the material. Also, the charge distribution on electrodes at the end of an IDT may differ substantially from those in the middle. Any technique which assumes an infinitely periodic system will be unable to account for these effects.

- Electrode resistivity - For devices with sharp resonance characteristics, the device quality factor may be reduced due to resistive losses in the IDT electrodes. This resistance may also affect the charge distribution on the electrodes, thus changing parameters such as wave generation and reception.

- Anisotropic effects - In an anisotropic material, properties such as propagation velocity and wave polarisation vary with direction. A piezoelectric material is necessarily anisotropic [36], since the piezoelectric effect is due to asymmetry in the crystal structure. Many other polycrystalline and single-crystal materials used in acoustics are also strongly anisotropic. This considerably complicates the analysis, and can result in unique effects such as beam steering, where the direction of power flow is not parallel to the wave propagation vector $\mathbf{k}$. The difference between these two angles is known as the power flow angle. In the anisotropic case, the material constants must be represented in tensor or matrix form.

- 3-dimensional effects - Almost all analysis techniques assume a 2-dimensional wave propagation model, which neglects all variations along the transversal direction. This means that diffraction in the surface plane and wave-guiding due to bus-bars are neglected. For RF filters with tight specifications on their frequency response, this can be a significant problem. A number of authors have studied these effects using both theoretical [44, 45] and experimental [46] methods. For most sensing applications these effects are of little concern, so the 2-dimensional approximation is used throughout this work.

- Temperature influence - The properties of an acoustic device always exhibit some dependance on temperature. This is commonly characterised by a temperature coefficient of delay (TCD), which includes the effect of thermal expansion and velocity change on the propagation time of a wave. This is extremely important for any frequency stabilising application including sensors, since high temperature sensitivity degrades the detection limit. For many oscillator applications substrate materials and orientations are selected so that the TCD has a zero near the desired operating temperature.

Depending on the particular application and device configuration, these effects will be of varying importance. For example, mechanical loading due to electrodes becomes more important at higher frequencies, where the electrode height relative to the wavelength becomes more significant. Electrode electrical loading, triple-transit interference

and conductometric sensitivity are more significant for devices with high electromechanical coupling K^2. End effects are more prominent in IDTs with few electrodes, and may be completely absent in a resonator structure which consists only of synchronously located electrodes.

It now remains to discuss the most important modelling techniques which may be applied to SAW sensors, with reference to the criteria discussed in this section.

2.3 Phenomenological Models

There are a number of phenomenological models which are commonly used for the design of SAW devices. They can be defined as models which do not have an accurate physical basis, but which nonetheless are able to replicate the important behaviour of a structure.

The strength of these models is their comparatively simple nature, which enables them to be used in an iterative design procedure, where many design variants are evaluated against some specified criteria. Their major disadvantage is that they require parameters to be extracted from some other source - either experiment or numerical simulation methods. They are usually only able to take into account a single mode of propagation, and may be limited in applicability to devices operating over a narrow frequency range. They tend to ignore many second order effects, so they are most applicable to situations where these effects are known to be negligible.

The delta function model [47] is one of the simplest models of a SAW device response. It considers the edges of each electrode of the input IDT to be the location of an impulsive source $\delta(x_1)$ with amplitude proportional to the electrode length. It allows a desired frequency response to be implemented in terms of a finite impulse response, much like a digital filter. However it contains no impedance information, and is only useful for specifying the shape (but not absolute magnitude) of ideal delay line filters. It ignores almost all second order effects and takes little account of material properties, and is thus ill-suited for sensor applications.

The equivalent circuit model [47] is based on the crossed field or in-line field models of the IDTs. This model assumes a highly simplified electric field distribution between electrodes, allowing analytical expressions to be derived for the input admittance of

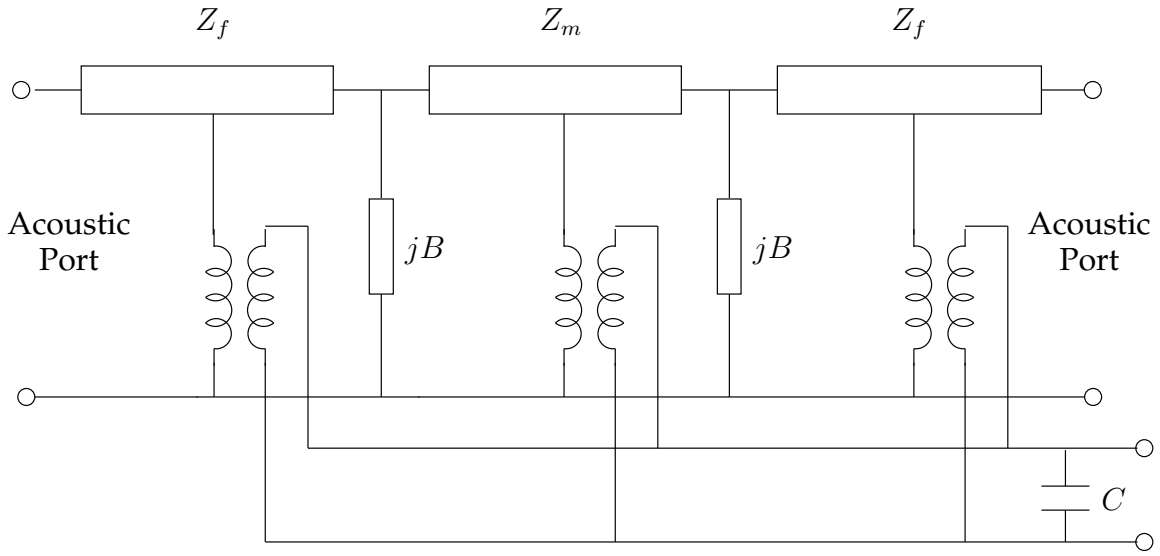

Figure 2.2: Equivalent circuit model for a single electrode

an IDT. By cascading 2-port and 3-port matrices based on these models, the complete device response is given. A more advanced equivalent circuit model was reported by Smith [48], and is illustrated in Figure 2.2. It models IDT electrodes and the spaces between as sections of transmission line of impedance Z_m and Z_f respectively, thus including electrode reflection. Triple-transit effects are automatically included in the equivalent circuit model. Susceptance jB between sections may also be added to take into account energy storage at electrode edges. A major advantage of the equivalent circuit model is that it can be implemented using standard circuit simulation software.

In the case of SAW resonators it is also possible to produce a simple RLC equivalent circuit to describe the resonance peak [49]. However, such a model is only useful for modelling the SAW's interaction with an external circuit, and is not useful for SAW device design.

Given the typical applications of SAW devices, it is not surprising that many microwave modelling techniques are commonly applied to their design. In the scattering (S-matrix) model, an IDT is modelled as a 3 port network with 2 acoustic ports and an electrical port. Each port is represented as generating outgoing waves in response to incident waves at any port. Reflectors and free or metallised sections are represented by 2 acoustic ports [50]. However, for the electrical port it is generally more convenient to use voltage and current rather than wave amplitudes. Making this modification re-

sults in the P-Matrix model, which was originally introduced by Tobolka [51]. It's primary advantage is that identical sections may be cascaded analytically, and differing sections may still be cascaded quite easily.

The Coupling of Modes (COM) model comes from a rich mathematical background developed for physical problems in periodic media [52]. It approximates the difference equation for the multiple reflections within an IDT or grating by a differential equation, thus allowing analytical solutions. It models the wave distribution in each electrode array as consisting of a single spatial harmonic coupled to another spatial harmonic propagating in the infinite direction. All higher order harmonics are neglected.

The model was extended by Chen and Haus [53] to include interaction between acoustic waves and the voltage and current in an IDT or metallic grating. They also developed variational expressions for all COM parameters, thus allowing the COM model to be used independently with acceptable accuracy for many applications. It has long been used in the design of resonant SAW structures, and despite the relatively high degree of approximation involved, it can show very good agreement with experimental results. The COM model may be used to give analytical expressions for the P-matrix of a transducer, thus to some extent these models are complementary. A thorough treatment of COM analysis can be found in [40]. It's major strength is its ability to characterise reflection, thus it is commonly applied to devices where reflection is a dominant phenomenon, such as resonators and low loss RF filters. Expressions for the COM parameters in Rayleigh wave devices which yield reasonably good agreement with experiment are reported in [53, 54]. Although they are based on perturbation methods, they are quite useful in many signal processing applications.

All phenomenological models have difficulty accurately simulating shear horizontal waves, due to the interaction between SH-SAW and SH-BAW modes [40]. Plessky [55] introduced a new model similar to COM, which is able to characterise these effects with moderate accuracy. However, this model can only be applied to reflective gratings, and not to IDTs. Abbot and Hashimoto [56] formally combined Plessky's model with the traditional COM model, thus allowing shear horizontal waves to be included in the COM model with acceptable accuracy. Koskela [57] presented a completely new phenomenological model based on a simplified Green's function model, which also

accounts for the effect of the finite length of a structure on bulk wave interaction.

The COM, P-matrix and equivalent circuit models are similar in their overall approach, with minor differences making them more suitable for different device types. The COM model is particularly appealing however, because the parameters it uses have a close correspondence to the physical phenomena of interest to a device designer. It should be noted that all these models have many variations and extensions which are too numerous to mention here. Any of these phenomenological models can be applied to a SAW sensor, since many of the design requirements are similar to those of devices for signal processing applications. This is because a SAW sensor also requires control over it's frequency response to ensure good signal-to-noise ratio. As these models rely on parameters derived elsewhere, they cannot directly include many of the effects which are important in sensing, such as mass loading or liquid interaction. However, if these effects have been characterised by some experimental or numerical technique, then their impact on device performance can be calculated using the COM, P-matrix or equivalent circuit models. This will then show the effect on the complete device frequency response.

2.4 Numerical Models

The phenomenological techniques presented in Section 2.3 all share the disadvantage that they must be fitted to a measured or simulated device, severely limiting their usefulness for predicting the response of devices using new materials, or new orientations or combinations of materials. The most rigourous method of analysing acoustic wave propagation is through the use of the piezoelectric constitutive relations, which are well known [36]. However, due to the anisotropy of piezoelectric materials, analytical solutions to these equations are only possible for selected orientations of materials having particular crystal symmetry. To calculate solutions for arbitrary orientations numerical techniques are required.

The advantages of using numerical techniques are:

- They can be calculated directly from material constants
- Being directly derived from the physics of the problem they give a high degree

of confidence in the solution

- They are valid for arbitrary symmetry classes of material
- All surface wave, bulk wave and electrostatic effects are directly included
- Differing material orientations and combinations can be analysed without experimental measurement

There are also a number of drawbacks:

- Stability issues - piezoelectric problems can be ill-conditioned, and require careful scaling to ensure accuracy [58].
- Iterative techniques are often required, which are susceptible to producing spurious results or finding local minima (convergence problems)
- Material constants are often unavailable for many of the materials which are used for sensing applications
- The numerically obtained answer does not isolate the effects of different input parameters on the calculated result, thus it is harder to gain insight into the mechanisms at work.

Numerical solution of the piezoelectric constitutive equations has been used for a wide variety of piezoelectric devices, including SAW devices. Examples can be found in [37, 59, 60] for a many differing material configurations. All of these techniques use the quasi-static approximation, which assumes that the electric field can be represented as the gradient of a scalar potential (i.e. the electromagnetic part of solution is neglected).

Complex wave propagation problems including a substrate, guiding layer, sensitive material, an analyte and a surrounding liquid are most readily solved using numerical methods. Thus they are highly suitable for sensing applications. Since these techniques are all based on the solution of the piezoelectric constitutive equations there is no great distinction between them in terms of applicability to the sensing case, discussion of which will be deferred to Section 2.7.4.

The most important classes of numerical techniques reported in the literature for SAW devices are based on the finite element, finite difference, partial wave and boundary element methods. The application of numerical models to periodic systems are also discussed.

2.4.1 Finite Element and Finite Difference Techniques

The most flexible approaches to the piezoelectric wave problem are finite element and finite difference, which discretise the field variables in all regions throughout the problem domain. The advantage of these techniques is that the problem can often be solved using available software. These methods are very flexible regarding the simulation of complex shapes. They can be extended to include the effects of other circuit elements such as pads, bonding wires and packaging. Layered structures require no special treatment, since each simulated region can have arbitrary material properties. The finite difference method is less flexible than the finite element method since it requires all points to be regularly arranged in a grid or grids.

The disadvantage of these techniques is the very large number of elements required, resulting in long computation time. Additionally, they have poor convergence for electrode arrays, which further increases the number of nodes required. This problem is caused by the discontinuities in charge distribution which occur at the electrode edges, violating the assumption that field variables are continuous. A surface wave is generally considered to propagate on a semi-infinite substrate, which does not reflect energy towards the surface. To represent this open boundary with a finite domain involves the use of a perfectly matched layer [61] in order to artificially absorb the wave energy.

Finite element models are usually used in the frequency domain for wave propagation problems, as this is where performance requirements are typically specified. However, finite difference time domain (FDTD) is a popular technique for solving electromagnetic wave propagation problems, as it requires no matrix inversions. It has been proposed to use this technique for studying piezoelectric wave propagation [62], however to the best of the author's knowledge no applications have been reported to date. The disadvantage of time domain techniques is that they cannot be applied specifically

to a region of interest in the frequency domain, thus becoming somewhat inefficient if a narrow frequency range needs to be simulated with high resolution.

2.4.2 Partial Wave Techniques

Partial wave techniques are those which represent the field inside a region as a sum of bulk wave solutions of the form $\exp\left[j\left(\omega t - k_1 x_1 - k_2 x_2 - k_3 x_3\right)\right]$, where terms k_i represent the complex wave number components along each Cartesian coordinate axis. These bulk modes can be found by solving the Christoffel equation (see Section 3.2.3). For acoustic waveguides such as SAW devices, the partial modes are combined to satisfy the boundary conditions between materials and at the boundaries. These partial modes can easily be applied to open devices boundaries, thus allowing simulation of a surface wave on a semi-infinite substrate. Various techniques based on this approach are able to account for most important effects in SAW devices, including beam steering, electromechanical coupling, capacitance, bulk wave generation and temperature induced variation.

A problem with the partial wave method is it's application to PSAW solutions, which have some finite propagation loss due to wave leakage into the substrate. This means that the corresponding singularities of the Green's function can be considered to be offset from the real slowness axis into the complex plane. Adler [63] gave a technique for partial mode selection when searching for PSAW poles in the complex plane, but gave no physical justification for this method. Biryukov and Weihnacht [64] investigated the question of partial mode selection in the complex plane. They concluded that by tracking the partial modes from the real axis, it is possible to uniquely identify the correct partial modes in the complex plane. This result is important because it makes the process of searching for PSAW solutions more rigourous, and less prone to finding solutions with no physical basis.

Partial wave techniques are useful in their own right, but are even more important because they form the basis of more advanced techniques, which are discussed next.

2.4.3 Green's Function and Spectral Domain Techniques

This section covers an important family of related techniques, variously known as spectral domain analysis [65], surface impedance or admittance [66], effective permittivity [67, 68] or spectral domain Green's function. The earliest example of this work is that of Ingebrigtsen [69], who gave analytical expressions for the electrical impedance of a piezoelectric material, assuming weak piezoelectric coupling. This was able to give analytical expressions for the input admittance of a SAW transducer at centre frequency.

Milsom et al. [68] developed a rigourous method for calculating the effective permittivity, and the accompanying Green's function. This Green's function approach is advantageous because it represents the piezoelectric equations in integral form. The 4 coupled partial differential equations in 4 tensor variables are reduced to a single scalar equation:

$$\varphi(x_1,\omega) = \int_{-\infty}^{\infty} G(x_1 - x_1',\omega) q(x_1',\omega)\,\mathrm{d}x_1', \tag{2.2}$$

where φ is the voltage and q is the charge density per unit width. The substrate is assumed to occupy the region $x_3 < 0$ and propagation is considered in the direction x_1 (see Figure 1.3). The Green's function $G(x_1,\omega)$ encapsulates the behaviour of the acoustic waveguide and is discussed further in Chapter 3. By choosing appropriate weighting and expansion functions for the voltage and charge distribution, an equation results of the form:

$$\varphi_i = \sum_{j=1}^{J} A_{ij} q_j, \tag{2.3}$$

where φ_i are the known[1] coefficients of the voltage weighting functions, and q_j are the unknown coefficients of the charge expansion functions. The form of matrix A depends upon the choice of weighting and expansion functions, the Green's function and problem geometry.

This method is highly suitable for computer implementation, since numerical integration is a well established area of numerical computing. Using this method it is possible to show how the desired SAW response and the undesired BAW response

[1]For structures with floating electrodes the electrode voltages are unknown, and can be found by requiring charge neutrality ($\sum q_n = 0$) on each electrode

contribute to the total admittance curve. Equation (2.2) can be regarded as an exact solution of the 2 dimensional piezoelectric wave propagation problem in a half-space, when there are no surface-normal stresses at $x_3 = 0$. Analysis based on the formulation of a Green's function is referred to as the Boundary Element Method (BEM) or Method of Moments (MOM). The Green's function is most readily calculated from a partial mode analysis in the spectral domain, where functions of the spatial variable x_1 are Fourier transformed to be functions of the spectral variable k_1. The resulting expression for the relationship between voltage and charge is:

$$\overline{\varphi}(k_1, \omega) = \overline{G}(k_1, \omega)\overline{q}(k_1, \omega), \tag{2.4}$$

where the bar notation is used to indicate quantities in the spectral domain which also have a representation in the spatial domain. It is closely related to the effective permittivity, which for real values of k_1 is expressed as [4]:

$$\varepsilon_{eff}(k_1, \omega) = \frac{\overline{q}(k_1, \omega)}{|k_1|\overline{\varphi}(k_1, \omega)} = \frac{1}{|k_1|\overline{G}(k_1, \omega)}. \tag{2.5}$$

The simplest application of the spectral domain Green's function is to search for homogenous solutions, corresponding to free or metallised surface velocities of SAW, PSAW or SSBW modes. Various techniques [39, 64, 68, 70, 71] are used to estimate the electromechanical coupling, power flow angle, attenuation and temperature dependance of these modes, which are based on or compatible with the Green's function formulation.

There is a simple Fourier transform relationship between $G(x_1, \omega)$ and $\overline{G}(k_1, \omega)$, the real-space and spectral Green's functions [4]:

$$G(x_1, \omega) = \frac{1}{2\pi} \int_{-\infty}^{\infty} \overline{G}(k_1, \omega) e^{jk_1 x_1} \mathrm{d}k_1. \tag{2.6}$$

In practice, singularities in the spectral Green's function require careful analytical treatment [68, 72, 73], which complicates the numerical integration of equation (2.6), and makes computer automation error prone. However, it was shown [74] that apart from bulk wave contributions, all elements of the matrix A in equation (2.3) can be calculated analytically from the tabulation of a single function. Despite the efficiency of Green's function based techniques, a large number of source terms need to be considered in

practical devices, particularly resonator structures which have many electrodes. Direct implementation of equation (2.3) to these device geometries results in long computation time. For this reason periodic techniques described were developed, which will be discussed in Section 2.4.4.

Another approach to remedy this problem, a quasi-static[2] Green's function analysis, was developed by Morgan [75], based on the weak-coupling approximation. This assumes that the Green's function terms due to electrostatic effects dominate the admittance of a transducer, and that transfer characteristics can be calculated by using only the surface wave terms. For many applications with delay line devices on low coupling substrates this is sufficiently accurate, and the transfer function can be computed rapidly. This method is very useful for structures where reflections have negligible effect on input admittance, particularly delay lines with split electrode geometries. It is not appropriate for modelling of resonant structures where reflection is an essential part of device operation, as it is not self consistent. A thorough treatment of SAW device modelling using quasi-static analysis was presented by Morgan [4].

An important limitation of the scalar Green's function in equation (2.2) is that it only includes the electrical contribution of the electrodes to reflection and velocity perturbation. In applications on low coupling substrates, with acoustically thick electrodes (i.e. electrode height is not negligible compared wavelength, or electrode material is of high density) the mechanical contribution is also significant. Milsom's results can be generalised to derive a dyadic Green's function (e.g. [76, 77]) which addresses these issues. It consists of a 4×4 matrix relating particle displacement and voltage to applied stress and charge, and in the spectral domain is expressed as:

$$\begin{bmatrix} \overline{u}_1 \\ \overline{u}_2 \\ \overline{u}_3 \\ \overline{\varphi} \end{bmatrix} = \begin{bmatrix} \overline{G}_{11} & \overline{G}_{12} & \overline{G}_{13} & \overline{G}_{14} \\ \overline{G}_{21} & \overline{G}_{22} & \overline{G}_{23} & \overline{G}_{24} \\ \overline{G}_{31} & \overline{G}_{32} & \overline{G}_{33} & \overline{G}_{34} \\ \overline{G}_{41} & \overline{G}_{42} & \overline{G}_{43} & \overline{G}_{44} \end{bmatrix} \begin{bmatrix} \overline{T}_{31} \\ \overline{T}_{32} \\ \overline{T}_{33} \\ \overline{q} \end{bmatrix}. \tag{2.7}$$

The dyadic Green's function allows both mechanical and electrical sources to be considered, and is again computed by partial mode methods. It is advantageous be-

[2]This should not be confused with the quasi-static approximation to the piezoelectric equations, which is used in almost all SAW analysis techniques.

cause it allows mechanical electrode interactions to be included in equation (2.3), and can be more readily extended to layered media (see Section 2.6). For situations where mechanical electrode interactions are negligible, only the element $\overline{G}_{44}$ need be used, thus retaining the simplicity of the scalar Green's function. The dyadic Green's function reveals the existence of acoustic modes which are not coupled to the electric field, and thus cannot be generated piezoelectrically. These modes are not included in the effective permittivity, but may be excited by mode conversion due to mechanical reflection. Further elaboration on the details of the dyadic Green's function will be deferred to Chapter 3.

Utilising the dyadic Green's function, Reichinger and Baghai-Wadji [78] combined a FEM model for electrodes with the BEM model of a substrate, using pulse expansion functions. This allows the semi-infinite substrate to be efficiently represented by using the BEM, and electrodes of arbitrary two dimensional shape to be represented by the FEM. Peach [79] and Ventura [80] presented variations of this technique, using Tchebychev expansion functions, which were previously shown [81] to give much more efficient representation of charge in a periodic system of electrodes. In order to make computation more efficient, Peach [79] used a rigourous Green's function for interaction between nearby electrodes, and a much faster analytical Green's function for long range electrode interactions. This shows the flexibility of methods based on a Green's function, which allow accuracy to be carefully balanced against computation time.

Biryukov [82] demonstrated a fast variational approach to modelling the mechanical fields within electrodes, assuming isotropic and homogeneous material. Using polynomial expansion functions, stress discontinuities at the electrode edge are well approximated with a technique which requires no meshing, making it much simpler than FEM. This method can be combined with the BEM model of the substrate[83].

Gamble and Malocha [84] combined the FEM/BEM model with lumped resistances in series with each electrode to represent the distributed electrode resistance. They also demonstrated a method to extract an angular power distribution from the FEM/BEM model, which allows power lost to bulk waves to be characterised. Previous techniques had not given exact information about the influence of the finite thickness electrodes

on generation of bulk waves, which can be particularly important in the case of shear horizontal waves.

Peverini et al. [85] presented a method to optimally represent the charge distribution on the electrodes of a SAW device. The solution was calculated at a number of widely spaced frequencies using pulse weighting functions. Using a model order reduction technique, the response at other frequencies was computed using the original solutions as expansion functions. This results in a significant reduction in computation time for structures with large numbers of electrodes. Although it was only demonstrated for the case of the scalar Green's function this approach could also be beneficial for fast computation of SAW device responses using the FEM/BEM method.

The disadvantage of boundary element methods is that they form a relationship between every point on the surface, thus creating a dense matrix, rather than a sparse matrix as in the case of FEM. However, the matrices in BEM are typically much smaller, because there is no need for a mesh the complete geometry of the device. BEM also requires the formulation of a Green's function and analytical treatment of singularities within it, whereas the FEM and FD techniques described in Section 2.4.1 follow much more directly from the piezoelectric constitutive equations. A significant advantage of BEM is that the discontinuities in the charge distribution can be much more readily accounted for than in FEM or FD, thus offering greatly improved convergence. Considering all these factors, it is the author's opinion that amongst numerical methods BEM is the best suited for modelling of SAW devices.

2.4.4 Modelling of Periodic Systems

The quasi-static Green's function provides a very good trade-off between accuracy, computation time and physical understanding. However, it is only appropriate for devices with weak piezoelectric coupling. An alternative approach to reducing the computational burden of the Green's function based calculations is to consider an infinitely periodic array of electrodes. This approximation is appropriate for any SAW device with a large arrays of identical electrodes, particularly reflective arrays where the fields decay strongly, so that end effects can be safely neglected. The advantage of this approach is that only a single period of the system needs to be analysed, of-

fering enormous savings in computation time. The periodic Green's function can be calculated directly from the spectral domain Green's function, often without needing to characterise the singularities, which is a difficult process to automate.

Bløtekjær et al. [67] introduced the concept of harmonic admittance (also referred to as strip admittance), based on Ingebrigtsen's approximation of the effective permittivity. The tangential electric field component E_1 between electrodes is represented in the spectral domain in the form:

$$E_1(\beta) = \sum_{n=-\infty}^{\infty} \sum_{m=-M}^{M+1} \alpha_m S_{n-m} P_{n-m} \left[\cos(l/p)\right] e^{-j(\beta+2\pi n/p)x_1}, \tag{2.8}$$

where S_n is the sign of n, P_n is the Legendre function of order n, l/p is the metallisation ratio of the electrodes, p is the period of a single electrode in the array and the product βp gives the phase shift between adjacent electrodes. The coefficients α are determined from the effective permittivity, and M determines the order of the approximation. The normal component of electric flux $D_3(\beta)$ is represented in a similar form, and the harmonic admittance is calculated as:

$$Y(\beta, \omega) = V(\beta, \omega)/I(\beta, \omega), \tag{2.9}$$

where voltage V is obtained by integrating E_1 between electrodes and current I is calculating by integrating $j\omega D_3$ beneath the electrodes. The result applies to any electrode in the array. This approach is very efficient, because although it only explicitly models interactions between a finite number of harmonics, it is able to account for an infinite number of non-interacting harmonics due to electrostatic effects. This allows the complicated charge distribution on electrodes to be taken into account using a very small number of coefficients. By solving for β as a function of ω, the dispersion curve can be obtained, which characterises the propagation in the electrode array.

This harmonic admittance formulation was combined with Milsom's rigourously derived effective permittivity by Zhang et al. [86]. This combined the advantages of an efficient method of representing electrode charge, with the exact analysis of the Green's function, which includes SAW, PSAW and bulk wave contributions. They showed that this harmonic admittance is related to the mutual admittance Y_n between electrodes,

sometimes referred to as the discrete Green's function, satisfying:

$$I_n(\omega) = \sum_{m=-\infty}^{\infty} Y_{m-n}(\omega) V_m(\omega), \tag{2.10}$$

$$Y_m(\omega) = \frac{p}{2\pi} \int_0^{2\pi/p} Y(\beta, \omega) e^{jm\beta p} \, \mathrm{d}\beta, \tag{2.11}$$

with $I_n(\omega)$ and $V_n(\omega)$ being the current and voltage on electrode n. Thus a structure of regular electrodes with arbitrary connections can be rigourously simulated, but differing electrode periods and gaps cannot be accounted for. Unfortunately this model requires extensive computation time and also requires analytical treatment of singularities at each frequency. However, this technique was used to show the behaviour of bulk wave propagation in a periodic array of electrodes, which had previously been neglected.

Hashimoto [65] extended Bløtekjær's theory to include the mechanical effects of electrodes, and named the technique FEM/SDA (spectral domain analysis). This retains the advantage of implicitly dealing with all higher harmonics of the charge distribution, but requires explicit calculation of higher harmonics for the mechanical effects. Thus it loses the advantage of faster computation and becomes complicated to implement. Working in the spectral domain is advantageous because it converts convolution to multiplication. On the other hand, complicated boundary conditions and electrode configurations are more difficult to deal with in the spectral domain.

Another approach is the periodic Green's function [73, 87], which was introduced in scalar form, neglecting mechanical interactions between the acoustic wave and the electrodes. This approach is an implementation of the techniques presented in Section 2.4.3 to the periodic case. The periodic Green's function G_p is the response of the substrate to an infinite number of regularly spaced impulse charge sources:

$$G_p\left(x_1\right) = \sum_{n=-\infty}^{\infty} G\left(x_1 - np\right). \tag{2.12}$$

Here p is the period of the electrodes. Charge distribution on the electrodes is represented either as a series of pulses, or in the form

$$q\left(x_1\right) = \frac{\sum_n q_n T_n(x_1/w)}{\sqrt{1-(x_1/w)^2}}, \tag{2.13}$$

where T_n is the Tchebychev polynomial of order n, w is the electrode half width and q_n is the charge expansion coefficient. It was shown that Tchebychev basis functions result in much faster convergence than pulse functions. The resultant BEM equation has the same form as equation (2.3), however the elements of matrix A are determined by sampling the spectral Green's function at an infinite number of spatial harmonics. In practice this summation can be limited to a finite number of harmonics, since the spectral domain representation of the weighting function converges to zero for large k_1.

As with the non-periodic case, mechanical electrode effects can also be included in the periodic Green's function. Peach [72] and Ventura et al. [88] presented periodic FEM/BEM methods using Tchebychev basis functions. Mathematically, the FEM/BEM and FEM/SDA techniques are equivalent. The spectral domain approach has difficulty handling arbitrary electrode configurations or other complicated boundary conditions. The FEM/BEM approach has the advantage of being able to simulate both finite devices and infinite electrode arrays with relatively minor modifications.

Noting that the FEM part accounts for most of the computational burden in the FEM/BEM model, Laude et al. [89] applied asymptotic waveform evaluation to the FEM/BEM model. The FEM part of the model is calculated only for a single frequency, and approximated at nearby frequencies by a Taylor series expansion. Although it shows great improvement in computation speed, care needs to be taken when using the technique over a wide frequency range, and for complete certainty comparison needs to be made with the exact method. As reported the method was unable to deal with resonant behaviour of electrodes, although it was claimed that it may be extended to cover this case. It has also been shown that this asymptotic waveform evaluation can accelerate the computation of oblique propagation in infinite gratings [90], which would allow these periodic techniques to efficiently account for some 3-dimensional effects.

Ballandras et al. [91] extended the FEM/BEM model to include buried electrodes and also applied this extended model to the study of boundary waves propagating between two semi-infinite materials [92]. This was achieved by using FEM for the region containing the electrodes, as well as some surrounding region, and using BEM only

to account for semi-infinite boundaries. This allows full simulation of electrical and mechanical electrode interactions in layered media. The disadvantage of this method is that it's computational cost is very high, whilst the implementation of the method in software is complex.

Jakoby [93] introduced an FFT-based method, which greatly speeds up the integration necessary to compute the elements of the $\mathbb{A}$ matrix in equation (2.3) for the case of pulse weighting functions in a periodic BEM simulation. This performance increase can result in significant computational savings in cases where the computational burden of calculating the elements of matrix $\mathbb{A}$ is much greater than that of solving it, which is often the case for a periodic system with a small number of weighting functions.

One drawback of any periodic analysis is that it is unable to account for wave scattering which may occur at the transition between an array of electrodes and a free or metallised gap, or the change in charge distribution towards the ends of an electrode array. Additionally, properties of SH surface waves and interfering bulk waves can have a strong dependance on the IDT length [57], which cannot be represented in a periodic model.

It should be noted that continuing advances in computer processing power mean that direct FEM/BEM analysis of finite devices has received renewed interest [84, 85, 94], and is likely to become more widely used for analysing the RF performance of SAW devices. However, this techniques is not applicable to structures with electrodes buried within layered media. An additional problem that remains with the direct application of non-periodic methods is that they numerically calculate the response of a specific geometry, without providing analytical insight. In order to understand how device properties change due to some parameter change such as layer thickness, extraction of phenomenological parameters from a numerical model is necessary. This topic is discussed in the next section.

2.5 Parameterisation of Periodic Numerical Models

Calculating the response of a periodic system is highly advantageous from a computational point of view. However, the problem remains how to use the resulting harmonic

admittance or dispersion curves, which have been shown to yield identical information [95]. In order to simulate the response of a device, the COM and P-matrix models are typically used (Section 2.3), since their parameters can be extracted from periodic models.

The simplest method is to identify the edges of the stop-band for short circuit and open circuit gratings [65]. The stop band is the frequency range over which waves are reflected in an infinite array. This method gives very good results for Rayleigh waves, however it is less accurate for shear horizontal modes such as SSBW and PSAW. In particular it does not account for propagation loss and bulk wave conversion. Ventura [96] presented a method to calculate the P-matrix parameters from the harmonic admittance. Examples were presented showing the effect of electrode size and shape on propagation velocity and reflection, including an analysis of the sensitivity of these parameters to fabrication error.

Koskela [97] presented a method based on the harmonic admittance of an infinite IDT. This method is quite suited for PSAW modes and lossy media, since it is able to characterise propagation loss. However, it is also unable to characterise bulk wave generation and energy storage effects, thus rendering it more suitable for narrow bandwidth devices. The advantage of this method is that it only requires calculation of two admittance values for each frequency, instead of a full search to find the dispersion curve. This means that the computational burden of the rigourous periodic simulation is minimised.

Hashimoto et al. [98] developed a technique which is able to account for many of the subtleties of SH wave propagation. The disadvantage of this method is most of the parameters calculated are allowed to vary arbitrarily with frequency. This means that the technique is suited to the task of accurate representation, but is unable to summarise the behaviour of the structure in a few simple variables. This technique must be fitted to a complete dispersion curve, which requires searching in the complex wavenumber plane for each frequency point. A similar approach was presented by Sveshnikov et al. [99]. This approach is similar to a numerical computation of the complete device response in that it emphasises accuracy at the expense of analytical insight.

Although these techniques are able to give near perfect representation of the harmonic admittance and dispersion behaviour of infinite structures, there is often some discrepancy which occurs in finite structures [57, 99], even if they have a large number of electrodes. This is due to the nature of bulk wave generation, which strongly depend on the IDT geometry. If accurate characterisation of bulk wave interaction is required, then the best solution is to perform a full FEM/BEM simulation of a finite structure. This is because all bulk wave effects are automatically included, and require no special characterisation.

On the other hand, if it is desirable to represent the results of rigourous simulations with a few analytical parameters, the extraction techniques discussed in this section are often quite adequate. They make it easy to identify the effect of process parameters such as electrode size and shape in a meaningful way. For resonator type structures these techniques are ideal. A resonator structure is well approximated by an infinite array, and does not need highly accurate representation at frequencies far from the resonance. For SAW resonators acting as sensors in liquid media, these techniques appear quite promising. This is because they have the accuracy and flexibility of the underlying numerical techniques, and represent device performance in terms of a few simple parameters. The dependence of these parameters on effects such as liquid and mass loading or the impact of using a layered device would be of great interest for sensor design, but has not been considered in the existing literature.

2.6 Modelling of Layered Devices

There are a number of SAW device applications which make use of a layered configuration. These include piezoelectric thin films such as ZnO deposited on non piezoelectric substrates such as glass or diamond, or dielectric films deposited onto piezoelectric substrates to achieve temperature compensation or to modify velocity or electromechanical coupling. For sensing applications layered media are very important, particularly for shear horizontal modes where mass sensitivity can be greatly increased (see Section 2.7.1). Layered media may also be used to protect a SAW sensor, or a sensitive material may be modelled as an additional layer on the surface of the device.

For simple configurations such as an isotropic layer on an isotropic substrate, or

a thin membrane, analytical solutions are available [37]. For the addition of a thin isotropic layer, the perturbation theory of Tiersten [37] can be used to estimate the change in parameters such as propagation velocity. The greatest weakness of perturbation theory is that it is valid only for small changes to the solution. Exactly what constitutes a small change depends on the specifics of the device being characterised. To be certain that perturbation theory is valid it is necessary to compare with numerical solutions, which undermines many of the advantages of perturbation theory.

Techniques for the numerical characterisation of mechanical wave propagation in non-piezoelectric layered media are well established [100]. The transfer matrix is the most commonly used approach, as it treats structures with any number of layers in a consistent and simple manner. It was adapted to the piezoelectric case by Adler et al. [63, 101, 102], and implemented in freely available software [103]. The vector of fields variables ψ (defined in Section 3.2.4) at the top and bottom of a layer can be related by a transfer matrix Φ:

$$\psi(x_3 + h, k_1) = \Phi(h, \omega, k_1)\psi(x_3, k_1). \tag{2.14}$$

This depends on the layer height h, frequency ω and propagation wavenumber k_1. To include the effect of multiple layers, the product of Φ matrices for each layer is taken. From this matrix product, a boundary condition function can be derived. A numerical search of this function is made for values of k_1 which best satisfy the free or metallised surface boundary condition. Adler et al. [63] also demonstrated how the effective permittivity can be calculated using the transfer matrix method.

Smith et al. [104] extended Adler's method to produce a frequency dependant dyadic Green's function of a layered system. This extends all the capabilities of the Green's function analysis to multi-layered structures. It was shown that this method suffers from numerical instability for thick layers at high frequencies, so a scattering matrix approach was developed to solve this problem [105–107]. This formulation retains all the advantages of Adler's approach, and can be used to calculate a Green's function. Another more recent approach is the layer impedance or layer stiffness method [108, 109]. The advantages of this method are almost identical to those of the scattering matrix approach, although implementation is slightly simpler.

The scattering matrix approach has been extended by Reinhardt [110] to include

perfectly conducting metal layers, as well as non-viscous liquids. Such a model is very useful for ultrasonic transducers in liquid media, but for typical operating frequencies of SAW sensors the assumption of a liquid having negligible viscosity is not appropriate. Further discussion of including liquid media in these models is contained in Sections 2.7.3 and 2.7.4.

In order to consider the problem of piezoelectric generation at a layer other than the surface (e.g. for IDTs sandwiched between a layer and substrate), it is necessary to take an approach such as the surface impedance methods of Hashimoto [76] and Zhang [66]. This allows an interface to be modelled under the assumption of infinitely thin grating electrodes, and a resultant Green's function to be calculated. This results in very efficient computation, but suffers from poor accuracy for devices with low electromechanical coupling, heavy electrode material, thick electrodes or high operating frequency, where mechanical reflections play a critical role in device operation.

Wang et al. [111] introduced an asymptotic model for layered systems. They demonstrated that this approximate model can give acceptable accuracy compared to the exact method whilst improving computation speed. However, for maximum accuracy the improvement in speed is only by a factor of 2, and the model is more complicated than the exact models. Additionally, for certain cases the approximations cannot be used, so exact methods must be resorted to. Although the authors show how to detect these cases, it is not clear that the reduction in computation time outweighs the extra complexity of implementation.

A common feature of all the techniques for multi-layer devices discussed in this section is that they assume that each layer is perfectly homogeneous, and that the interface between layers is perfectly smooth. In practice such a conditions are never met, particularly in the case of poly-crystalline thin films. Nonetheless, good agreement is generally achieved. For problems with highly irregular layer boundaries a finite element approach would be more suitable.

For accurate modelling of layered SAW filter and sensor structures, it is necessary to account for electrodes of finite height buried between a layer and substrate. The FEM/BEM models discussed in Section 2.4.3 cannot be applied because they treat each electrode separately, whereas within layered media they are directly coupled to each

other by the layer material. To date only Ballandras et al. [91] have reported a solution to this problem based on using FEM to mesh most of the problem, leaving most of the semi-infinite substrate or homogenous layers to be simulated via a Green's function analysis. This solution is very crude, since it uses the FEM for the most critical sections of the problem, resulting in poor convergence and long computation time. Thus there is a requirement for a simpler model to handle this case.

2.7 Modelling of SAW Sensor Response

For SAW and other acoustic sensors, the analysis requirements are somewhat different from those of signal processing components. Factors such as precise control of the operating frequency are of less concern. More importance is placed on the change in these parameters due to the quantity being sensed, as well as interfering effects. To model sensor performance it is necessary to know the mechanism by which it will operate. The most common is a mass response, whereby a mass adsorbed into or deposited onto the sensitive layer causes a change in wave velocity. Another mechanism is through a change in conductivity of a thin film, which causes a change in velocity due to acousto-electric interaction between the wave and a conductive material. Other common mechanisms include loading of the wave by the density, viscosity, conductivity or permittivity of a liquid medium. Usually only one of these mechanisms corresponds to the desired response, so other mechanisms will results in some interference. For mass sensing there may be additional effects due to the elastic properties and geometry of the additional mass. Techniques to calculate the sensitivity to mass will be reviewed in Section 2.7.1, and sensitivity to conductivity changes will be reviewed in Section 2.7.2, since these are the parameters of greatest interest in sensing applications. This will be followed in Section 2.7.3 by a discussion of techniques to characterise the operation of SAW sensors in liquid media, and in Section 2.7.4 by a review of numerical techniques for the determination of sensitivity.

2.7.1 Mass Sensitivity

Mass sensitivity represents the change in output signal caused by a mass bound to the surface of a sensor. The most widely used definition of the mass sensitivity of a SAW mode is [112]:

$$S_m^v = \lim_{\Delta m \to 0} \left(\frac{\Delta v / v_p}{\Delta m / a} \right), \tag{2.15}$$

where v_p is the SAW phase velocity and Δv is velocity change due to mass change Δm per area a. In practice, it can be regarded as the fractional velocity change due to loading by a small mass per unit area, and is commonly expressed in cm^2/g. A quantity which is often useful in deriving the velocity sensitivity is the sensitivity of the wavenumber k_1:

$$S_m^k = \lim_{\Delta m \to 0} \left(\frac{\Delta k / k_1}{\Delta m / a} \right), \tag{2.16}$$

Since frequency is typically the parameter which is experimentally measured, the corresponding sensitivity of the output frequency [16]:

$$S_m^f = \lim_{\Delta m \to 0} \left(\frac{\Delta f / f_0}{\Delta m / a} \right) = \left(\frac{v_g}{v_p} \right) S_m^v = - \left(\frac{v_g}{v_p} \right)^2 S_m^k, \tag{2.17}$$

is of more practical interest, where v_g is the group velocity of the SAW mode, which can be calculated from the phase velocity. In a non-layered device the group and phase velocities are equal, thus S_m^f, S_m^v and S_m^k are identical. In layered devices with significant velocity dispersion this equality no longer holds.

Perturbation theory is commonly used to describe the variation of SAW propagation properties due to the addition of a layer, or a change in its properties. A thorough explanation of this theory can be found in [37]. This theory gives the expression for the wavenumber shift due to the addition of a thin isotropic layer as:

$$\frac{\Delta k}{k_1} = -\frac{v_p h}{4|P|} \left[\left(\rho' - \frac{4c'_{44}}{v_p^2} \frac{c'_{12} + c'_{44}}{c'_{11}} \right) |v_1|^2 + \left(\rho' - \frac{c'_{44}}{v_p^2} \right) |v_2|^2 + \rho' |v_3|^2 \right]_{x_3 = 0}, \tag{2.18}$$

where ρ' and c' are the density and stiffness constants of the perturbing layer, v_p is the phase velocity of the underlying device, $v_{1..3}$ are the particle velocity components of the unperturbed mode and $|P|$ is the integrated SAW power flow per unit width. These can be readily calculated using the numerical techniques discussed in Section 2.6. Assuming that the shear wave velocity of the perturbing material is much less than the phase velocity of the SAW mode (ie. $c'_{44}/\rho' \ll v_p^2$), the coefficient of $|v_2|^2$ in equation

2.18 reduces to ρ'. Also, noting that the term $\left(c'_{12}+c'_{44}\right)/c'_{11}$ must lie between 0.5 and 1 for physically realisable materials, the coefficient of v_1 will also reduce to ρ' if the shear wave velocity of the perturbing material is low. By making these simplifications and combining with equation 2.18, the following expression for mass sensitivity is obtained [113]:

$$S_m^v = -\frac{v_p}{4|P|}\left(|v_1|^2+|v_2|^2+|v_3|^2\right)\Big|_{x_3=0}. \tag{2.19}$$

Perturbation theory can only be meaningfully applied to small changes, and it's range of validity can generally only be determined by comparing with exact numerical solutions. The assumption that the shear wave velocity of the perturbing material is low means that mass of the material can only be independently measured when it has low stiffness and high density, even for very thin layers.

By approximating the guiding layer and substrate as being isotropic, Wang et al. [112] obtained analytical expressions for the mass sensitivity of a layered SAW and plate mode devices. For a Love wave device, they showed that optimum mass sensitivity is achieved when quarter wave resonance occurs in the layer, and is given as

$$\left(S_m^f\right)_{max} = -4\frac{v_{s1}}{v_{s2}\rho_2\lambda_1}, \tag{2.20}$$

where v_{s1} and λ_1 are the substrate shear wave velocity and propagation wavelength and v_{s2} is the guiding layer shear velocity. Thus maximum sensitivity is expected when using a high velocity substrate and a guiding layer with a low density and velocity. It should be noted that this approach is strictly only valid for structures with pure SH polarisation, but would be expected to qualitatively apply to structures with quasi-SH polarisation.

The useful property of these methods is that they give an indication of which parameters have an impact on device performance, thus providing some design insight. Although the resultant mass sensitivity is useful for comparison of devices, it does not necessarily correspond to the response that will be observed in a given experimental situation. This is because any practical analyte will also have finite geometry and stiffness or viscosity, which also affect wave propagation.

A limitation of these models is that they do not account for the specific geometry of the SAW sensor, which can result in different sensitivity from that predicted by models which assume propagation along an infinite substrate [25]. In addition, these models

assume that the device is loaded by a homogeneous layer. In practical applications such as bio-sensing, this is not necessarily the case.

2.7.2 Conductometric Sensitivity

Conductometric sensitivity gives the velocity change due to a change in conductivity of a layer on the surface of the SAW device. For sensing oxidising and reducing gasses this is the most common mechanism used, in combination with an appropriate sensing layer. Ricco and Martin [34] developed the basic theory of a SAW sensor responding to a conductivity change. Using perturbation theory, assuming weak electromechanical coupling, and neglecting the thickness of the layer, they showed that the velocity shift $\Delta v/v_p$ and normalised attenuation α/k_1 of a non-layered SAW device in contact with a thin conductive layer are:

$$\frac{\Delta v}{v_p} = -\frac{K^2}{2}\frac{\sigma_{sh}^2}{\sigma_{sh}^2 + v_p^2\varepsilon_p^2}, \tag{2.21a}$$

$$\frac{\alpha}{k_1} = \frac{K^2}{2}\frac{v_p\varepsilon_p\sigma_{sh}}{\sigma_{sh}^2 + v_p^2\varepsilon_p^2}, \tag{2.21b}$$

where K^2 is the electromechanical coupling of SAW mode at the device surface, ε_p is the permittivity of the structure (including free space permittivity), v_p is the phase velocity and σ_{sh} is the sheet conductivity of the layer. A normalised plot of equations (2.21) is given in Figure 2.3. It is important to note that the conductivity sensitivity is a function of the sheet resistance of the thin layer (σ_{sh}), and is largest when $\sigma_{sh} = v_p\varepsilon_p$, which coincides with maximum power dissipation into the layer. This indicates that to achieve high sensitivity the sheet conductivity of the layer must be matched to the velocity-permittivity product of the SAW mode.

Conductometric sensitivity is linearly proportional to electromechanical coupling coefficient K^2. An important distinction which must be made in the case of layered SAW devices is between K^2 at the device surface, and at the substrate-layer interface. For modelling acoustic wave generation and detection K^2 should be calculated where the IDT is located, which is often at the interface between the guiding layer and the substrate. For conductivity sensing purposes K^2 should be calculated at the device surface, since this is where the conductometric sensitive layer is deposited. In both cases the same techniques can be used to calculate the coupling.

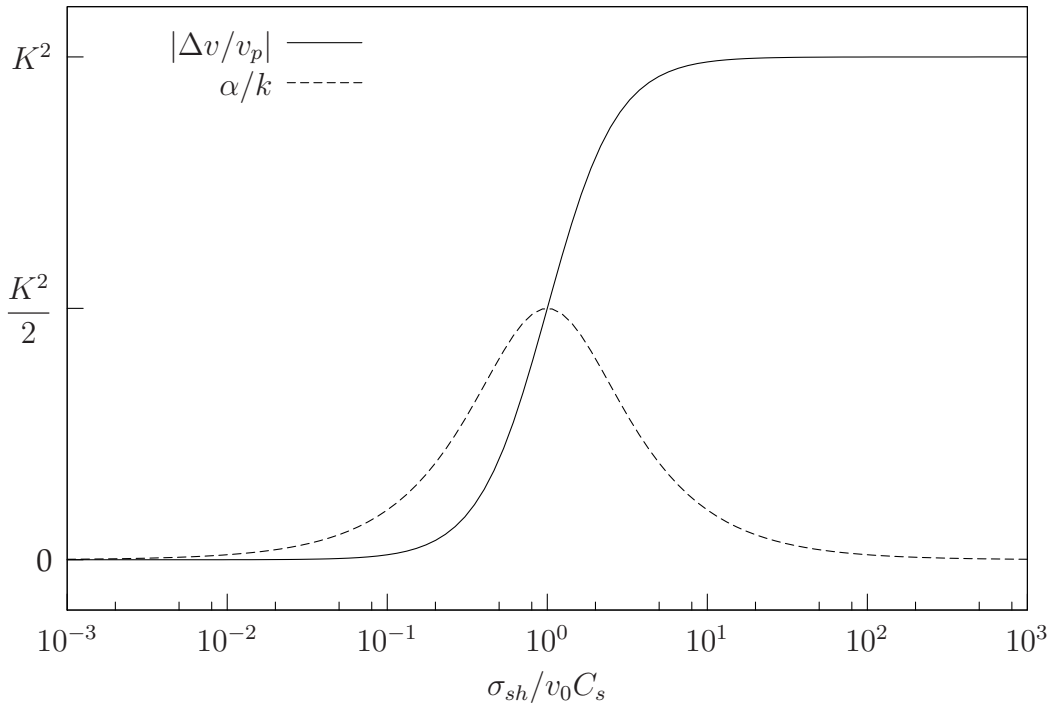

Figure 2.3: Surface wave velocity and attenuation as a function of layer conductivity

2.7.3 Influence of Liquid Media

Operation in liquid media has a significant impact on the wave propagation characteristics of a device. The conductivity and viscosity of the liquid can significantly increase attenuation and shift the phase velocity. In addition, acoustic modes with substantial shear vertical components may be strongly attenuated due to radiation of energy into the liquid.

Niemczyk et al. [114] and Josse and Shana [115] derived perturbation relations for the effect of liquid conductivity σ on the velocity and attenuation of a surface acoustic wave. As expected, these equations have similar form to the response of a SAW to a thin conductive film given in equations (2.21):

$$\frac{\Delta v}{v_p} = \frac{-K^2}{2} \frac{(\varepsilon_s + \varepsilon_0)\,\sigma^2}{(\varepsilon_s + \varepsilon_l)\left[\sigma^2 + \omega^2 (\varepsilon_s + \varepsilon_l)\right]}. \tag{2.22a}$$

$$\frac{\alpha}{k} = \frac{K^2}{2} \frac{(\varepsilon_s + \varepsilon_0)\,\omega\sigma\,(\varepsilon_s + \varepsilon_l)}{(\varepsilon_s + \varepsilon_l)\left[\sigma^2 + \omega^2 (\varepsilon_s + \varepsilon_l)\right]}. \tag{2.22b}$$

Here ε_s is the permittivity of the structure excluding the area above the substrate, ε_l is the liquid permittivity, ε_0 is the free space permittivity and ω is the angular frequency. The most significant difference from the case of a thin conducting layer is that this

result is frequency dependant, and is sensitive to both changes in conductivity and permittivity of the liquid. The matching conditions for maximum sensitivity to liquid conductivity are dependant on the permittivity of the liquid.

The viscosity sensitivity of a shear horizontal SAW device operating in liquid media is closely related to its mass sensitivity. The velocity change due to a change of Newtonian liquid of viscosity from η_l to η_l' and density from ρ_l to ρ_l' is calculated via perturbation theory as [116]:

$$\frac{\Delta v}{v_p} = -\frac{v_g \left|v_2\right|^2}{4\omega|P|}\left(\sqrt{\frac{\omega\eta_l'\rho_l'}{2}} - \sqrt{\frac{\omega\eta_l\rho_l}{2}}\right), \tag{2.23}$$

where v_2 is the shear particle velocity. By comparison with equation (2.19) it can be seen that a SAW device with high mass sensitivity must also have high viscosity sensitivity. However, viscosity sensitivity is also enhanced by surface roughness and porosity, but this cannot be characterised so easily in an analytical form. Some differentiation between the mass and viscosity responses can be achieved because a perfectly elastic material does not cause wave attenuation, whereas a viscosity change will cause attenuation change of

$$\frac{\Delta\alpha}{k} = \frac{v_g \left|v_2\right|^2}{4\omega|P|}\left(\sqrt{\frac{\omega\eta_l'\rho_l'}{2}} + \sqrt{\frac{\omega\eta_l\rho_l}{2}}\right). \tag{2.24}$$

A more in-depth study of the effect of liquid viscosity on Love wave devices was presented by Tamarin et al. [117]. By assuming isotropic materials, dispersion relations were obtained showing the effect of liquid viscosity on the SAW velocity. This work also showed that a viscous liquid can actually increase the mass sensitivity, due to the trapping effect of the liquid.

McHale et al. [118] presented an analysis of Love wave devices loaded with viscoelastic materials, thus unifying the theory of the response to mass and viscosity changes. The influence of viscoelastic characteristics of the guiding layer were also shown, which are significant when a polymer is used. Analytical formulas for the mass sensitivity in liquid and vacuum media were given. An important result is that the effects of mass loading and liquid loading cannot be considered to be independent additive effects, but must be considered together. It was shown that for mass loading in liquid media, the sensitivity S_m^{liq} has an extra factor compared to the sensitivity in

the vacuum case S_m^{vac}:

$$S_m^{liq} \approx \frac{1 - \frac{j\omega}{c_{44}^{(m)} k_3^{(m)}} \sqrt{\frac{1}{2}\rho_l \eta_l \omega}}{1 - \frac{j\omega}{c_{44}^{(g)} k_3^{(g)}} \sqrt{\frac{1}{2}\rho_l \eta_l \omega}} \, S_m^{vac}. \tag{2.25}$$

In this expression k_3 refers to the surface-normal component of the wave vector, quantities with superscripts (g) and (m) are those of the guiding layer and perturbing mass layer respectively. It is important to note that unlike equation (2.19), where the contribution of the elastic properties was shown to be negligible when the perturbing material has high density and low stiffness, no such limit occurs in this case. Instead, there is an explicit dependance on the properties of the liquid, guiding layer and the perturbing mass.

These analytical techniques provide useful insight, but do not give a complete picture of device operation in liquid media. This is due to the assumption of isotropic materials, and the neglecting of electrode effects, which are particularly important for resonator structures.

2.7.4 Numerical Models for Sensing Application

The analytical techniques presented so far in this section give a great deal of useful insight, but do not necessarily reveal the complete device behaviour. Numerical techniques can give a much more accurate picture, assuming that all the underlying parameters are well known. Most of the techniques presented in Section 2.6 were developed for signal processing applications, where dielectric, piezoelectric and ideal conducting layers are modelled. The adaptation of these techniques to the sensing case will be considered here. Numerical techniques are also quite applicable to SAW sensors operating in liquid media, as the liquid can be considered another semi-infinite layer with well known properties.

Furukawa et al. [119] modelled a viscous liquid as a dielectric solid with complex stiffness constants, by manipulating the equations for a Newtonian liquid into a stress and displacement form. This allows a viscous liquid to be included in the analysis techniques presented in Section 2.4. A more formal approach by Ballandras et al. [120] considering interaction with a viscous liquid gave essentially the same result. They

combined this approach with the layered Green's function, to calculate the harmonic admittance of infinitesimally thin electrodes directly exposed to water.

Zaitsev et al. [121] used a similar numerical approach to model a conductive liquid, finding significant differences between the numerical approach and perturbation theory of equations (2.22). The major difference that liquid viscosity or conductivity introduces to the analysis of liquids is the frequency dependance of the material constants. Since the velocity and other properties of a layered structure are almost always frequency dependant, this does not significantly increase the computational complexity. For narrow bandwidth acoustic devices such as resonators, the values at centre frequency are likely to be sufficiently accurate over the bandwidth of interest.

Briot et al. [122] analysed the sensitivity of a shear plate mode device using the harmonic admittance. Utilising a simple spectral representation of the charge distribution, the dispersion curve was calculated and an equivalent circuit derived. The change in resonant frequency of this equivalent circuit due to mass loading was calculated to give the mass sensitivity.

The conclusion which can be drawn from these works is that many numerical techniques suitable for SAW device analysis can be applied to SAW devices operating in liquid media. Some obvious exceptions exist, such as using the FEM/BEM method for electrodes directly covered in liquid. In practice this is not a useful configuration, since the liquid will cause excessive electrical loading. The most common situation is liquid/guiding layer/IDT/substrate. As discussed in Section 2.6 this configuration can readily be modelled, however the problem of finite height electrodes and non-smooth guiding layer is likely to be even more significant, since a corrugated surface has been shown [31] to strongly affect SAW/liquid interaction. There is a significant need for a relatively simple model which accurately characterises the effect of mechanical interactions with electrodes buried within layered media, due to the common use of this configuration in liquid media sensing.

Another area of concern is the sensitivity expressions given in Sections 2.7.1 and 2.7.2. These equations assume that the device interaction with the analyte is uniform over the surface. However, in applications such as bio-sensing, this assumption is not well grounded. Using analytical models it is not possible to conclude which part of the

device surface is most sensitive to surface perturbations. It has previously been shown by Harding [25] that for a SAW delay line with electrodes exposed to the analyte, sensitivity varies significantly over the device surface. For resonator type SAW devices even stronger sensitivity variation is expected, since acoustic energy decays exponentially into the reflective gratings. Thus there is a strong need for a model which characterises the effect of inhomogeneous loading, in order to find the region of the SAW where sensitivity is highest. This is particularly important in cases where only a small quantity selective material is available, so that it can be placed on the most sensitive region of the SAW device. It is also important when a limited amount of analyte is available.

2.8 Other Modelling Considerations

None of the methods mentioned in this section include electromagnetic feed-through, or the effects of packaging. These issues can be quite important in sensor design. Electromagnetic feed-through can distort the frequency response, which can cause the startup frequency to be unpredictable. The effect of bond leads and packaging are typically included separately in signal processing applications via electromagnetic simulations [123]. Packaging is an important issue in its own right which can impact on sensor performance by affecting thermal insulation, electrical interference, mechanical stresses and vibration isolation. This area has not received such a great deal of attention in the literature. In the author's opinion this is because packaging details are considered commercially sensitive, due to their highly critical importance in the performance of the sensor system.

Many other techniques also exist in the literature to study effects such as unidirectionality and non-linear interaction. These effects are almost always insignificant for SAW sensors, so they will not be considered here.

2.9 Conclusion

It was shown that modelling techniques for SAW device analysis vary between simple analytical models and computationally intensive numerical models. Numerical methods such as those based on the Green's function give greater accuracy but can require

long computation time. Analytical or phenomenological methods are much quicker to use and easier to understand, but are often quite limited in their applicability. Techniques also exist which extract analytical parameters from the results of rigourous simulation methods, thus combining the merits of both approaches. In the author's opinion, these techniques are highly appealing because they give results rigourously based on the physics of the problem, whilst still being relatively quick to compute and providing useful insight.

The rigourous numerical techniques which were discussed in this chapter were developed primarily for signal processing applications. In order to apply them to layered SAW resonator sensors operating in liquid media, a new model is required to account for mechanical electrode interactions when the electrodes are buried within layered media. In subsequent chapters of this thesis, the author will propose a new model which accurately describes the behaviour of resonant layered SAW sensors operating in liquid media.

The author's novel approach to this problems will be presented in Chapter 4, utilising the periodic Green's function. In order to develop this function the spectral domain Green's function is required, so this is outlined in Chapter 3, and extended to include material classes used in SAW sensors. As the spectral domain Green's function can also be used for the analysis of delay line structures, examples of this analysis will be given and compared with experimental results.

When considering SAW sensors specifically, an important limitation is the simplistic nature of the existing models. Although they provide useful insight, they are not always sufficiently accurate for optimisation of sensor performance. In particular, all of these models assume that the SAW device is homogeneously loaded by the analyte, thus they are unable to determine which areas of the sensor are most sensitive. The author's approach to this problem will be detailed in Chapter 6, based on the novel technique developed in Chapter 4.

[This page has intentionally been left blank.]

Chapter 3

Spectral Domain Green's Function Model

3.1 Introduction

In Chapter 2 it was shown that techniques based on the extraction of phenomenological parameters from a periodic numerical model are the most suitable for analysing SAW resonator structures. These techniques will form the basis of the author's novel approach to modelling layered SAW resonators for liquid media sensing applications. In order to present this approach, it is necessary to first introduce the spectral domain Green's function, which will be done in this chapter.

The spectral domain Green's function will be presented in such a manner as to lead naturally to the periodic analysis, which will be discussed in Chapter 4. In this chapter it will be shown how the spectral domain Green's function can be used as an analytical tool in it's own right. This technique will be employed to determine propagation velocity, electromechanical coupling and mass sensitivity, which are the most important properties for both delay line and resonator SAW structures. Example calculations will be presented of the ZnO/36°-YX $LiTaO_3$ configuration, alongside the author's measurements of delay line SAW devices, which are used to validate the model.

Section 3.2 covers the derivation of the layered spectral domain Green's function from the constitutive and governing equations for piezoelectric and other materials. From the spectral domain Green's function it is possible to gain insight into the performance of SAW sensors before proceeding to the more complicated periodic analysis. Section 3.3 describes the techniques used to extract useful parameters describing SAW

sensor performance from the Green's function, and gives several examples of these parameters. It also includes a comparison with parameters extracted from measurement of devices. Although the analysis undertaken in this chapter is applicable to SAW resonator sensors, it does not include several effects which are specific to them. These effects will be discussed and methods to account for them will be developed in Chapter 4.

3.2 Development of Spectral Domain Green's Function

In this section the derivation of the spectral domain Green's function is given. This is a powerful analytical tool which can be used to solve partial differential equations, and forms the basis of all subsequent analysis. For SAW devices the equations to be solved are the piezoelectric constitutive and governing equations, which will be introduced first. For the analysis of wave propagation problems, it is most convenient to work in the frequency domain with all field quantities proportional to $e^{j\omega t}$, with ω being the angular frequency. This convention will be used throughout this thesis.

3.2.1 Constitutive and Governing Equations for Piezoelectric Materials

The piezoelectric constitutive and governing equations [36] can be used to describe the behaviour of almost all piezoelectric micro-devices. The essential details are reproduced here, and in Section 3.2.2 they will be extended to describe the behaviour of other materials which are important for liquid media sensing applications.

The linearised strain tensor S represents the deformation of a material under the acoustic approximation. The acoustic approximation implies that the deformation of the material is small ($\partial u_i/\partial x_j \ll 1$) and that the material response can be assumed to be linear. Strain is related to the particle displacement u_i by

$$S_{ij} = \frac{1}{2}\left(\frac{\partial u_i}{\partial x_j} + \frac{\partial u_j}{\partial x_i}\right). \tag{3.1}$$

Diagonal elements $(i = j)$ represent the expansion or contraction of a material along direction x_i. Off-diagonal elements $(i \neq j)$ represent shear deformation in the (x_i, x_j) plane.

Stress tensor element T_{ij} is the force per unit area in the direction x_j on an infinitesimal surface normal to the direction x_i. It is related to the acceleration of an infinitesimal volume of material, having density ρ, via the governing equation:

$$\frac{\partial}{\partial x_j} T_{ij} = -\rho\omega^2 u_i. \tag{3.2}$$

In this equation the Einstein notation is used [36] whereby summation is implied over repeated indices.

The stress and strain tensors are coupled to each other, as well as the electric field E and electric flux D, via the piezoelectric constitutive equations:

$$T_{ij} = -e_{ijk} E_k + c^E_{ijkl} S_{kl}. \tag{3.3a}$$

$$D_i = \varepsilon^S_{ij} E_j + e_{ijk} S_{jk}. \tag{3.3b}$$

The stress and strain tensors are related by the stiffness tensor c_{ijkl}, with the superscript ^{E} indicating that the stiffness is defined at constant electric field. The dielectric tensor ε_{ij} represents the relationship between electric field and flux density, with the superscript ^{S} indicating that it is defined at constant strain. The piezoelectric tensor e_{ijk} is responsible for the interaction between electrical and mechanical fields.

The divergence of electrical flux is equal to volume charge density q_v:

$$\nabla \cdot \mathbf{D} = q_v. \tag{3.4}$$

In this work the volume charge density is taken to be zero in all regions except for on electrodes and metal layers, where it takes the form of a surface charge density.

The quasi-static approximation is almost always used in the analysis of piezoelectric wave propagation. It assumes that the electric field can be represented as the gradient of a scalar voltage field φ, such that:

$$E_i = -\frac{\partial}{\partial x_i} \varphi. \tag{3.5}$$

Another quantity which is often used is particle velocity, which is the time derivative of particle displacement:

$$v_i = j\omega u_i. \tag{3.6}$$

Due to the high degree of symmetry in the tensors S_{ij}, T_{ij}, c_{ijkl} and e_{ijk} they can be represented in a more compact matrix form as S_I, T_I, c_{IJ} and e_{iJ}. The dielectric tensor ε_{ij}

remains unchanged in this matrix notation. The stress and strain matrices are formed from the tensor elements as follows:

$$\mathbf{T} = \begin{bmatrix} T_{11} & T_{22} & T_{33} & T_{23} & T_{13} & T_{12} \end{bmatrix}^T. \tag{3.7}$$

$$\mathbf{S} = \begin{bmatrix} S_{11} & S_{22} & S_{33} & 2S_{23} & 2S_{13} & 2S_{12} \end{bmatrix}^T. \tag{3.8}$$

Superscript ^{T} indicates the matrix transpose operation. Apart from the factors of 2 in the strain matrix, all of the equations are consistent with the tensor form. Stress and strain matrices obey the following equations:

$$\underline{\underline{\nabla}}^T \mathbf{T} = -\rho\omega^2 \mathbf{u} \tag{3.9}$$

$$\mathbf{S} = \underline{\underline{\nabla}} \mathbf{u}, \tag{3.10}$$

where the operator $\underline{\underline{\nabla}}$ represents the tensor divergence in matrix form and is given by the expression:

$$\underline{\underline{\nabla}} = \frac{\partial}{\partial x_1}\mathrm{N}_1 + \frac{\partial}{\partial x_2}\mathrm{N}_2 + \frac{\partial}{\partial x_3}\mathrm{N}_3. \tag{3.11}$$

The effect of elements N_i is to select the direction of tensor quantities expressed in matrix form, and they are defined as [124]:

$$\mathrm{N}_1 = \begin{bmatrix} 1 & 0 & 0 \\ 0 & 0 & 0 \\ 0 & 0 & 0 \\ 0 & 0 & 0 \\ 0 & 0 & 1 \\ 0 & 1 & 0 \end{bmatrix} \qquad \mathrm{N}_2 = \begin{bmatrix} 0 & 0 & 0 \\ 0 & 1 & 0 \\ 0 & 0 & 0 \\ 0 & 0 & 1 \\ 0 & 0 & 0 \\ 1 & 0 & 0 \end{bmatrix} \qquad \mathrm{N}_3 = \begin{bmatrix} 0 & 0 & 0 \\ 0 & 0 & 0 \\ 0 & 0 & 1 \\ 0 & 1 & 0 \\ 1 & 0 & 0 \\ 0 & 0 & 0 \end{bmatrix}. \tag{3.12}$$

In matrix form the constitutive equations are as follows:

$$\mathbf{T} = -\mathrm{e}\mathbf{E} + \mathrm{c}^E \mathbf{S}, \tag{3.13a}$$

$$\mathbf{D} = \varepsilon^S \mathbf{E} + \mathrm{e}^T \mathbf{S}, \tag{3.13b}$$

where c^E is a 6×6 symmetric matrix, e is a 6×3 matrix and ε is a 3×3 symmetric matrix. For most materials there are further constraints upon the elements of these matrices, based on the crystal symmetry of the material, which reduce the number of independent elements. A very important class of materials are the isotropic ones, which have

only two independent elastic constants c_{11} and c_{44}, and a single dielectric constant ε_{11}. They greatly simplify the analysis because their properties such as propagation velocity are independent of direction. However the piezoelectric materials used to generate acoustic waves are necessarily anisotropic, and so are many of the crystalline materials used in SAW devices.

An important practical consideration is the numerical stability of equation (3.13) and of the many subsequent equations which are derived from it. Based on data from the literature [36], Table 3.1 gives the typical orders of magnitude of the material constants when expressed in SI units.

Table 3.1: Typical order of magnitude of material constants

Parameter	SI Unit	Magnitude
c	$\mathrm{N/m^2}$	10^{11}
e	$\mathrm{C/m^{-2}}$	1
ε	$\mathrm{F/m}$	10^{-11}

These greatly differing numbers are highly problematic for numerical computation, since the smaller numbers can easily be much less than the rounding errors of the larger numbers. In many matrix based computations these quantities will be added to each other, thus the smaller quantities will be obliterated and the resultant solution will be erroneous. This problem can be remedied by introducing scaled versions of the field variables as follows:

$$D_i' = \frac{D_i}{D_0} \qquad\qquad u_i' = \frac{u_i}{u_0}. \tag{3.14}$$

By substituting equation (3.14) into equations (3.9), (3.10) and (3.13), it is seen that working with the normalised variables has the effect of scaling the material constants:

$$\underline{\underline{\nabla}}^T\mathbf{T} = -u_0\rho\omega^2\mathbf{u}'. \tag{3.15a}$$

$$\mathbf{S}' = \underline{\underline{\nabla}}\mathbf{u}'. \tag{3.15b}$$

$$\mathbf{T} = -\mathrm{e}\mathbf{E} + u_0\mathrm{c}^E\mathbf{S}'. \tag{3.15c}$$

$$\mathbf{D}' = \frac{1}{D_0}\varepsilon^S\mathbf{E} + \frac{u_0}{D_0}\mathrm{e}^T\mathbf{S}'. \tag{3.15d}$$

For consistency it is required that the scaling on e and e^T are identical, so that:

$$D_0 = u_0. \tag{3.16}$$

This then allows the following normalised material constants to be defined, which then simplify equations (3.15):

$$\rho' = u_0\rho. \qquad \mathrm{c}' = u_0\mathrm{c}. \qquad \varepsilon' = \frac{\varepsilon}{u_0}. \tag{3.17}$$

Examining Table 3.1 and equations (3.15), it can be seen that $u_0 = 10^{-11}$ would be sufficient to bring the typical value of all 3 constitutive constants to near unity. Density is also scaled in order to ensure that characteristic velocities of the materials are unchanged, since these have dimensions of $\sqrt{c/\rho}$ (see Section 3.2.3).

In all further analysis in this thesis, it is assumed that the normalised parameters are used, so the symbol ' will be omitted. Once the piezoelectric equations have been solved the scaling is simply reversed, thus giving the correct result in SI units. The values of the material constants used in this thesis are given in Appendix A.

3.2.2 Extension to Other Classes of Material

The theory in Section 3.2.1 was developed for piezoelectric solids. It can also be extended to other classes of material which are of interest in SAW sensor modelling. Non-piezoelectric solids are represented by setting all elements of piezoelectric matrix e to zero, thus decoupling the electrical and mechanical fields. These material models are adequate for most acoustic devices used for signal processing applications. For sensing applications a variety of materials are used which have much less ideal characteristics. Viscoelastic materials and liquid loading are commonly encountered in such applications.

Viscoelastic materials, such as the polymer layers often used in SAW sensors, can also be represented in a similar form to a non-piezoelectric solid [118]. Assuming isotropic media, the shear stiffness constant c_{44} can be replaced by a complex shear modulus of the form:

$$c'_{44} = \frac{j\omega\eta}{1 + j\omega\eta/c_{44}}, \tag{3.18}$$

where η is the shear viscosity coefficient. At low frequencies ($\omega\eta/c_{44} \ll 1$) such a material will have a viscous limit: $c'_{44} \sim j\omega\eta$, whereas at high frequencies ($\omega\eta/c_{44} \gg 1$)

it will have an elastic limit: $c'_{44} \sim c_{44}$. In the case of elastic solids [36], losses can be considered in a much simpler form by making the substitution

$$c'_{IJ} = c_{IJ} + j\omega\eta_{IJ}. \tag{3.19}$$

This complex stiffness will result in absorption of energy by the material. For sufficiently low frequencies this loss will be negligible, and the term $j\omega\eta_{IJ}$ can be neglected. It should be noted that these loss coefficients for solids are generally more difficult to determine than the stiffness constants, and are not commonly available in the literature.

To include liquid media in the model, a constitutive relationship for it must also be derived. A viscous liquid is commonly represented using the Newtonian model with negligible bulk viscosity[60, 120, 125], which allows for the propagation of both longitudinal and shear waves. To allow the constitutive equation to be incorporated with existing models, it is expressed in terms of the stress and strain tensors:

$$T_{ij} = \left(K - j\omega\frac{2}{3}\eta\right)\sum_{k=1}^{3} S_{kk}\delta_{ij} + 2j\omega\eta S_{ij}. \tag{3.20}$$

Here K is the bulk modulus of the liquid and η is its shear viscosity.

By converting equation 3.20 to matrix form, it can be seen that the symmetry of the equations is identical to that for an isotropic solid. The most important differences are the presence of the time dependant viscosity terms $j\omega\eta$, and that for the shear component there is no real term of the material parameters. This is because shear stresses are not supported by a non-viscous liquid. To account for such a case the numerical techniques used need to be modified [110], however this case is not of interest in this thesis. As the liquids in this model are isotropic, they can be given equivalent stiffness constants [119]:

$$c'_{11} = K + \frac{4}{3}j\omega\eta. \tag{3.21a}$$

$$c'_{44} = j\omega\eta. \tag{3.21b}$$

By substituting these appropriate c' elements into the equations of Section 3.2.1, the analysis undertaken in this and subsequent chapters can be applied to liquids, viscoelastic materials, and lossy elastic solids. The most important difference which

needs to be taken into consideration is that for these materials, the stiffness matrix is frequency dependant, which will introduce a frequency dependency into several quantities which would otherwise be frequency independent.

The final class of media which must be considered is the gaseous media surrounding a SAW device. For high precision oscillator applications the SAW device may be contained within a sealed evacuated package, in order to eliminate the influence of gas on the device response and aging. These effects are of no significance for the work undertaken in this thesis, since they many orders of magnitude weaker than the effects of interest. Therefore, no distinction is made between the performance of the device operating in vacuum, or in gas media. A vacuum is much simpler to model than gas media, since it supports no acoustic wave propagation and has a well-known permittivity of $\varepsilon_0 = 8.854 \times 10^{-12}$. In this thesis the analysis conducted for devices in vacuum media should be understood to be applicable to the case of gas media which has negligible influence on the device performance.

3.2.3 Bulk Waves in Infinite Media

It was shown in Section 3.2.2 that the piezoelectric constitutive and governing equations can represent the behaviour of materials composing a SAW sensor and its liquid environment. However, direct solution of these equations is usually impractical, since in the most general cases analytical solutions do not exist.

If the solution is assumed to be an infinite plane wave of the form $\exp(j\omega t - \mathbf{k}\cdot\mathbf{x})$, the piezoelectric constitutive equations can be reduced to the piezoelectric Christoffel equation [36]:

$$\frac{1}{\rho}\left(\mathcal{K}_{iN}\left\{c^{E}_{NM} + \frac{\left[e_{Nj}\hat{k}_j\right]\left[\hat{k}_i e_{iM}\right]}{\hat{k}_i, \varepsilon^{S}_{ij}\hat{k}_j}\right\}\mathcal{K}_{Mj}\right) v_j = \left(\frac{\omega}{|\mathbf{k}|}\right)^2 v_i, \tag{3.22}$$

where the unit wave-vector $\hat{\mathbf{k}}$ defined as:

$$\hat{\mathbf{k}} = \frac{\mathbf{k}}{|\mathbf{k}|}, \tag{3.23}$$

gives the propagation direction. The tensor divergence operator results in the quantity $\mathcal{K}$, defined as:

$$\mathcal{K} = \hat{k}_1\mathrm{N}_1 + \hat{k}_2\mathrm{N}_2 + \hat{k}_3\mathrm{N}_3. \tag{3.24}$$

Equation (3.22) converts the complicated system of equations (3.13) to an algebraic eigenvalue problem. Each eigenvalue $(\omega/|\mathbf{k}|)^2$ is the square of the propagation velocity, with the corresponding eigenvector $\mathbf{v}$ being the particle velocities (or polarisation) of the mode. There will be 3 eigenvalues corresponding to the 3 different polarisations possible, although it is quite common to have degenerate solutions (e.g. the two shear modes in an isotropic solid).

These solutions correspond to the partial modes discussed in Section 2.4.2. It is important to note that $|\mathbf{k}|$ and ω only appear as a ratio in equation (3.22), unless ω appears in the material constants as described in Section 3.2.2. This is a property of non-dispersive media and structures, where the phase velocity is independent of frequency. In such cases the wavenumber $\mathbf{k}$ can be expressed in normalised form as $\mathbf{s} = \mathbf{k}/\omega$, where $\mathbf{s}$ is termed the slowness, since it has dimensions of inverse velocity. For convenience this notation is retained even in situations where the material properties or device geometry result in dispersive behaviour.

3.2.4 Spectral Domain Green's Function

The solution presented in Section 3.2.3 is adequate for modelling structures such as thickness shear mode (TSM) resonators, where the wave propagation is well described by a single plane wave. However, it is not directly applicable to guided-wave structures such as SAW devices, so the necessary modifications will be presented in this section. They are based on the partial mode analysis described in Section 2.4.2, and will be extended to develop the spectral domain Green's function. For simplicity the non-layered case will be presented first, with the modifications for the layered case being presented in Section 3.2.5.

When modelling the propagation in a non-layered SAW device, the structure considered is a semi-infinite half space occupying the region $x_3 < 0$. The coordinate convention used throughout this thesis is given in Figure 1.3. The material constants c, ε and e can be rotated to give the correct alignment of crystal axes relative to the device coordinates. The wave propagation is taken to be in the positive x_1-direction, and it is assumed that there is no variation along the x_2-direction, so that:

$$\frac{\partial}{\partial x_2} \equiv 0. \tag{3.25}$$

This means that diffraction and wave-guiding effects in the (x_1, x_2)-plane are ignored. In the co-ordinate system used here, the field variables of interest can be composed into a vector $\boldsymbol{\psi}^{(n)}$ for each partial mode as:

$$\begin{aligned}\boldsymbol{\psi}^{(n)} &= \left[\begin{array}{cccccccc} \overline{v}_1^{(n)} & \overline{v}_2^{(n)} & \overline{v}_3^{(n)} & j\omega\overline{\varphi}^{(n)} & \overline{T}_{13}^{(n)} & \overline{T}_{23}^{(n)} & \overline{T}_{33}^{(n)} & \overline{D}_3^{(n)} \end{array}\right]^T. \\ &= \left[\begin{array}{cccc} \overline{\mathbf{v}}^{(n)T} & j\omega\overline{\varphi}^{(n)} & \overline{\boldsymbol{\tau}}^{(n)T} & \overline{\mathcal{D}}^{(n)} \end{array}\right]^T.\end{aligned} \tag{3.26}$$

Superscript $^{(n)}$ refers to the partial mode. These elements are chosen because any boundary normal to the x_3 direction will place continuity conditions on these variables. Additionally, for frequency-independent material constants, this column vector will be frequency independent. Equation (3.26) also shows the short-hand notation which will be used subsequently. In cases where the frequency dependance has been explicitly introduced, the variables $\overline{\mathbf{u}}$ and $\overline{\varphi}$ will be used instead of $\overline{\mathbf{v}}$ and $j\omega\overline{\varphi}$.

In Section 3.2.3 the wave vector magnitude $|\mathbf{k}|$ and direction $\hat{\mathbf{k}}$ were treated separately. In the analysis used here, it is more convenient to use the propagation component of the slowness vector s_1 as an independent variable, and to find the corresponding partial modes. The complete solution for each value of s_1 is a sum of these partial modes, and can be expressed as:

$$\boldsymbol{\psi}\left(s_1, x_3\right) = \sum_{n=1}^{8} w^{(n)} \boldsymbol{\psi}^{(n)} \exp j\omega\left(t - s_1 x_1 - s_3^{(n)} x_3\right). \tag{3.27}$$

Each partial mode is weighted by a factor $w^{(n)}$ which is determined by boundary conditions. The depth slowness component $s_3^{(n)}$ and corresponding polarisation vector $\boldsymbol{\psi}^{(n)}$ are calculated by reformulating the Christoffel equation (3.22). Instead of specifying propagation direction of the partial mode by the vector $\hat{\mathbf{k}}$, the propagation component s_1 is specified *a priori* and the depth components $s_3^{(n)}$ are determined.

The equation to perform this operation is well known [102, 126]. However, to allow easy generalisation to later results, an alternate form [124] is chosen:

$$\left[\begin{array}{cc} \mathcal{L}_{11} & \mathcal{L}_{12} \\ \mathcal{L}_{21} & \mathcal{L}_{22} \end{array}\right] \left[\begin{array}{c} \overline{\mathbf{u}} \\ \overline{\varphi} \\ \overline{\boldsymbol{\tau}} \\ \overline{\mathcal{D}} \end{array}\right] = \frac{\partial}{\partial x_3} \left[\begin{array}{c} \overline{\mathbf{u}} \\ \overline{\varphi} \\ \overline{\boldsymbol{\tau}} \\ \overline{\mathcal{D}} \end{array}\right]. \tag{3.28}$$

This is a more general approach, since it can be used in a full 3-dimensional analysis, and allows inhomogeneous material constants to be used. The 3-dimensional case is

not considered in this thesis, and the case of inhomogeneous material constants will considered in Chapter 4. Adapting this operator to the 2-dimensional case where $\frac{\partial}{\partial x_2} \equiv 0$ results in:

$$\mathcal{L}_{11} = -\mathrm{M}_{33}^{-1}\mathrm{M}_{31}\frac{\partial}{\partial x_1}. \tag{3.29a}$$

$$\mathcal{L}_{12} = \mathrm{M}_{33}^{-1}. \tag{3.29b}$$

$$\mathcal{L}_{21} = -\underline{\underline{\rho}}\omega^2 - \frac{\partial}{\partial x_1}\left[\mathrm{M}_{11} - \mathrm{M}_{13}\mathrm{M}_{33}^{-1}\mathrm{M}_{31}\right]\frac{\partial}{\partial x_1}. \tag{3.29c}$$

$$\mathcal{L}_{22} = -\frac{\partial}{\partial x_1}\mathrm{M}_{13}\mathrm{M}_{33}^{-1}. \tag{3.29d}$$

The matrix $\underline{\underline{\rho}}$ is defined as:

$$\underline{\underline{\rho}} = \begin{bmatrix} \rho & 0 & 0 & 0 \\ 0 & \rho & 0 & 0 \\ 0 & 0 & \rho & 0 \\ 0 & 0 & 0 & 0 \end{bmatrix}. \tag{3.30}$$

Matrices M_{ij} are based on the material constants:

$$\mathrm{M}_{ij} = \begin{bmatrix} \mathrm{N}_i^T c \mathrm{N}_j & \mathrm{N}_i^T e n_j \\ n_i^T e^T \mathrm{N}_j & -n_i^T \varepsilon n_j \end{bmatrix}. \tag{3.31}$$

Each matrix n_i represents a column vector with a 1 in component i, and the matrices N_i were defined in equation (3.12). A solution of the form $\exp\left(-jk_1x_1 - jk_3x_3\right)$ is substituted into equation (3.28), assuming that the material constants are independent of $\mathbf{x}$. By changing the choice of variables and scaling the equations, the following matrix eigenvalue problem results:

$$\begin{bmatrix} -s_1\mathrm{M}_{33}^{-1}\mathrm{M}_{31} & -\mathrm{M}_{33}^{-1} \\ s_1^2\left(-\underline{\underline{\rho}} + \mathrm{M}_{11} - \mathrm{M}_{13}\mathrm{M}_{33}^{-1}\mathrm{M}_{31}\right) & -s_1\mathrm{M}_{13}\mathrm{M}_{33}^{-1} \end{bmatrix} \boldsymbol{\psi}^{(n)} = s_3^{(n)}\boldsymbol{\psi}^{(n)}. \tag{3.32}$$

The eigenvectors $\boldsymbol{\psi}^{(n)}$ give the polarisation of the partial modes, and the eigenvalues $s_3^{(n)}$ describe their propagation or decay in the x_3-direction.

The eight partial modes can be divided into radiating modes having purely real s_3, and evanescent modes with imaginary or complex s_3. The Poynting vector component $P_3^{(n)}$ [36] of the radiating partial modes must be analysed to determine whether radiating modes propagate in the positive or negative x_3 direction. For evanescent modes,

the sign of the imaginary component of s_3 determines whether the mode decays in the positive or negative x_3 direction. For a non-layered, semi-infinite substrate occupying the region $x_3 < 0$, partial modes should be selected to decay or propagate in the $-x_3$ direction. For calculations made to characterise PSAW velocity and attenuation, complex values of s_1 are used, and different partial mode selection rules should be applied as discussed in Section 2.4.2.

Once the partial modes have been selected, the spectral dyadic Green's function (defined in Equation (2.7)) can be calculated as [104]:

$$\overline{G}(s_1) = \frac{1}{j\omega} \begin{bmatrix} \overline{\mathbf{v}}^{(d)} \\ j\omega\overline{\varphi}^{(d)} \end{bmatrix} \begin{bmatrix} \overline{\boldsymbol{\tau}}^{(d)} \\ \overline{q}^{(d)} \end{bmatrix}^{-1} . \tag{3.33}$$

The superscript $^{(d)}$ indicates the column-wise arrangement of partial modes which decay or propagate in the "downward" $-x_3$ direction. Surface charge $\overline{q}$ is calculated for each partial mode from the discontinuity in electrical flux:

$$\overline{q}^{(n)} = -\overline{\mathcal{D}}^{(n)} - j\varepsilon_0 s_1 \left(j\omega\overline{\varphi}^{(n)}\right) . \tag{3.34}$$

An important feature of the Green's function for *non-layered structures consisting of non-dispersive media* is that it has trivial dependance on frequency. Thus it only needs to be calculated once and scaled appropriately for each frequency. The Green's function can be symbolically partitioned as follows:

$$\begin{bmatrix} \overline{\mathbf{u}} \\ \overline{\varphi} \end{bmatrix} = \begin{bmatrix} \overline{G}_{u\tau} & \overline{G}_{uq} \\ \overline{G}_{\varphi\tau} & \overline{G}_{\varphi q} \end{bmatrix} \begin{bmatrix} \overline{\boldsymbol{\tau}} \\ \overline{q} \end{bmatrix} , \tag{3.35}$$

where $\overline{G}_{u\tau}$ has size 3×3, $\overline{G}_{uq}$ has size 3×1, $\overline{G}_{\varphi\tau}$ has size 1×3 and $\overline{G}_{\varphi q}$ is a scalar.

Having developed the spectral domain Green's function of a piezoelectric half-space, the next task is to extend it to the case of a layered structure.

3.2.5 Extension to Layered Media

As was discussed in Section 2.6, a number of techniques exist for numerically calculating the dyadic Green's function of a layered structure. It is well established that the transfer matrix approach can become numerically unstable for thick layers at high frequency, so the scattering matrix approach [107] has been used in this work.

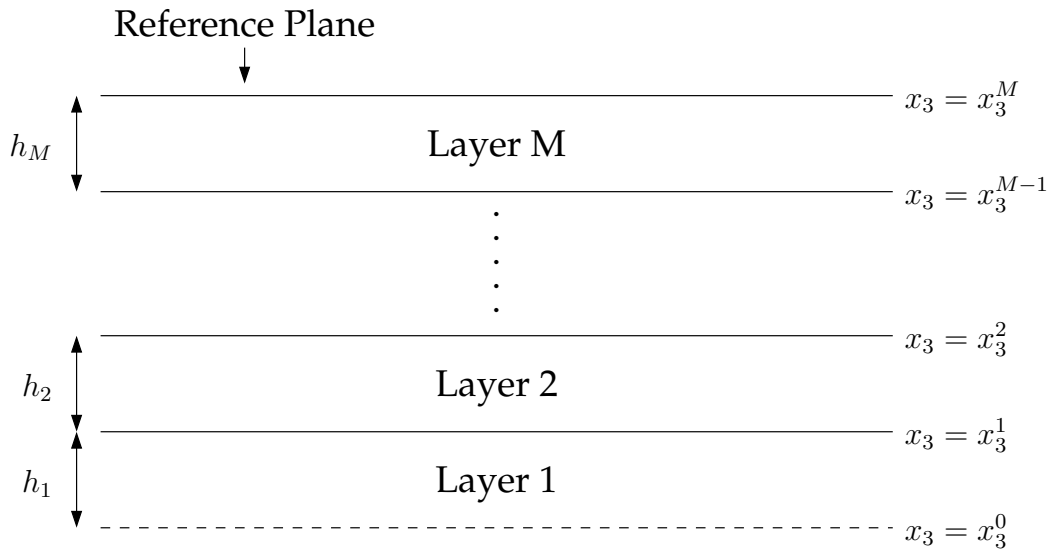

Figure 3.1: Layered configuration to be modelled by Green's function

At the interface between layers, it is always assumed that all components of ψ are continuous, so that rigid coupling occurs, and there is no charge. This model is almost always used for solids [36], and for liquids it is equivalent to assuming that slip effects are negligible. The device consists of an arbitrary number of layers M underneath a reference plane $x_3 = x_3^M$. The reference is the location where the Green's function is calculated; usually this would be the location of the IDTs. Non-zero charge is allowed for at this interface. The case where there is material both above and below the reference plane will be discussed later in this section. Within each layer m the partial modes $\boldsymbol{\psi}_m^{(n)}$ are distinct from those in other layers, and are calculated as discussed in Section 3.2.4:

$$\boldsymbol{\psi}_m^{(n)} = \left[\begin{array}{cccc} \overline{\mathbf{v}}_m^{(n)T} & j\omega\overline{\varphi}_m^{(n)} & \overline{\boldsymbol{\tau}}_m^{(n)T} & \overline{\mathcal{D}}_m^{(n)} \end{array} \right]^T . \tag{3.36}$$

Using the criteria discussed in Section 3.2.4, they are divided into upward and downward bounded partial modes, labelled with a superscript (u) and (d) respectively. It should be noted that from here on subscripts will be used to indicate layer number, thus $\overline{\mathcal{D}}_1$ indicates $\overline{D}_3$ evaluated at $x_3 = x_3^1$.

Next a diagonal matrix $\mathcal{P}_m(h)$ is defined representing the propagation or decay of partial modes in layer m over distance h_m in the x_3 direction :

$$\mathcal{P}_m(h_m) = \mathrm{diag}\left(\left[\begin{array}{ccc} e^{-jk_{3,m}^{(1)}h_m} & \dots & e^{-jk_{3,m}^{(8)}h_m} \end{array} \right] \right). \tag{3.37}$$

For each layer m a vector of partial mode weighting coefficients W_m at the top of the

layer can be calculated:

$$W_m(x_3^m) = \left[\begin{array}{c} \mathcal{P}_m(x_3^m) \end{array} \right] \left[\begin{array}{ccc} w_m^{(1)} & \dots & w_m^{(8)} \end{array} \right]^T . \tag{3.38}$$

These weighting coefficients can also be divided into those belonging to upward and downward bounded modes. The scattering matrix algorithm works by iteratively constructing a reflection matrix $R_{m,m-1}$ at the interface between layers m and $m-1$. This reflection matrix relates the upward and downward propagating modes in layer m:

$$W_m^{(u)} = R_{m,m-1} W_m^{(d)} \tag{3.39}$$

The recursive process is initiated by considering the bottom layer interface at $x_3 = x_3^1$, and constructing a reflection matrix $R_{1,0}$, which accounts for all the material below (but not including) the interface. There are two possible cases for this bottom layer. If it is semi-infinite, then there will be no reflection, so $R_{1,0} = 0$. For a layer of finite thickness bordered by a vacuum, the reflection coefficient can be calculated by imposing the boundary condition of normal stress $\boldsymbol{\tau}$ and the discontinuity in normal flux $\mathcal{D}$ vanishing at the interface:

$$R_{1,0} = -\mathcal{P}_1^{(u)}(h_1) \left[\begin{array}{c} \overline{\boldsymbol{\tau}}_1^{(u)} \\ \overline{\mathcal{D}}_1^{(u)} - j s_1 \varepsilon_0 (j\omega\overline{\varphi}) \end{array} \right] \left[\begin{array}{c} \overline{\boldsymbol{\tau}}_1^{(d)} \\ \overline{\mathcal{D}}_1^{(d)} - j s_1 \varepsilon_0 (j\omega\overline{\varphi}) \end{array} \right]^{-1} \mathcal{P}_1^{(d)}(-h_1) . \tag{3.40}$$

Once the reflection coefficient has been calculated at the top of a layer ($x_3 = x_3^{m-1}$), it can be calculated at the top of the next layer ($x_3 = x_3^m$) by applying the following recursive formula:

$$R_{m,m-1} = \left[\begin{array}{cc} \mathcal{P}_m^{(u)}(h_m) & 0 \end{array} \right] \left[\begin{array}{cc} -\psi_m^{(u)} & \psi_{m-1}^{(u)} R_{m-1,m-2} + \psi_{m-1}^{(d)} \end{array} \right]^{-1} \left[\begin{array}{c} \psi_m^{(d)} \mathcal{P}_m^{(d)}(-h_m) \end{array} \right] . \tag{3.41}$$

At the reference plane ($x_3 = x_3^M$) the Green's function for the structure below the reference interface can be calculated based on the partial modes and the reflection coefficient:

$$\begin{aligned} \overline{G}^b &= \frac{1}{j\omega} \left[\left(\begin{array}{c} \overline{\mathbf{v}}_M^{(u,M)} \\ j\omega\overline{\varphi}_M^{(u)} \end{array} \right) R_{M,M-1} + \left(\begin{array}{c} \overline{\mathbf{v}}_M^{(d)} \\ j\omega\overline{\varphi}_M^{(d)} \end{array} \right) \right] \left[\left(\begin{array}{c} \overline{\boldsymbol{\tau}}_M^{(u)} \\ \overline{\mathcal{D}}_M^{(u)} \end{array} \right) R_{M,M-1} + \left(\begin{array}{c} \overline{\boldsymbol{\tau}}_M^{(d)} \\ \overline{\mathcal{D}}_M^{(d)} \end{array} \right) \right]^{-1} \\ &= \frac{1}{j\omega} \left[\begin{array}{c} \overline{\mathbf{v}}^b \\ j\omega\overline{\varphi}^b \end{array} \right] \left[\begin{array}{c} \overline{\boldsymbol{\tau}}^b \\ \overline{\mathcal{D}}^b \end{array} \right]^{-1} . \end{aligned} \tag{3.42}$$

It can be seen for a non-layered structure $R_{M,M-1} = 0$, and the spectral domain Green's function is similar to that given in equation (3.33).

If a structure is present above the reference plane then its Green's function can be calculated in a similar way by swapping upward and downward bounded quantities in the algorithm to yield G^a. Here a and b indicate quantities in the region above and below the reference interface respectively. Alternatively, if there is a vacuum above the the reference plane, it's dielectric effect should be included for accurate representation of charge at an interface. It should be noted that equation (3.42) is expressed in terms of electrical flux component $\overline{\mathcal{D}}$, instead of charge. However, the following procedure results in a Green's function in terms of charge $\overline{q}$.

For a configuration with material above and below the reference plane, use of the quantities $\Delta\overline{\boldsymbol{\tau}} = \overline{\boldsymbol{\tau}}^{\,a} - \overline{\boldsymbol{\tau}}^{\,b}$ and $\overline{q} = \overline{\mathcal{D}}^{\,a} - \overline{\mathcal{D}}^{\,b}$ simplifies the analysis. It is assumed that there is rigid contact between the materials, so that $\overline{v}^{\,a} = \overline{v}^{\,b}$ and $\overline{\phi}^{\,a} = \overline{\phi}^{\,b}$. For the regions above and below the reference interface, instead of solving equation (3.42), the following equation is solved for $\overline{Z}^{\,a}$ and $\overline{Z}^{\,b}$:

$$\overline{Z}^{a,b} = j\omega \begin{bmatrix} \overline{\boldsymbol{\tau}}^{\,a,b} \\ \overline{\mathcal{D}}^{\,a,b} \end{bmatrix} \begin{bmatrix} \overline{\mathbf{v}}^{\,a,b} \\ j\omega\overline{\varphi}^{\,a,b} \end{bmatrix}^{-1}. \tag{3.43}$$

The quantity $\overline{Z}$ is known as the surface impedance, and is the inverse of the dyadic Green's function. It will sometimes be more convenient to refer to this quantity in frequency independent form as $Z' = \frac{1}{j\omega}Z$. Therefore $\overline{q}$ and $\Delta\overline{\boldsymbol{\tau}}$ can be found from:

$$\begin{bmatrix} \Delta\overline{\boldsymbol{\tau}} \\ \overline{q} \end{bmatrix} = \left(\overline{Z}^{\,a} - \overline{Z}^{\,b}\right) \begin{bmatrix} \overline{\mathbf{v}} \\ j\omega\overline{\varphi} \end{bmatrix}. \tag{3.44}$$

This result is then inverted to form the Green's function of the complete structure:

$$\overline{G} = \left(\overline{Z}^{\,a} - \overline{Z}^{\,b}\right)^{-1}. \tag{3.45}$$

To apply this model directly to a layered SAW device requires the assumption of infinitely thin electrodes causing no mechanical perturbation. The author's novel approach which more accurately models buried electrodes within layered media will be presented in Chapter 4.

Having calculated the spectral domain Green's function of a layered SAW structure, device analysis using this function will be undertaken in Section 3.3. This function will also be used in the periodic analysis developed in Chapter 4.

3.3 Device Analysis Using the Spectral Domain Green's Function

The spectral domain Green's function was developed as a means of calculating the spatial domain Green's function, which is used to directly solve for the electrical and mechanical fields within a SAW device. However, since it encapsulates the solution to the piezoelectric waveguide problem excluding electrode interactions, the spectral domain Green's function also serves as an excellent analytical tool in its own right. The quantity $k_1\overline{G}_{\varphi q}(s_1)$ is typically considered since it remains constant with frequency for a non-layered device, and shows all the important behaviour in the absence of mechanical interactions at the surface. For a layered SAW device this function will change with angular frequency ω and layer thickness h. Examining equation (3.37), and substituting $k_3 = \omega s_3$, it can be seen that the product ωh determines the frequency dependance. This dependance is discussed further in Section 3.3.3, and is compared with experimental results. Firstly the important features of the spectral domain Green's function will be discussed in Section 3.3.1. This will be followed in Section 3.3.2 by the calculation and experimental verification of phase velocity, electromechanical coupling and mass sensitivity as a function of layer thickness.

3.3.1 Parameter Extraction

To illustrate the techniques used, examples will be given for the ZnO/$LiTaO_3$ device configuration [127]. Figure 3.2 shows $k_1\overline{G}_{\varphi q}$ for a 1µm ZnO layer on a 36°-YX $LiTaO_3$ substrate, calculated at 100MHz. The most important features are the pole and zero at approximately 2.4×10^{-4}s/m. These correspond respectively to the free surface and metallised surface phase velocities of the PSAW mode. There is also a pole-zero pair at 3.2×10^{-4}s/m corresponding to the phase velocities of the Rayleigh mode.

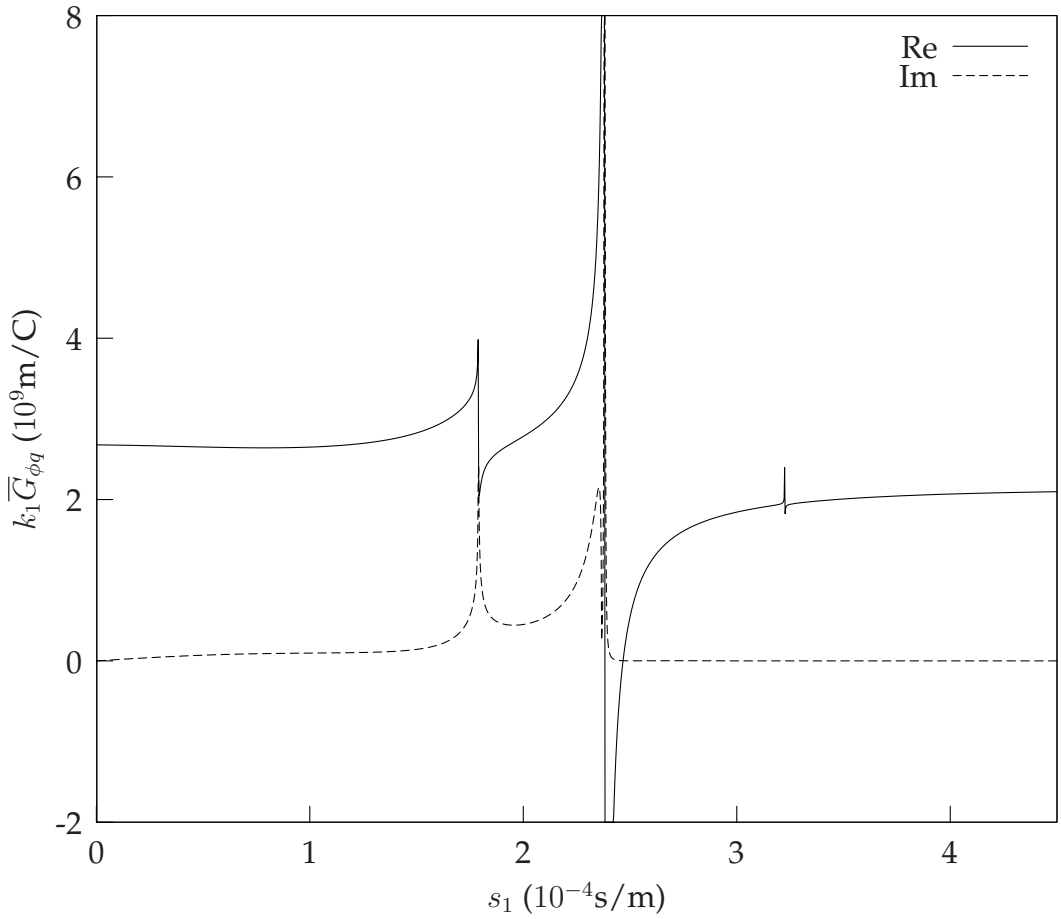

Figure 3.2: Green's function for 1µm ZnO on 36°-YX $LiTaO_3$ substrate at 100MHz

Recalling the definition of the spectral domain electrical Green's function in equation (2.4), it can be seen that for the surface charge $\overline{q}$ to be zero whilst voltage $\overline{\varphi}$ remains finite, a singularity must occur. In the region of the singularity, the electrical Green's function is well approximated by [67]:

$$k_1\overline{G}_{\varphi q}(s_1) = \frac{1}{\varepsilon_{eff}(\infty)}\frac{s_1^2 - s_m^2}{s_1^2 - s_f^2}. \tag{3.46}$$

With reference to equation (3.33), it can be seen that the matrix containing $\overline{\boldsymbol{\tau}}$ and $\overline{q}$ of the partial modes will become singular when the free-surface boundary conditions are satisfied. When considering wave propagation at the interface between two materials using the surface impedance approach, values of s_1 are sought which satisfy the continuity requirement of ψ at the interface between materials. Both these cases can be catered for by solving:

$$\det\left[\overline{Z}(s_f)\right] = 0. \tag{3.47}$$

In practice a numerical search is performed to find a minimum in the absolute value

of this determinant [63]. The function $|\det \overline{Z}'(s_1)|$ is shown in Figure 3.3 (a boundary determinant scan), corresponding to the spectral domain Green's function in Figure 3.2. The minima corresponding to the propagating modes are much easier to find with a search algorithm than poles of the $\overline{G}_{\varphi q}$, since their shape does not depend on the electromechanical coupling.

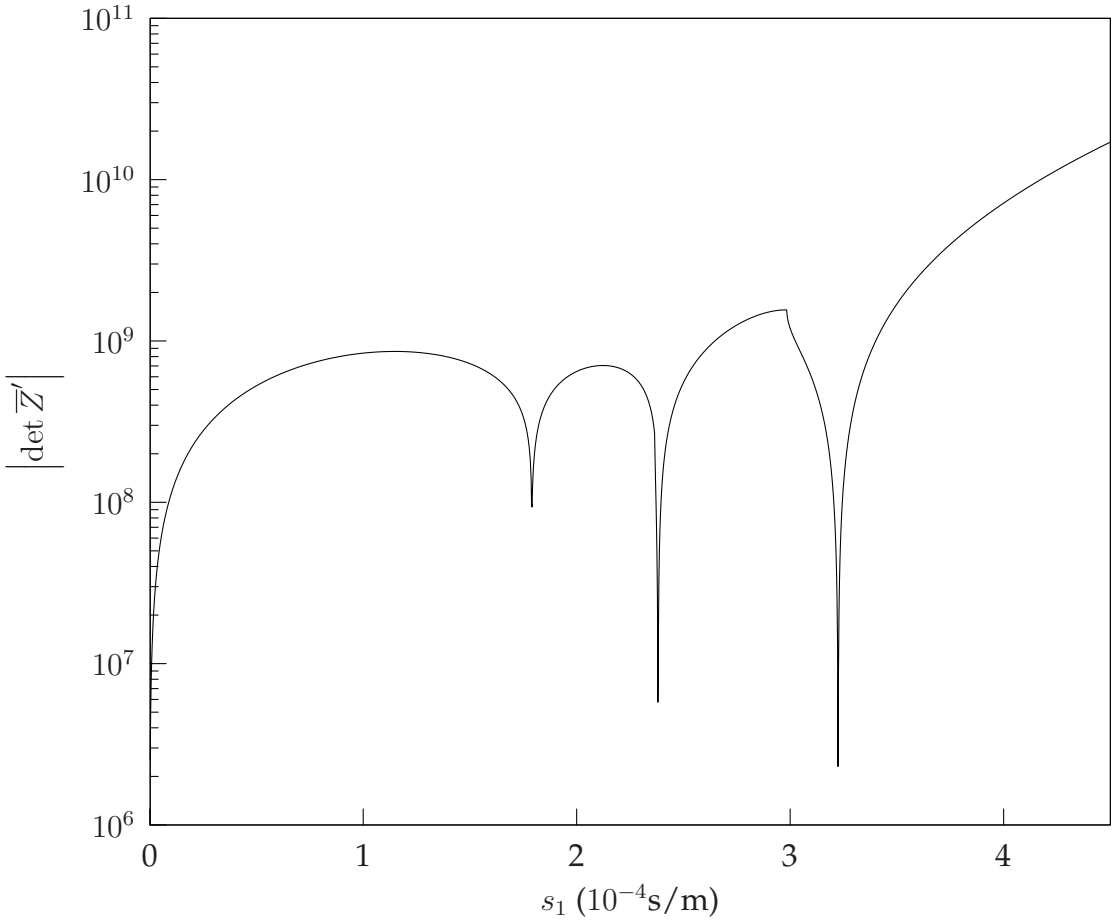

Figure 3.3: Determinant scan for 1µm ZnO on 36°-YX $LiTaO_3$ substrate at 100MHz

The free surface velocity of the acoustic mode is then found from $v_f = 1/\mathrm{Re}(s_f)$, where Re indicates that the real part is taken. The determinant scan may also reveal singularities which do not appear in the electrical part $G_{\varphi q}$. This indicates a mode which cannot be excited piezoelectrically (i.e. $K^2 = 0$). However, mode conversion due to mechanical discontinuities at an electrode may cause such a mode to be excited in a device.

To find the metallised surface velocities, the surface impedance Z' must be modi-

fied, to yield Z'_{met}:

$$\overline{Z}'_{met} = \begin{bmatrix} \overline{\mathbf{v}} \\ \overline{q} \end{bmatrix} \begin{bmatrix} \Delta\overline{\boldsymbol{\tau}} \\ j\omega\overline{\varphi} \end{bmatrix}^{-1} = \frac{1}{\overline{Z}'_{q\varphi}} \begin{bmatrix} \overline{Z}'_{\tau u}\overline{Z}'_{q\varphi} - \overline{Z}'_{qu}\overline{Z}'_{\tau\varphi} & \overline{Z}'_{qu} \\ -\overline{Z}'_{\tau\varphi} & 1 \end{bmatrix}. \tag{3.48}$$

The zeros of $\det \overline{Z}'_{met}(s_1)$ can be searched for to yield the metallised surface velocities. In these examples the free or metallised condition is at the interface between the substrate and the layer, where an IDT is most likely to be placed in a layered SAW sensor.

Once the free surface and metallised surface phase velocities have been found, the electromechanical coupling coefficient K^2 can be estimated from $K^2 = 2\left(v_f - v_m\right)/v_m$. Although more accurate methods can be used to calculate K^2, this definition is acceptable for the analysis performed here. A more precise picture of electromechanical coupling is given in Section 4.2.3 using the COM model, which expresses acousto-electric transduction using a different parameter, and which also includes the influence of electrode geometry.

An important difference between the Rayleigh SAW and PSAW modes is that for PSAW modes the values of s_f and s_m will be complex. Thus for the PSAW mode, once the minimum has been found along the real axis, the determinant must then be minimised along the negative imaginary axis (which corresponds to wave attenuation). Viscoelastic and liquid media will result in losses, as discussed in Section 3.2.2, so if these materials are included in the model a similar search must be performed. It is simple to show that the attenuation α expressed in dB/wavelength can be found from:

$$\alpha_{f,m} = 40\pi \log_{10}(e) \frac{\mathrm{Im}(s_{f,m})}{\mathrm{Re}(s_{f,m})}, \tag{3.49}$$

where Re and Im indicate the real and imaginary parts respectively. As well as the poles corresponding to SAW modes, another feature can be seen in Figures 3.2 and 3.3 at 1.8×10^{-4}s/m. This is a branch point singularity [72], corresponding to the limiting velocity of a bulk wave. This limiting velocity corresponds to the lowest frequency at which a bulk wave can be generated by surface sources. In this example the mode is a longitudinal bulk wave, having polarisation predominantly in the x_1 direction.

If the influence of the BAW, SAW and PSAW modes were to be subtracted from Figure 3.2, the remaining part would correspond to the electrostatic response of the structure. Recalling from (2.5) that $G_{\varphi q}$ is closely related to the effective permittivity,

the quantity:

$$\varepsilon_{eff}(\infty) = \lim_{k_1 \to \infty} \frac{1}{|k_1| G_{\varphi q}(k_1/\omega)} \tag{3.50}$$

can be used for calculating capacitance of an electrode structure. In a layered structure the dielectric contribution varies with k_1, so this parameter is not as meaningful.

When performing the determinant scan for non-layered media, the quantity plotted is $|\det(Z'(s_1))|$. For a layered structure, the quantity $s_1 = k_1/\omega$ is no longer a constant. Z' now depends on both k_1 and ω independently, so the complete SAW solution cannot be shown by a 2-dimensional figure. When analysing a dispersive structure, it is normally desirable to know the centre frequency at which the IDT will generate acoustic waves. For an IDT of period λ_0 per electrode pair, the centre frequency will occur when:

$$k_1 = \frac{2\pi}{\lambda_0}. \tag{3.51}$$

By enforcing equation (3.51), the function $|Z'(s_1)|$ can now by unambiguously defined. A zero of the determinant now corresponds to the phase velocity at centre frequency, allowing both quantities to be calculated.

3.3.2 Sensitivity Analysis

The techniques presented in Section 3.3.1 allow phase velocity and electromechanical coupling coefficient to be extracted from the spectral domain Green's function analysis. In this section, it will be shown how these techniques can be extended to calculate mass sensitivity.

As discussed in Section 2.7, analytical techniques are normally used to characterise the mass sensitivity of a SAW sensor. Equation (2.15) is considered the definition of mass sensitivity, however it makes no reference to the parameters of the mass being measured. The expression for sensitivity based on perturbation theory (equation (2.18)) indicates the conditions under which the mass will dominate the response. To reiterate, these conditions are that the mass layer is much thinner than the acoustic wavelength, and that it's acoustic velocity is much lower than that of the substrate.

To measure mass sensitivity, the velocity is calculated for the structure, then it is calculated for the structure with an additional isotropic layer on the device surface, to represent the perturbing mass. Mass sensitivity can then be calculated by numerically

evaluating equation (2.17). This is preferable to the perturbation approach because it can be applied to leaky SAW eigenmodes which become unbounded as $x_3 \rightarrow -\infty$, and can also be combined with the electrode models which will be presented in Chapter 4. However, the disadvantage of this technique is the difficulty in correctly choosing the material constants and thickness.

Table 3.2: Parameters of mass loading layer

c_{11}	10^6 N/m^2
c_{44}	3×10^6 N/m^2
ρ	10^6 kg/m^3
ε	ε_0
h_{mass}	10^{-12}m

The constants chosen for this work are listed in Table 3.2, where h_{mass} is the thickness of the mass loading layer. In order to validate this choice of material constants, sensitivity calculations were performed and compared with the results of a simpler analytical method [112] for the case of a gold layer on a silica substrate. The results are shown in Figure 3.4 as a function of normalised gold layer thickness. This is not an interesting configuration in itself, since it is non-piezoelectric, but the isotropic nature of the materials allows the simple analytical theory to be used. The solid curve in this figure shows the results when using the chosen material parameters, and is visually indistinguishable from the analytical result at the this scale of the graph. For comparison purposes results are shown with a higher thickness layer, which shows an additional contribution due to finite thickness effects. In addition, results are shown for a lower density, which has resulted in a very small relative frequency shift, and hence is corrupted by numerical error.

It is assumed here that the mass of the perturbing layer is the complete cause of the device response. This assumption is made, not because experiments necessarily satisfy the conditions, but rather because it serves as a useful benchmark. It allows for a comparison of SAW devices based on different materials or geometries without having to understand the mechanical properties of the analyte.

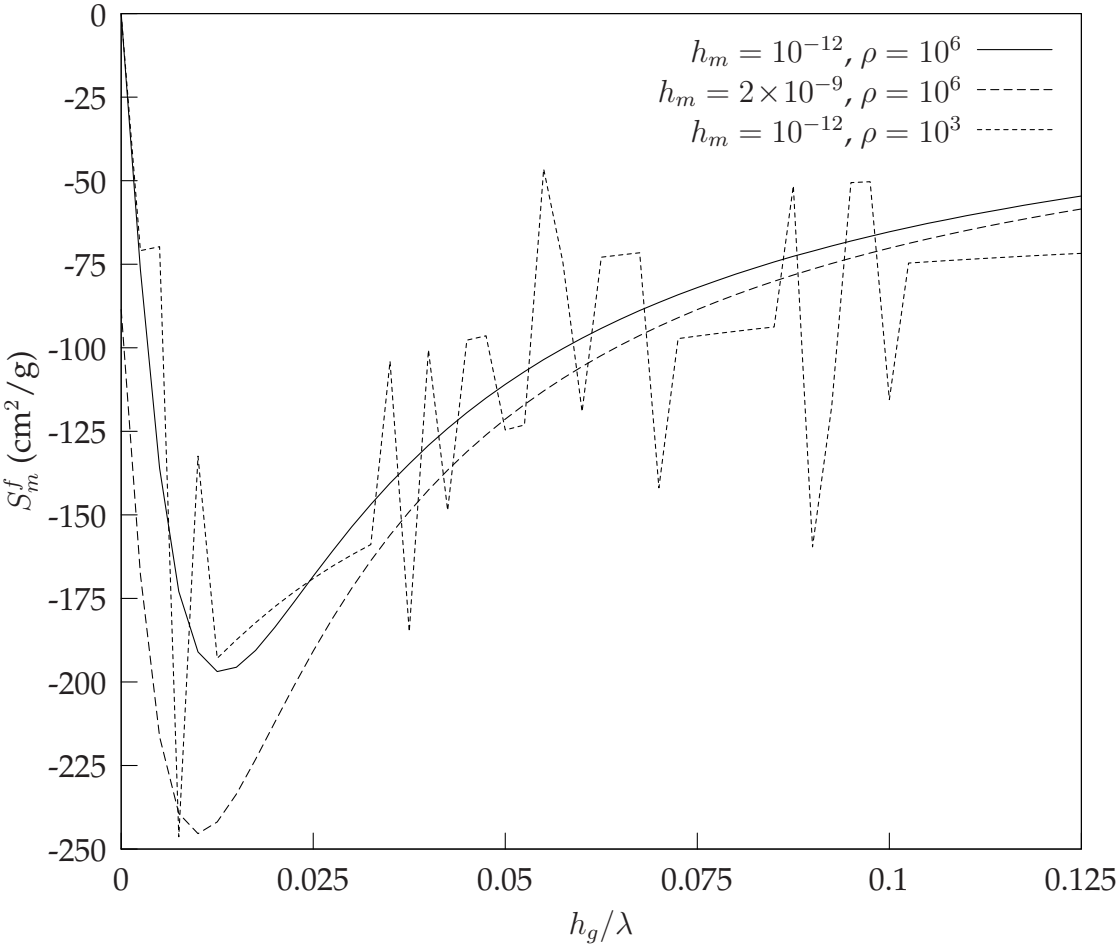

Figure 3.4: Influence of mass layer properties on mass sensitivity simulation for Au layer on SiO_2 substrate (height in metres, density in kg/m^3)

Sensitivity examples will be given in the next section, since for layered SAW devices it is most useful to study these parameters as a function of layer thickness.

3.3.3 Parameter Variation with Layer Thickness

The techniques discussed in Sections 3.3.1 and 3.3.2 allow the spectral domain Green's function to be used for the analysis of a SAW sensor. For layered SAW sensors, it is important to know how these properties vary with layer thickness. In this section extracted results will be presented for devices fabricated with a ZnO layer on a $LiTaO_3$ substrate.

In a layered device the Green's function is frequency (and hence wavelength) dependant, and it will be most useful to consider parameters as a function of normalised layer thickness h/λ_0, where λ_0 is this period of the IDT electrode pairs. The reference

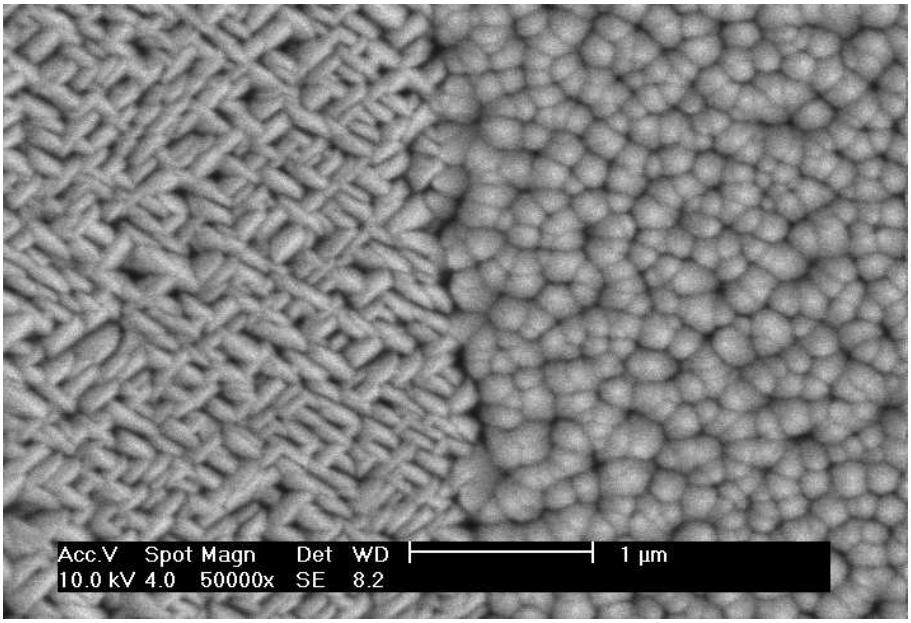

Figure 3.5: SEM image of ZnO growth on bare $LiTaO_3$ (left) and metallised region (right)

plane used is the substrate-layer interface, which corresponds to the location of the IDT.

3.3.3.1 Delay-Line Device Configuration

Devices were fabricated on 36°-YX $LiTaO_3$ wafers, using an Al metallisation layer and Cr adhesion layer deposited by electron beam evaporation. IDTs with a period λ_0 of 40µm were fabricated using a wet-etch process to create delay line devices. ZnO films were deposited by RF magnetron sputtering. Devices were fabricated with film thickness h ranging from 0 to 8µm, with corresponding operating frequencies between 101.5MHz and 78.5MHz. The full details of the device fabrication techniques can be found in Chapter 5.

Figure 3.5 shows an SEM micrograph of the thin film ZnO grown on 36°-YX $LiTaO_3$. As was previously reported [128, 129], the grain growth and corresponding crystal orientation of ZnO is (001) on the metallised region and (110) on the bare substrate. This implies that acoustic wave properties will also differ. Thus separate Green's functions are required for the (001) and (110) ZnO orientations. The examples given in Section 3.3.1 were for the (110) ZnO orientation.

3.3.3.2 Phase Velocity

Figure 3.6 shows the theoretically derived phase velocity for a ZnO layer on a $LiTaO_3$ substrate. Velocity was experimentally determined by measuring the frequency of the peak of the radiation conductance, which is the real part of the input admittance of the device. It was found that the measured propagation velocity was almost identical to the velocity calculated for metallised regions. The slight discrepancy may be attributed to the mechanical loading by the electrodes of the IDT, which is not accounted for in these calculations.

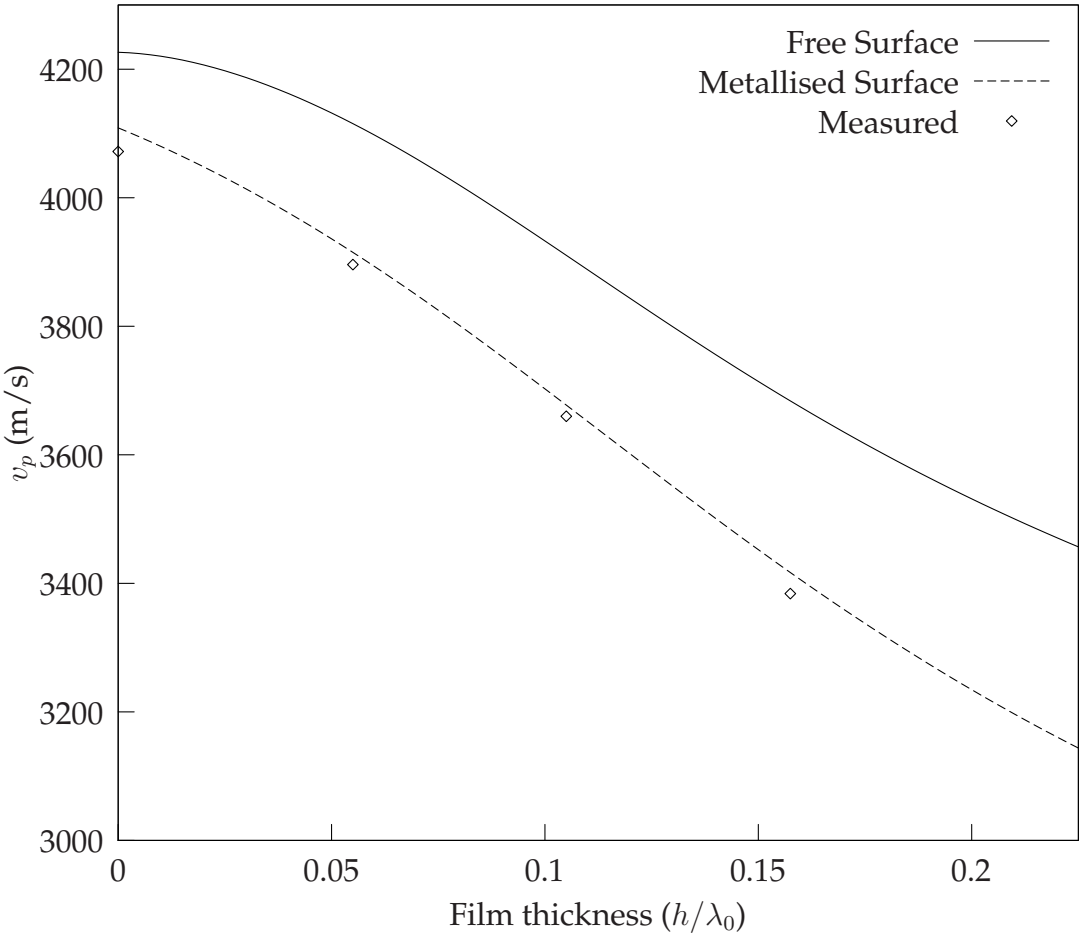

Figure 3.6: Measured and calculated phase velocity

3.3.3.3 Electromechanical Coupling

The electromechanical coupling coefficient was measured via the radiation conductance. According to the crossed-field model, the radiation conductance G_a, at centre

frequency f_0, can be expressed as [130]:

$$G_a(f_0) = 8k^2 f_0 C N, \tag{3.52}$$

where N is the number of electrode pairs in the IDT, and C is the input capacitance, which was measured using a 1MHz capacitance meter. Figure 3.7 shows the measured coupling coefficient, which achieves a maximum of ~7.5% for $h/\lambda_0 = 0.05$. As with propagation velocity, the modelled values for (001) ZnO on the metallised surface show best agreement with the experimental results. This suggests that the properties of delay-line structures on a $LiTaO_3$ substrate can be easily predicted by analysing the parameters in the metallised surface case.

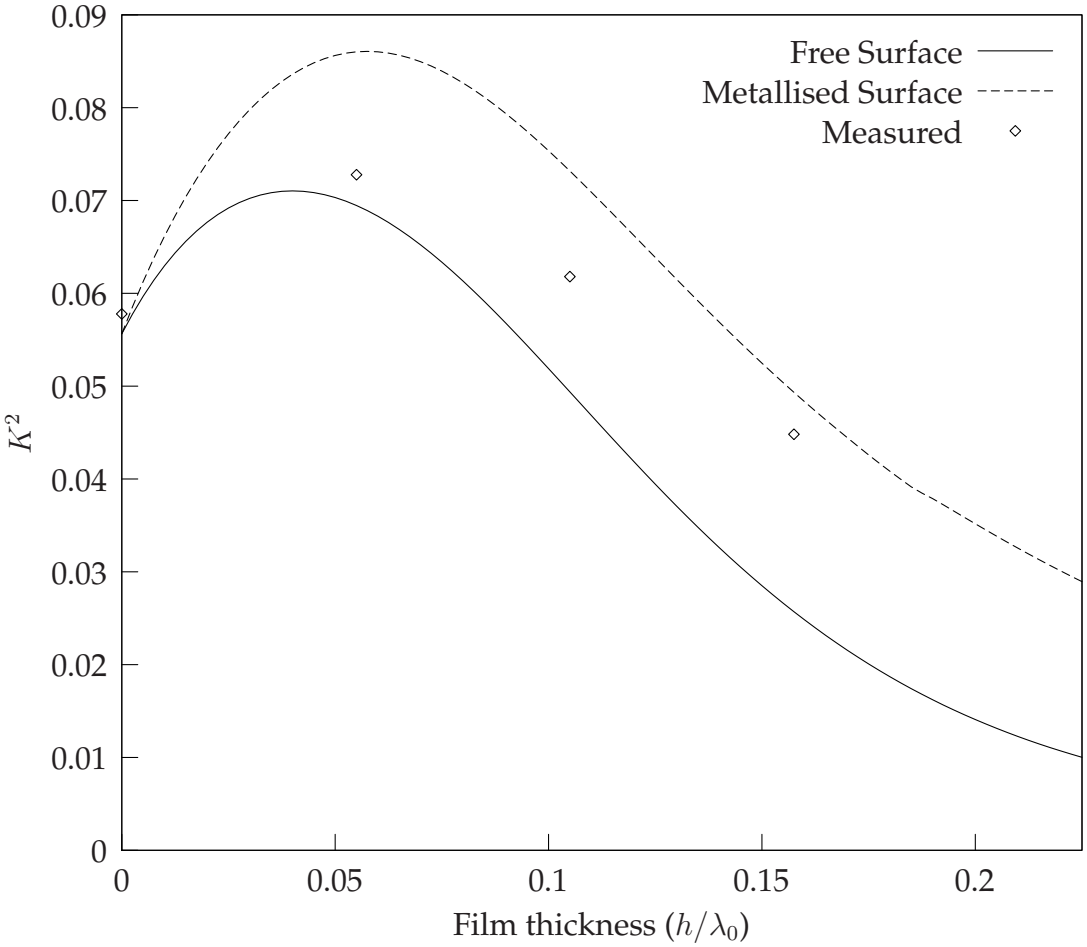

Figure 3.7: Measured and calculated electromechanical coupling coefficient

3.3.3.4 Mass Sensitivity

Figure 3.8 shows both the theoretically derived and experimentally measured mass sensitivity of the devices. Calculation was based on the metallised surface velocity

shift determined by the Green's function analysis. The additional mass was modelled using the procedure outlined in Section 3.3.2.

To verify these results experimentally, a 150nm SiO_2 layer was sputter-deposited onto the surface of the devices, to act as a perturbing mass layer. The frequency shift in the maximum radiation conductance was measured and from this the mass sensitivity shown in Figure 3.8 was derived. It is useful to compare this $LiTaO_3$ substrate/ZnO layer device with the previously reported $LiTaO_3$ substrate/ZnO layer device [131]. It can be seen that the ZnO device has higher mass sensitivity for h/λ_0 up to 0.2, and that this range of layer thickness is of most interest due to difficulties in depositing thicker films.

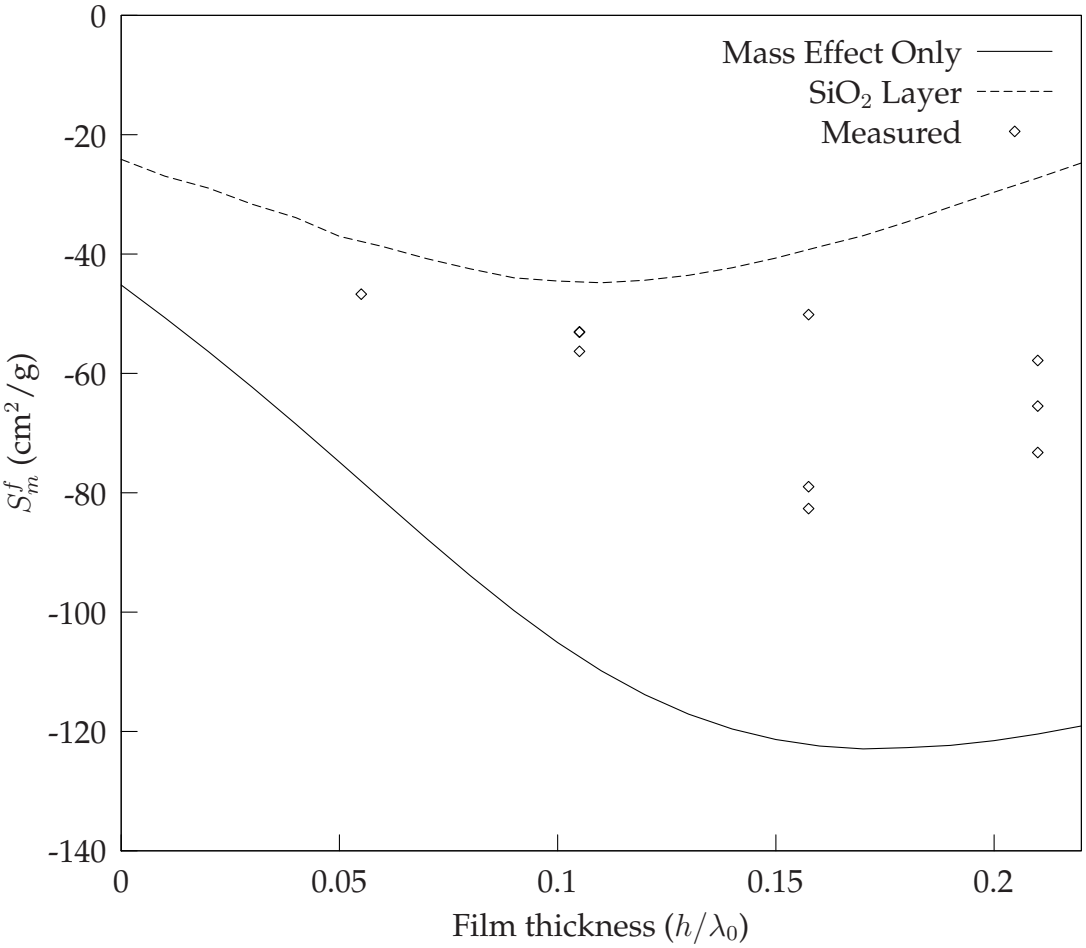

Figure 3.8: Measured and calculated mass sensitivity

It can be seen that the measured sensitivity of the $LiTaO_3$/ZnO devices is much less than that predicted. This is due to the relatively high shear velocity of the SiO_2 layer (2800m/s), which violates the assumptions made when selecting the modelled mass

layer, resulting in an additional elasticity effect.

The dotted curve in Figure 3.8, allows a comparison of the measurements with a simulation including the elastic constants of thin film SiO_2 (see Appendix A). It can be seen that sensitivity is somewhat higher than predicted, but that agreement is much better than when the idealised mass layer was modelled. Further improvement could be achieved by assuming a reduced shear stiffness of the deposited SiO_2 perturbing layer, however this would need to be independently verified. Some discrepancy may also be attributed to the effect of the measurement probes, as well as the approximation of modelling poly-crystalline ZnO as a homogeneous layer with a flat surface.

The effect of the elasticity of the sputtered SiO_2 layers is similar to that due to viscosity occurring in practical bio-sensing measurements [132]. This suggests that mass sensitivity does not necessarily correspond to the response observed in an experimental situation. Ogilvy [18] also describes difficulties in reconciling the theoretically derived mass sensitivity of SiO_2/quartz devices with that obtained by experimental deposition of a thin perturbing film.

3.4 Conclusion

In this chapter the spectral domain Green's function was described, based on the piezoelectric equations in the quasi-static approximation. It was shown that this technique is applicable to layered devices and to elastic, piezoelectric, viscoelastic and liquid media. It was also demonstrated that the spectral domain Green's function is able to yield a great deal of useful information regarding the propagation properties of surface acoustic waves, and the sensitivity of SAW sensors. An example was presented comparing calculated results with measurements of a ZnO/$LiTaO_3$ layered SAW configuration.

However, the analysis presented here is not able to take into account the electrode interactions which are fundamental to the operation of SAW resonator devices. As discussed in Chapter 2 there is a need for an improved periodic model, and this will be presented in Chapter 4. The mathematical form of the analysis undertaken in this chapter has been carefully chosen to be readily extensible to the the author's novel developments made on the periodic model.

[This page has intentionally been left blank.]

Chapter 4

Periodic Green's Function Model

4.1 Introduction

In this chapter techniques based on the formulation of a periodic Green's function will be developed and described in detail. The basis for the author's novel approach will be presented. This approach combines existing work with the author's novel developments and applies them to a new problem - *characterising the performance of layered SAW resonators operating in liquid media*.

In Section 4.2 a description of the calculation of the periodic Green's function will be given. This will begin with the approximate model for infinitesimally thin electrodes in Section 4.2.1, which allows for very efficient computation. The author's novel model which accounts for the mechanical interactions between the acoustic wave and electrodes buried within layered media will be derived in Section 4.2.2. In Section 4.2.3 it will be shown how the results of these periodic models can be used to calculate parameters for the Coupling-of-Modes (COM) model.

Having rigourously derived parameters for the COM model, this will be used for the analysis of SAW resonator sensors in Section 4.3. The first part of this analysis, presented in Section 4.3.1, considers the change in the COM parameters due to choice of layer thickness, including the effects of liquid loading. This represents a new application of the COM model. Calculations of the mass sensitivity of an electrode grating are also presented, and compared with the results obtained for a delay lines structure, as was presented in Section 3.3.3. In Section 4.3.2 the COM parameters will be used to

calculate the complete 2-port response of a SAW resonator based sensor.

The techniques presented here will be used for the design of SAW resonator sensors, which will be presented in Chapter 5. This will be followed in Chapter 6 by an analysis of the variation of sensitivity across the surface of the device, which will also be based on the work of this chapter.

4.2 Development of Periodic Model

As discussed in Section 2.4.4, periodic models are the most efficient for dealing with structures having a large number of electrodes. There are a number of techniques which may be used to model such structures. The method used here is based on the formulation of a periodic Green's function. This is chosen because it is rigourous, flexible and can be readily extended to the problem of mechanical interactions with electrodes buried within layered media.

Figure 4.1 shows the basic periodic structure to be modelled. It consists of an electrode sandwiched between a guiding layer and a substrate. Parameters p, l and h_e indicate the electrode period, width and thickness respectively, whilst h is the guiding layer thickness. The theory developed in Section 3.2.5 allows for an arbitrary number of layers to be considered, and this also applies to the work of this chapter. However, the focus of this chapter will be on resonator devices with a single guiding layer, which is the most commonly employed configuration.

It should be noted that in this analysis, the periodic cell is considered to be that of a single electrode. Thus the geometry is periodic in $p = \lambda_0/2$, whereas in the analysis in Chapter 3 the quantity λ_0 was used. The fact that electrodes are connected with opposite polarity can be accounted for in the parameter β, which will be introduced shortly. For convenience, when considering the height of the guiding layer, parameter h refers to the height of the layer above the electrode region, rather than the complete layer height. For the electrode thickness range considered in this work, this difference is negligible.

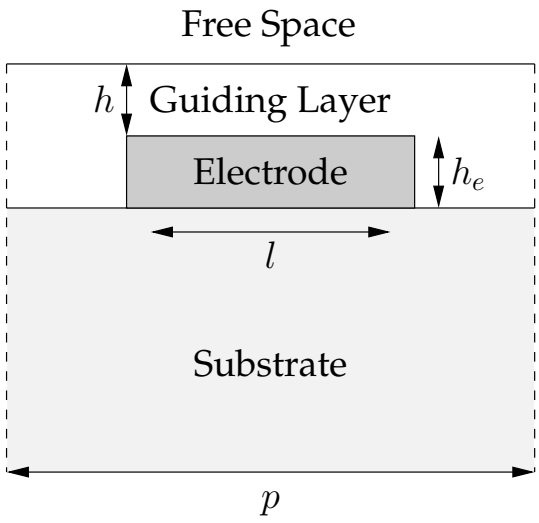

Figure 4.1: Basic periodic structure to be modelled

4.2.1 Boundary Element Model with Electrical Approximation

In this section the existing electrical Green's function model is considered, which has the limitation that the electrode height h_e must be approximated as being zero. An additional consideration is that, depending on the deposition technique used, the top of the guiding layer may not be perfectly flat, but may instead be conformal with the underlying electrode shape. This effect is not included in this thesis. The charge is assumed to be concentrated at the bottom surface of the electrode, as it greatly simplifies the computation with a minimal loss of accuracy. Thus the solution can be based on a Green's function calculated with the reference plane ($x_3 = 0$) set to the bottom of the electrodes.

In a system with period p in the x_1 direction, Floquet's theorem dictates that the field quantities obey the following relationship [52]:

$$\psi\left(x_1, x_3\right) = \psi\left(x_1 + np, x_3\right) \exp\left(j\beta np\right), \tag{4.1}$$

where n is an integer, and a β is a phase shift between periods which may be unknown. A solution to this equation must be of the form:

$$\psi\left(x_1, x_3\right) = \psi_0\left(x_1, x_3\right) \exp\left(j\beta x_1\right), \tag{4.2}$$

where ψ_0 is periodic with period p, and the phase shift between periods due to the term $\exp(j\beta x_1)$ corresponds to the propagation of a wave in the structure with wavenumber β.

Figure 4.2 illustrates the so called "Floquet-periodic" distribution of field variables for the case of charge distribution. There are an infinite number of charge distributions q_0 (nonzero only in the range $-p/2 < x_1 < p/2$), periodically arrayed at the surface with phase shift β between periods. The periodic Green's function represents the response of a periodic system to excitation of this form.

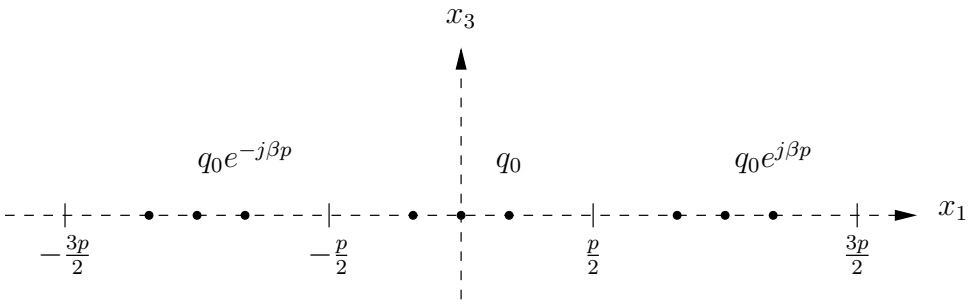

Figure 4.2: Floquet-periodic charge distribution

The most straightforward way of deriving the periodic Green's function is to perform the calculations in the spectral domain [73]. Since the charge distribution obeys equation 4.1, it can be represented in the following form:

$$q(x_1, \beta, \omega) = \exp(j\beta x_1) \sum_{n=-\infty}^{\infty} q_0(x_1 - np, \beta, \omega), \tag{4.3}$$

where in contrast with equation (4.2) the periodic component is explicitly represented as a sum over all periods. The periodic component of this function can be represented by a Fourier series:

$$q(x_1, \beta, \omega) = \exp(j\beta x_1) \sum_{l=-\infty}^{\infty} \overline{q}_l(\beta, \omega) \exp(jlQx_1) \tag{4.4a}$$

$$= \sum_{l=0}^{\infty} \overline{q}_l(\beta, \omega) \exp(j\beta_l Q x_1), \tag{4.4b}$$

where the following symbols have been introduced:

$$Q = \frac{2\pi}{p} \tag{4.5}$$

$$\beta_l = \beta + lQ. \tag{4.6}$$

The constant Q can be considered to be the characteristic wavenumber of the structure, and depends only on the period. It will be shown that the relationship between the

wavenumber of the propagating wave and this parameter Q is critical in determining the behaviour of the wave. Each value of β_l represents one of the spatial harmonics of the propagating wave, and the relative amplitude of these harmonics $\overline{q}_l$ is used to describe the field distribution within the periodic array.

The inverse Fourier series relationship for the charge distribution is:

$$\overline{q}_l(\beta,\omega) = \frac{1}{p}\int_{-p/2}^{p/2} q_0(x_1,\beta,\omega)\exp(-j\beta_l x_1)\mathrm{d}x_1. \tag{4.7}$$

A Fourier representation also exists for the voltage:

$$\varphi(x_1,\beta,\omega) = \sum_{l=-\infty}^{\infty} \overline{\varphi}_l(\beta,\omega)\exp(j\beta_l Q x_1). \tag{4.8}$$

Combining equation (4.8) with the Green's function of equation (3.35) and neglecting mechanical interactions, the voltage can be expressed in the spatial domain as a function of the Fourier coefficients of the charge distribution:

$$\varphi(x_1,\beta,\omega) = \sum_{l=-\infty}^{\infty} \overline{G}_{\varphi q}(\beta_l,\omega)\exp(j\beta_l Q x_1)\overline{q}_l(\beta,\omega). \tag{4.9}$$

With reference to equations (4.9) and (4.7), the case where the charge distribution within the each period is an impulse function can be considered:

$$q_0(\beta,\omega) = \delta(x_1 - x'). \tag{4.10}$$

$$\varphi(x_1,\beta,\omega)) = \frac{1}{p}\sum_{l=-\infty}^{\infty} \overline{G}_{\varphi q}(\beta_l,\omega)\exp\left(j\beta_l Q\left(x_1 - x'\right)\right). \tag{4.11}$$

The right hand side of equation (4.11) is known as the periodic Green's function, and is the response of the system to a periodic array of phase shifted impulse functions. It can be used in a convolution operation in a similar way to the spatial domain Green's function defined in equation (2.2). In practice it is much more convenient to use equation (4.9) directly in the spectral domain.

Having developed a relationship between charge and voltage at the plane $x_3 = 0$ for a periodic problem, the boundary conditions must be applied and the problem discretised. This will allow an equation of the form of (2.3) to be obtained, describing the relationship between voltage and current on a single period of the structure, which can then be solved using standard matrix inversion algorithms.

The boundary conditions which must be applied to this problem are that the voltage V is specified on the electrodes and charge q is zero outside the electrodes. To apply these boundary conditions, basis and weighting functions are used which can easily satisfy these conditions. Pulse function are chosen since they are the simplest orthogonal functions, they are flexible and do not enforce any particular shape on the solution. It should be emphasised that the author's novel developments made in this chapter are not contingent on the choice of basis functions. The pulse functions are of unit area and of width w_m, each located at position x_m. They are non-overlapping with no gaps between them to ensure orthogonality and completeness. The normalised pulse function is defined as:

$$\Pi_m = \begin{cases} \dfrac{1}{2w_m}, & |x_1 - x_m| < w_m. \\ 0, & \text{otherwise.} \end{cases} \tag{4.12}$$

The pulses representation of charge is is illustrated in Figure 4.3, and can be written as:

$$q_0(x_1, \beta, \omega) = \sum_{m=1}^{M} q_m(\beta, \omega)\Pi_m, \tag{4.13}$$

where M is the number of pulse basis functions. Multiplying this equation by $\exp(-j\beta x_1)$ and taking a Fourier integral results in:

$$\frac{1}{p}\int_{-p/2}^{p/2} q_0(x_1, \beta, \omega)e^{-j\beta_l x_1}\mathrm{d}x_1 = \frac{1}{p}\int_{-p/2}^{p/2}\sum_{m=1}^{M} q_m(\beta, \omega)\Pi_m e^{-j\beta_l x_1}\mathrm{d}x_1. \tag{4.14}$$

$$\overline{q}_l(\beta, \omega) = \sum_{m=1}^{M} q_m(\beta, \omega)\frac{1}{p}\int_{-p/2}^{p/2}\Pi_m e^{-j\beta_l x_1}\mathrm{d}x_1. \tag{4.15}$$

$$\overline{q}_l(\beta, \omega) = \frac{1}{p}\sum_{m=1}^{M} q_m(\beta, \omega)e^{-j\beta_l x_m}\frac{\sin(\beta_l w_m)}{\beta_l w_m}. \tag{4.16}$$

Substituting equation (4.16) into equation (4.9) and limiting the summation over l to the range $[-L, L]$ results in:

$$\varphi(x_1, \beta, \omega) = \frac{1}{p}\sum_{l=-L}^{L}\overline{G}_{\varphi q}(\beta_l, \omega)\sum_{m=1}^{M} q_m(\beta, \omega)\frac{\sin(\beta_l w_m)}{\beta_l w_m}e^{j\beta_l(x_1 - x_m)}. \tag{4.17}$$

For finite values of L and M it is not possible to exactly satisfy the boundary conditions for φ, so some finite error is inevitable. Using the method of weighted residuals

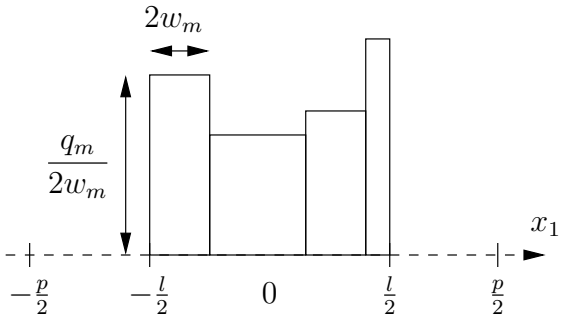

Figure 4.3: Pulse representation of charge distribution at $x_3 = 0$

[133] it is possible to minimise the error averaged over some weighting function. Using pulse weighting functions, the result is as follows:

$$\int_{-p/2}^{p/2} \Pi_n \varphi(x_1, \beta, \omega) \mathrm{d}x_1 = \int_{-p/2}^{p/2} \Pi_n \frac{1}{p} \sum_{l=-L}^{L} \overline{G}_{\varphi q}(\beta_l, \omega) \sum_{m=1}^{M} q_m(\beta, \omega) \frac{\sin(\beta_l w_m)}{\beta_l w_m} e^{j\beta_l(x_1 - x_m)} \mathrm{d}x_1. \tag{4.18}$$

$$\varphi_n(\beta, \omega) = \frac{1}{p} \sum_{l=-L}^{L} \overline{G}_{\varphi q}(\beta_l, \omega) \sum_{m=1}^{M} \frac{\sin(\beta_l w_m)}{\beta_l w_m} \frac{\sin(\beta_l w_n)}{\beta_l w_n} e^{j\beta_l(x_n - x_m)} q_m(\beta, \omega). \tag{4.19}$$

The coefficient φ_n is just the average value of the voltage across pulse n. It can be seen that if pulses of equal width are taken ($w_m = w_n = w$), (4.19) will become greatly simplified. Jakoby showed that in this case the computational burden of evaluating equation (4.19) can be reduced by using a Fast Fourier Transform (FFT)-based method [93]. This has the minor disadvantage of reducing the flexibility of computation by fixing the number of harmonics used in the integration for a given number of pulse function. By retaining pulses of differing width, it is possible to use wider pulses towards the middle of the electrode, where there is less variation, and smaller pulses at the edges where singular behaviour is observed, thus reducing the number of pulses required for a given level of accuracy [85].

It is also worth noting that the procedure resulting in equation (4.19) can be applied to any of the 16 elements of the dyadic Green's function. This forms the basis of the FEM/BEM methods discussed in Section 2.4.3. More complicated periodic electrode configurations can also be included with no change to the form of equation (4.19), however only a single electrode per period is considered here.

Using equation (4.19) the charge distribution can be solved for any choice of β and ω, by setting $\varphi_n = V$, where V is the applied voltage. The current flowing into each electrode can be calculated by integrating the charge over the electrode width, and differentiating with respect to time:

$$I(\beta,\omega) = j\omega \int_{-l/2}^{l/2} q(x_1,\beta,\omega)\mathrm{d}x_1. \tag{4.20}$$

$$= j\omega \sum_{m=1}^{M} q_m(\beta,\omega). \tag{4.21}$$

Since no account is taken of the electrode width in the x_2-direction, I must be interpreted as current per unit aperture width. The aperture width of the device will be introduced into the analysis in Section 4.2.3. As discussed in Section 2.4.4, the applied voltage and the resultant current yield the harmonic admittance, which is the most convenient way to express the solution to the periodic problem:

$$Y(\beta,\omega) = I(\beta,\omega)/V(\beta,\omega). \tag{4.22}$$

The harmonic admittance function will be discussed in detail in Section 4.2.3, where it will be used for the extraction of COM parameters.

4.2.2 Extension of Model to Mechanical Interactions with Electrodes

In order to improve accuracy in the case where the height or mass of the electrodes makes a significant contribution to the device performance, a model which includes these effects must be developed. Since the problem with electrodes sandwiched between the substrate and guiding layer is quite different from the well known problem of electrodes upon the device surface, a new technique developed by the author is described here. This is based on the matrix eigen-operator previously utilised in Section 3.2.4, which is known to be valid for inhomogeneous media [124].

4.2.2.1 Matrix Eigen-Operator for Periodic Media

For the approach presented here to be valid, it is necessary to assume that the electrode shape is perfectly rectangular. This is because in the electrode region, this eliminates the x_3 dependence of the material constants. The assumption that charge is restricted to

the reference plane $x_3 = 0$ will be retained for simplicity. Abandoning this assumption would significantly complicate the model but would grant negligible improvement in accuracy.

Referring to Figure 4.4, the aim is to create a model for region (ii), which contains the electrodes, since regions (i) and (iii) can already be accounted for in the existing model. This model will yield a matrix relating the values of stress and displacement at $x_3 = 0$ (substrate surface) to those at $x_3 = h_e$. This matrix will then be incorporated into a periodic model similar to that developed in Section 4.2.1.

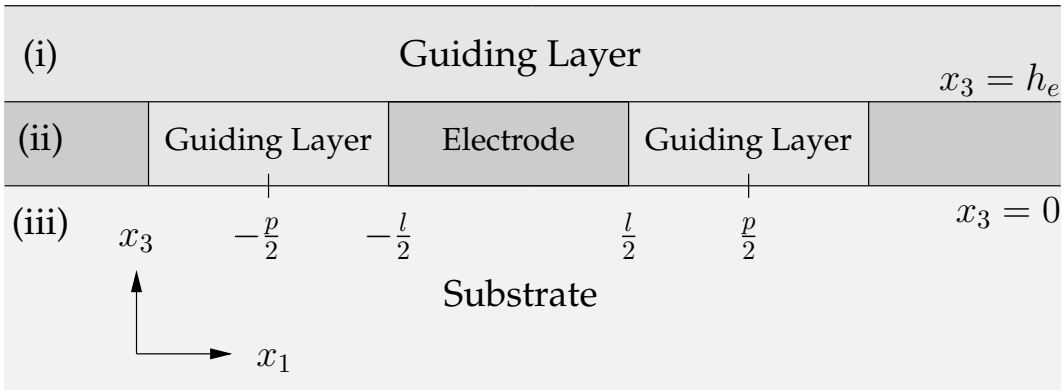

Figure 4.4: Division of periodic structure for electrode model

The acoustic and electrical fields in the electrode region obey the eigenvalue operator equation (3.28), so this will form the basis for this approach. The most significant change is that the matrices M_{ij} and $\underline{\underline{\rho}}$ now exhibit a periodic dependance on x_1. Defining the following material matrices simplifies the subsequent analysis:

$$\mathcal{M}^{11} = \mathrm{M}_{33}^{-1}\mathrm{M}_{31}. \tag{4.23a}$$

$$\mathcal{M}^{12} = \mathrm{M}_{33}^{-1}. \tag{4.23b}$$

$$\mathcal{M}^{21} = \mathrm{M}_{11} - \mathrm{M}_{13}\mathrm{M}_{33}^{-1}\mathrm{M}_{31}. \tag{4.23c}$$

$$\mathcal{M}^{22} = \mathrm{M}_{13}\mathrm{M}_{33}^{-1}. \tag{4.23d}$$

Each of these matrices depends only on the material constants. In order to represent material constants which are inhomogeneous along the x_1 direction, a Fourier expan-

sion is used:

$$\mathcal{M}^{kl}(x_1) = \sum_{n=-\infty}^{\infty} \mathcal{M}_n^{kl} e^{jnQx_1}. \tag{4.24}$$

$$\underline{\underline{\rho}}(x_1) = \sum_{n=-\infty}^{\infty} \underline{\underline{\rho}}_n e^{jnQx_1}. \tag{4.25}$$

Referring to Figure 4.4, the region $-l/2 < x_1 < l/2$ of each period in region (ii) is considered to consist of the electrode material, the remainder to consist of the guiding layer material. This can be illustrated by considering the generalised density matrix $\underline{\underline{\rho}}$, which has a constant values $\underline{\underline{\rho}}^{(e)}$ and $\underline{\underline{\rho}}^{(g)}$ in the electrode and guiding layer regions. Each Fourier coefficient $\underline{\underline{\rho}}_n$ can be calculated from:

$$\begin{aligned}
\underline{\underline{\rho}}_n &= \frac{1}{p} \int_{-p/2}^{p/2} \underline{\underline{\rho}}(x_1) e^{-jn2\pi/px_1}. \\
&= \frac{1}{p} \int_{-p/2}^{-l/2} \underline{\underline{\rho}}^{(g)} e^{-jn2\pi/px_1} + \frac{1}{p} \int_{-l/2}^{l/2} \underline{\underline{\rho}}^{(e)} e^{-jn2\pi/px_1} + \frac{1}{p} \int_{l/2}^{p/2} \underline{\underline{\rho}}^{(g)} e^{-jn2\pi/px_1}.
\end{aligned} \tag{4.26}$$

The result of these integrals is:

$$\underline{\underline{\rho}}_n = \begin{cases} \frac{l}{p}\underline{\underline{\rho}}^{(e)} + \left(1 - \frac{l}{p}\right) \underline{\underline{\rho}}^{(g)}, & n = 0. \\ \left(\underline{\underline{\rho}}^{(e)} - \underline{\underline{\rho}}^{(g)}\right) \dfrac{\sin\left(\pi n \frac{l}{p}\right)}{\pi n}, & n \neq 0. \end{cases} \tag{4.27}$$

For the field variables $\psi(x_1, x_3)$, the Floquet solution given in equation (4.2) applies. In this case the value of the field variables must be considered throughout the range $0 < x_3 < h_e$, rather than only at $x_3 = 0$ as was assumed for the thin electrode model. Again a phase-shifted Fourier series representation is used:

$$\psi(x_1, x_3, \beta, \omega) = \sum_{n=-\infty}^{\infty} \psi_n(x_3, \beta, \omega) \exp(jnQx_1) \exp(j\beta x_1). \tag{4.28}$$

The x_3 dependency can be accounted for by making the substitution:

$$\psi_n(x_3, \beta, \omega) = \psi_n(0, \beta, \omega) \exp(-jk_3^n(\beta, \omega)x_3). \tag{4.29}$$

At this stage it will be convenient to consider only the non-piezoelectric case, which decouples the electrical and mechanical solutions. The most significant difference be-

tween the full electrode model considered here and the infinitesimal electrode approximation discussed in Section 4.2.1 is the influence of mechanical properties. Considering also that the dielectric tensor of a metal layer is not well-defined, it is a justifiable simplification to consider the dielectric problem separately and to ignore the electrical inhomogeneity. The electrical part of the problem will be discussed later in this section. Substituting equations (4.24), (4.28) and (4.29) into the eigen-operator equation (3.28), and truncating the Fourier series representations to the range from $[-N, N]$, an algebraic form L results:

$$\sum_{n=-N}^{N} \begin{bmatrix} \mathrm{L}^{11}_{mn} & \mathrm{L}^{12}_{mn} \\ \mathrm{L}^{21}_{mn} & \mathrm{L}^{22}_{mn} \end{bmatrix} \begin{bmatrix} \overline{\mathbf{u}}_n \\ \overline{\boldsymbol{\tau}}_n \end{bmatrix} = (-jk_3) \begin{bmatrix} \overline{\mathbf{u}}_m \\ \overline{\boldsymbol{\tau}}_m \end{bmatrix}. \tag{4.30}$$

The elements of $\mathcal{L}$ have the following equivalent algebraic forms:

$$\mathrm{L}^{11}_{mn} = -(j\beta_n)\,\mathcal{M}^{11}_{m-n}, \tag{4.31a}$$

$$\mathrm{L}^{12}_{mn} = \mathcal{M}^{12}_{m-n}, \tag{4.31b}$$

$$\mathrm{L}^{21}_{mn} = -\omega^2 \underline{\underline{\rho}}_{\,m-n} + \left[\beta_n\,(m-n)\,Q + \beta_n^2\right] \mathcal{M}^{21}_{m-n}, \tag{4.31c}$$

$$\mathrm{L}^{22}_{mn} = \left[-j\,(m-n)\,Q - j\beta_n\right] \mathcal{M}^{22}_{m-n}, \tag{4.31d}$$

where matrices $\mathcal{M}$ were defined in equation (4.23). Expanding equation (4.30) explicitly in terms of all harmonics, the following algebraic eigenvalue problem results:

$$\begin{bmatrix} \mathrm{L}^{11}_{-N,-N} & \dots & \mathrm{L}^{11}_{-N,N} & \mathrm{L}^{12}_{-N,-N} & \dots & \mathrm{L}^{12}_{-N,N} \\ \vdots & & \vdots & \vdots & & \vdots \\ \mathrm{L}^{11}_{N,-N} & \dots & \mathrm{L}^{11}_{N,N} & \mathrm{L}^{12}_{N,-N} & \dots & \mathrm{L}^{12}_{N,N} \\ \mathrm{L}^{21}_{-N,-N} & \dots & \mathrm{L}^{21}_{-N,N} & \mathrm{L}^{22}_{-N,-N} & \dots & \mathrm{L}^{22}_{-N,N} \\ \vdots & & \vdots & \vdots & & \vdots \\ \mathrm{L}^{21}_{N,-N} & \dots & \mathrm{L}^{21}_{N,N} & \mathrm{L}^{22}_{N,-N} & \dots & \mathrm{L}^{22}_{N,N} \end{bmatrix} \begin{bmatrix} \overline{\mathbf{u}}_{-N} \\ \vdots \\ \overline{\mathbf{u}}_N \\ \overline{\boldsymbol{\tau}}_{-N} \\ \vdots \\ \overline{\boldsymbol{\tau}}_N \end{bmatrix} = (-jk_3) \begin{bmatrix} \overline{\mathbf{u}}_{-N} \\ \vdots \\ \overline{\mathbf{u}}_N \\ \overline{\boldsymbol{\tau}}_{-N} \\ \vdots \\ \overline{\boldsymbol{\tau}}_N \end{bmatrix}, \tag{4.32}$$

where $-jk_3$ are the eigenvalues, and give the x_3 dependance of the eigenvectors as shown in equation (4.29). This equation is analogous to equation (3.32), which was derived for the case of homogeneous material constants. In the inhomogeneous non-piezoelectric case there are $6(2N+1)$ eigenvalues, whereas the homogeneous piezoelectric case results in only 8. The extra capability of equation (4.32) in dealing with periodically varying media comes at the expense of having coupling between all harmonics, thus greatly increasing the computational complexity.

For this thesis only isotropic media will be considered for the inhomogeneous region, however this technique is equally valid for anisotropic and piezoelectric media. Substituting stiffness matrix c for an isotropic material into equations (3.31) and (4.23), and removing the components corresponding to the dielectric and piezoelectric interaction, it turns out that most of the components of $\mathcal{M}^{kl}$ are zero:

$$\mathcal{M}^{11} = \begin{bmatrix} 0 & 0 & 1 \\ 0 & 0 & 0 \\ \frac{c_{12}}{c_{44}} & 0 & 0 \end{bmatrix} \qquad \mathcal{M}^{12} = \begin{bmatrix} \frac{1}{c_{44}} & 0 & 0 \\ 0 & \frac{1}{c_{44}} & 0 \\ 0 & 0 & \frac{1}{c_{11}} \end{bmatrix} \tag{4.33a}$$

$$\mathcal{M}^{21} = \begin{bmatrix} c_{11} - \frac{c_{12}^2}{c_{11}} & 0 & 0 \\ 0 & c_{44} & 0 \\ 0 & 0 & 0 \end{bmatrix} \qquad \mathcal{M}^{22} = \begin{bmatrix} 0 & 0 & \frac{c_{12}}{c_{44}} \\ 0 & 0 & 0 \\ 1 & 0 & 0 \end{bmatrix}. \tag{4.33b}$$

In addition, it can be seen that the shear component (column 2 and row 2) decouples from the sagittal components (columns 1 and 3 and rows 1 and 3), thus further simplifying calculation. By substituting equation (4.33) into equation (4.31), a simplified equation in the form of (4.32) is derived. Equation (4.32) can be rewritten as:

$$\mathrm{L} \begin{bmatrix} \overline{\mathbf{u}}(x_3, \beta, \omega) \\ \overline{\boldsymbol{\tau}}(x_3, \beta, \omega) \end{bmatrix} = (-jk_3) \begin{bmatrix} \overline{\mathbf{u}}(x_3, \beta, \omega) \\ \overline{\boldsymbol{\tau}}(x_3, \beta, \omega) \end{bmatrix}. \tag{4.34}$$

The solution of this equation is:

$$\begin{bmatrix} \overline{\mathbf{u}}(x_3, \beta, \omega) \\ \overline{\boldsymbol{\tau}}(x_3, \beta, \omega) \end{bmatrix} = \Phi^{mech}(\beta, \omega, h_e) \begin{bmatrix} \overline{\mathbf{u}}(x_3 + h_e, \beta, \omega) \\ \overline{\boldsymbol{\tau}}(x_3 + h_e, \beta, \omega) \end{bmatrix}. \tag{4.35}$$

$$\Phi^{mech}(\beta, \omega, h_e) = \exp\left(-\mathrm{L}h_e\right). \tag{4.36}$$

The matrix exponentiation is most readily carried out by an eigenvalue decomposition of the matrix L:

$$\mathrm{L} = \mathrm{V}\mathrm{D}\mathrm{V}^{-1}, \tag{4.37}$$

$$\exp(-\mathrm{L}h_e) = \mathrm{V}\exp(-\mathrm{D}h_e)\mathrm{V}^{-1}, \tag{4.38}$$

where V is the column-wise arrangement of eigenvectors, and D contains the corresponding eigenvalues on the main diagonal. This operation can be regarded as a mapping the space harmonics to a sum of eigenmodes. These eigenmodes each propagate

over distance h_e in the x_3 direction at a different rate, as given by the $\exp(-\mathrm{D}h_e)$ operation, and are then mapped back to a sum of space harmonics.

This is equivalent to Adler's chain-matrix formulation which was discussed in Section 2.6, but has been extended to cover the case of inhomogeneous media. As with the case of homogeneous media, it is possible to use impedance, admittance and reflection matrix forms. Since electrode thicknesses in practical devices are much less than the acoustic wavelength, numerical instability is not a significant problem and the simpler chain-matrix technique is adequate.

In order to complete the analysis, the electrical transmission across the inhomogeneous region must also be characterised. Since it is difficult to define a dielectric constant for the electrode region, the region is assumed to be homogeneous and to have the same dielectric constant as the layer material. Simplifying the results from [134] for isotropic media and the invariance of fields in the x_2 direction, the matrix operator form for this problem can be written:

$$\begin{bmatrix} \mathcal{L}^{11} & \mathcal{L}^{12} \\ \mathcal{L}^{21} & \mathcal{L}^{22} \end{bmatrix} \begin{bmatrix} \overline{\varphi} \\ \overline{\mathcal{D}} \end{bmatrix} = \frac{\partial}{\partial x_3} \begin{bmatrix} \overline{\varphi} \\ \overline{\mathcal{D}} \end{bmatrix}, \tag{4.39}$$

where

$$\mathcal{L}^{11} = 0 \qquad \mathcal{L}^{12} = -\frac{1}{\varepsilon} \qquad \mathcal{L}^{21} = \frac{\partial}{\partial x_1}\varepsilon\frac{\partial}{\partial x_1} \qquad \mathcal{L}^{22} = 0. \tag{4.40}$$

Unlike equation (4.36), the matrix exponential corresponding to equation (4.39) can be solved analytically, yielding a transmission matrix:

$$\Phi^{elec}(\beta, h_e) = \begin{bmatrix} \Phi^{\varphi\varphi} & \Phi^{\varphi\mathcal{D}} \\ \Phi^{\mathcal{D}\varphi} & \Phi^{\mathcal{D}\mathcal{D}} \end{bmatrix} \tag{4.41}$$

$$= \delta_{nm} \begin{bmatrix} \cosh\left[(\beta + nQ)\, h_e\right] & \dfrac{1}{(\beta + nQ)\varepsilon} \sinh\left[(\beta + nQ)\, h_e\right] \\ (\beta + nQ)\varepsilon \sinh\left[(\beta + nQ)h_e\right] & \cosh\left[(\beta + nQ)h_e\right] \end{bmatrix}. \tag{4.42}$$

The matrices Φ^{mech} and Φ^{elec} are partitioned and combined, in order to gain a complete description of electrical and mechanical field transmission across the layer. The following equation is obtained, where the subscripts k and l refer to the harmonic

number:

$$\begin{bmatrix} \overline{\mathbf{u}}_k(x_3) \\ \overline{\varphi}_k(x_3) \\ \overline{\boldsymbol{\tau}}_k(x_3) \\ \overline{\mathcal{D}}_k(x_3) \end{bmatrix} = \sum_l \begin{bmatrix} \Phi_{kl}^{uu} & 0 & \Phi_{kl}^{u\tau} & 0 \\ 0 & \Phi_{kl}^{\varphi\varphi} & 0 & \Phi_{kl}^{\varphi D} \\ \Phi_{kl}^{\tau u} & 0 & \Phi_{kl}^{\tau\tau} & 0 \\ 0 & \Phi_{kl}^{\mathcal{D}\varphi} & 0 & \Phi_{kl}^{\mathcal{D}\mathcal{D}} \end{bmatrix} \begin{bmatrix} \overline{\mathbf{u}}_l(x_3 + h_e) \\ \overline{\varphi}_l(x_3 + h_e) \\ \overline{\boldsymbol{\tau}}_l(x_3 + h_e) \\ \overline{\mathcal{D}}_l(x_3 + h_e) \end{bmatrix}. \tag{4.43}$$

It should be noted that if the electrodes consist of multiple metal layers, then this technique can be applied for each layer. It can be seen that equation (4.43) can be iteratively applied for an arbitrary number of layers, with the transmission matrix calculated separately for each layer. These transmission matrices are cascaded to form a single transmission matrix, so no change is required in the analysis.

4.2.2.2 Incorporation with Periodic Green's Function

The mechanical and electrical behaviour of region (ii) having been characterised by transfer matrices Φ^{mech} and Φ^{elec}, the problem remains to integrate these into a Green's function based analysis. To proceed further, the concept of the spectral domain Green's function must be generalised. In the case of homogeneous media, equation (4.9) allows the structure to be characterised by a sum of weighting coefficients, each having the following form:

$$\overline{\varphi}(\beta + kQ, \omega) = \overline{G}(\beta + kQ, \omega)\overline{q}(\beta + kQ, \omega). \tag{4.44}$$

The inhomogeneous nature of the layer containing buried electrodes means that a relationship of the following form exists:

$$\overline{\varphi}(\beta + kQ, \omega) = \sum_l \overline{G}_{kl}(\beta, \omega)\overline{q}(\beta + lQ, \omega). \tag{4.45}$$

$$\overline{\varphi}_k(\beta, \omega) = \sum_l \overline{G}_{kl}(\beta, \omega)\overline{q}_l(\beta, \omega). \tag{4.46}$$

The matrix containing these elements shall be denoted as $\mathcal{G}(\beta, \omega)$, the multi-spectral Green's function, and as with the spectral domain Green's function it has an inverse $\mathcal{Z}(\beta, \omega)$. Obviously (4.44) can be included in equation (4.46) by making the substitution:

$$\overline{G}_{kl} = \delta_{kl}\overline{G}(\beta + lQ, \omega). \tag{4.47}$$

Referring to Figure 4.4, the substrate and homogeneous layer can be described by this means, and will be represented by multi-spectral impedance matrices $\mathcal{Z}^{(iii)}$ and $\mathcal{Z}^{(i)}$ respectively. Combining equation (4.43) with $\mathcal{Z}^{(i)}(\beta,\omega)$, the impedance matrix of the region above the reference plane, $\mathcal{Z}^{(a)}(\beta,\omega)$, is calculated from the expression:

$$\mathcal{Z}^{(a)} = \left(\begin{bmatrix} \Phi^{\tau u} & 0 \\ 0 & \Phi^{\mathcal{D}\varphi} \end{bmatrix} + \begin{bmatrix} \Phi^{\tau\tau} & 0 \\ 0 & \Phi^{\mathcal{D}\mathcal{D}} \end{bmatrix} \mathcal{Z}^{(i)} \right) \left(\begin{bmatrix} \Phi^{uu} & 0 \\ 0 & \Phi^{\varphi\varphi} \end{bmatrix} + \begin{bmatrix} \Phi^{u\tau} & 0 \\ 0 & \Phi^{\varphi\mathcal{D}} \end{bmatrix} \mathcal{Z}^{(i)} \right)^{-1}. \quad (4.48)$$

The multi-spectral impedance matrix of the complete structure can now be calculated by:

$$\mathcal{Z}(\beta,\omega) = \left[\mathcal{Z}^{(a)}(\beta,\omega) - \mathcal{Z}^{(iii)}(\beta,\omega) \right]. \quad (4.49)$$

Since all mechanical interactions are already included in this formulation, the problem can be reduced to a purely electrical one. From the inverse of a partitioned matrix [135], the multi-spectral electrical Green's function can be calculated as:

$$\mathcal{G}^{\varphi q}(\beta,\omega) = \left(\mathcal{Z}^{q\varphi} - \mathcal{Z}^{qu} \left(\mathcal{Z}^{\tau u} \right)^{-1} \mathcal{Z}^{\tau\varphi} \right)^{-1}. \quad (4.50)$$

Substituting equation (4.16) into equation (4.46) and summing over all harmonics:

$$\varphi(x,\beta,\omega) = \frac{1}{p} \sum_k \sum_l \overline{G}_{kl}^{\varphi q}(\beta,\omega) \sum_m q_m(\beta,\omega) e^{-j\beta_l x_m} \frac{\sin(\beta_l w_m)}{\beta_l w_m} e^{j\beta_k x_1}. \quad (4.51)$$

Utilising the method of weighted residuals and following a similar procedure to that outlined in Section 4.2.1, the resulting matrix equation is:

$$\varphi_n(\beta,\omega) = \frac{1}{p} \sum_{k=-L}^{L} e^{j\beta_k x_n} \frac{\sin(\beta_k w_n)}{\beta_k w_n} \sum_{l=-L}^{L} \overline{G}_{kl}(\beta,\omega) \sum_{m=-N}^{N} e^{-j\beta_l x_m} \frac{\sin(\beta_l w_m)}{\beta_l w_m} q_m(\beta,\omega). \quad (4.52)$$

It can be seen that if equation (4.47) is substituted directly into equation (4.52), the result is identical to equation (4.19), showing that this technique simplifies to the existing BEM formulation in case of homogeneous material constants.

As with the case of the infinitesimal electrode approximation, the charge distribution as a function of β and ω can be used to calculate the harmonic admittance. In the next section, the harmonic admittance function will be discussed further, along with the technique used to extract the COM parameters

4.2.3 Harmonic Admittance and COM Parameterisation

In Sections 4.2.1 and 4.2.2, the rigourous solution of the wave propagation problem in periodic media was shown to be represented by the harmonic admittance function $Y(\beta, \omega)$. Figure 4.5 shows the harmonic admittance for an electrode array with $p =$ 20µm, $l = 10$µm and $h_e = 0$, calculated using the simplified electrical Green's function model. The materials of the structure consist of a 1µm SiO_2 film on a 36°-YX $LiTaO_3$ substrate.

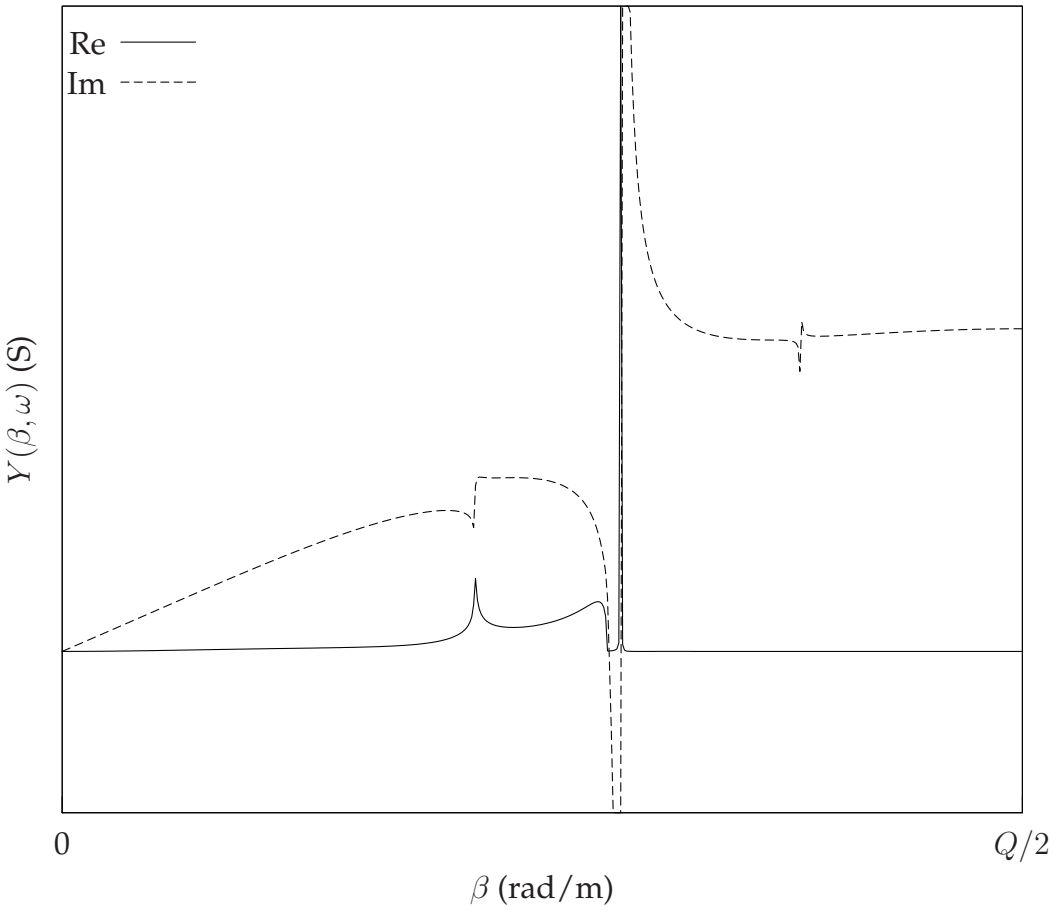

Figure 4.5: Harmonic admittance of a SiO_2/36°-YX $LiTaO_3$ SAW device at 60MHz

This plot is calculated for a fixed frequency of 60MHz, which was chosen as it clearly shows all the relevant features. The range of wavenumber β shown is $[0, Q/2]$, which is called the first Brillouin zone. The harmonic admittance in the second Brillouin zone $[Q/2, Q]$ is a reflection of the first Brillouin zone about $\beta = Q/2$, and the harmonic admittance repeats with period Q. Thus all the information available from the function can be obtained from the first Brillouin zone.

In Section 3.3.1 it was shown that the poles and zeros of the spectral domain Green's function could be used to find the propagating eigenmodes of the combination of substrate and layers. It will be shown here that a similar procedure can be performed for the harmonic admittance function in order to find the eigenmodes of such a configuration including the influence of an electrode array.

Wave propagation in an infinite electrode array can be characterised by two important eigenmodes, having short circuit and open circuit connections between the electrodes. In the short circuit case the voltage on each electrode is considered to be zero, thus according to equation (4.22) the harmonic admittance will become infinite. Similar to the case of the spectral domain Green's function, a singularity will be observed. The opposite case occurs for an open circuit electrode grating, where the current flowing into each electrode must be zero, so a zero of the harmonic admittance occurs. In Figure 4.5 the influence of these singularities can be observed, although their actual location will occur at a complex value of β. As with the case of the spectral domain Green's function, singularities with non-zero imaginary parts indicate that the wave amplitude is reducing. This may be caused by the same attenuation phenomena as were discussed in Section 2.2.2. However, an additional effect in a grating is the reflection from electrodes, which will manifest itself as an imaginary component of β.

By searching for the singularities at each frequency, open circuit and short circuit dispersion curves can be calculated. For illustrative purposes, Figure 4.6 shows an idealised dispersion curve, where the real and imaginary parts of β are on separate vertical scales. Over a range of frequencies known as the stop band, the imaginary part of the wavenumber is non-zero, corresponding to the decay in wave amplitude caused by Bragg reflection. In a practical SAW device other features may be observed in this curve due to bulk wave and leakage effects. Propagation losses will cause the imaginary component of β to be non-zero at all frequencies, except for bulk wave radiation which only occurs above a certain cut-off frequency. Calculation of the complete dispersion curve is not undertaken in this work, as it requires a large computational effort, and as will be shown shortly, is not required to characterise the electrode array.

To avoid the computationally intensive and error-prone process of searching for singularities at each frequency, the harmonic admittance can be calculated for each fre-

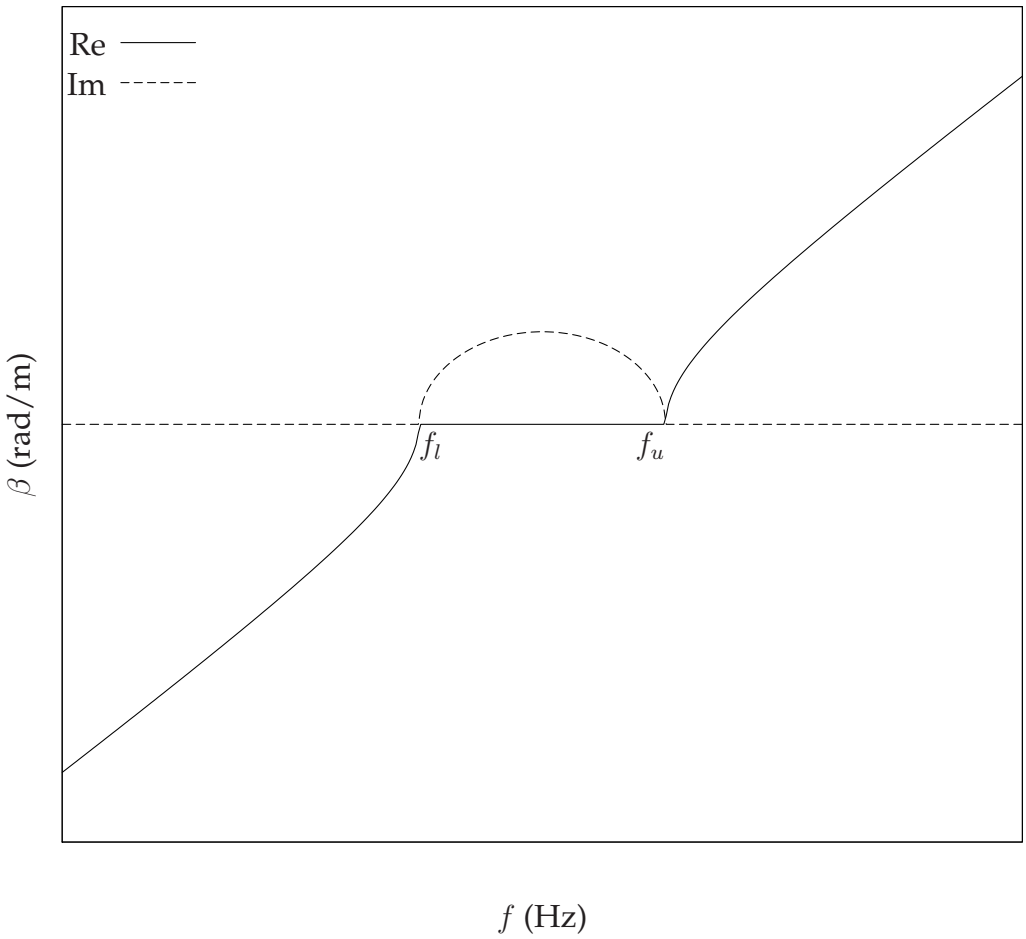

Figure 4.6: Idealised short circuit dispersion curve of an electrode array

quency at $\beta = Q/2$, and one additional wavenumber near this point. This corresponds to the admittance per electrode of an infinite length IDT, since for $\beta = Q/2$ the electrode voltages alternate in polarity. An example curve of this type is shown in Figure 4.7 for the same device configuration as was used to calculate Figure 4.5. Also shown are the curves produced by fitting a COM model, which will be discussed subsequently. The most important characteristic of this curve is the resonant peak, where the real part of the admittance reaches a maximum. For a lossless device this peak will be infinitely narrow, however the resonant frequency can be tracked via the minimum of the boundary determinant. The other important feature is the anti-resonant frequency, where the imaginary part of the admittance becomes zero.

The admittance of an infinite transducer is advantageous to use because it requires only two admittance calculations per frequency, but this does mean that it contains less information than the dispersion curve. This lack of information can be problematic if

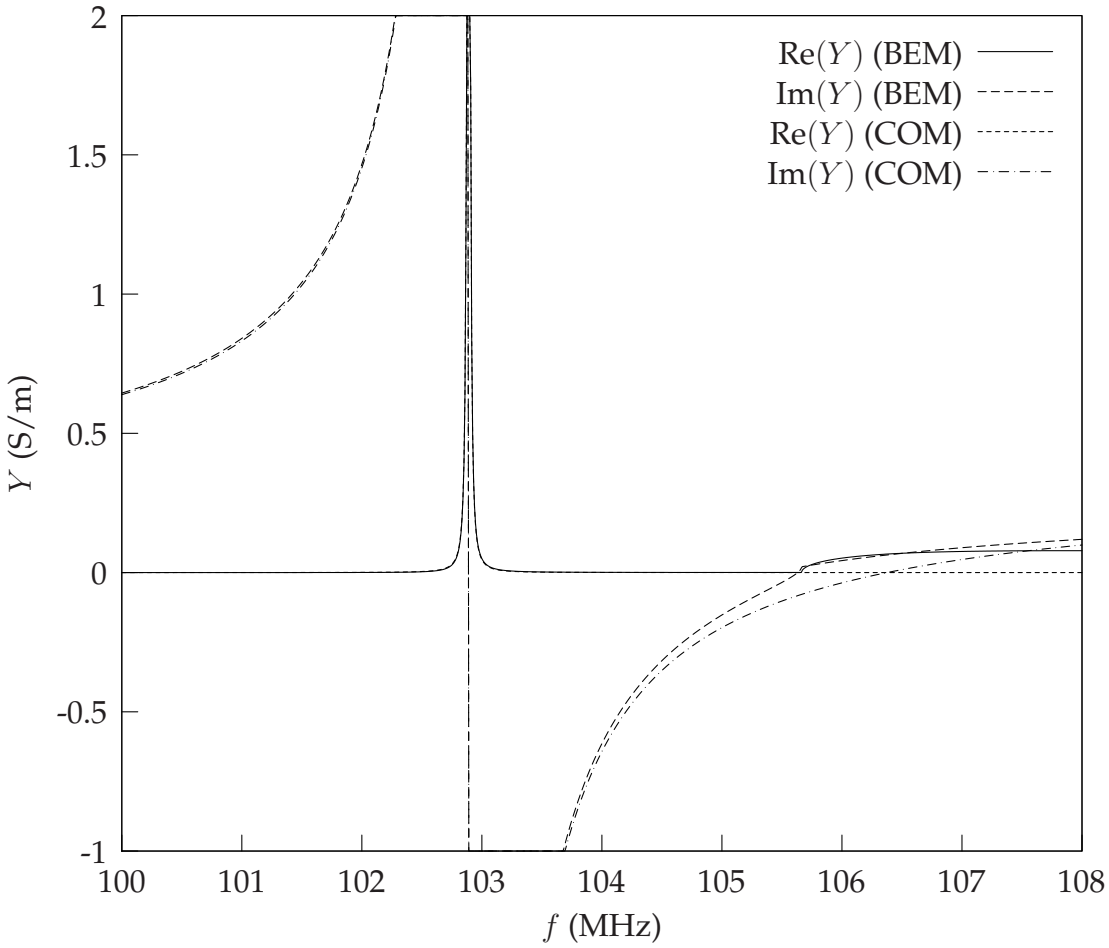

Figure 4.7: Harmonic admittance of 36°-YX $LiTaO_3$ for $\beta = Q/2$, $p = 20$µm, $l = 10$µm and $h_e = 0$.

the interaction of SH SAW and BAW modes needs to be parameterised, which is not important for this work.

Before discussing the COM parameterisation algorithm, a brief overview will be given of the COM model in its most common form. The characteristics of an electrode array are represented by three coupled differential equations:

$$\frac{\mathrm{d}w_+}{\mathrm{d}x_1} = -j\delta w_+ - j\kappa^* w_- + j\alpha V. \tag{4.53a}$$

$$\frac{\mathrm{d}w_-}{\mathrm{d}x_1} = -j\kappa w_+ - j\delta w_- - j\alpha^* V. \tag{4.53b}$$

$$\frac{\mathrm{d}I}{\mathrm{d}x_1} = -2j\alpha^* w_+ - 2j\alpha w_- + j\omega C V. \tag{4.53c}$$

The quantities w_+ and w_i represent the intensity of waves travelling in the positive and negative x_1 directions respectively, V represents the bus-bar voltage and I is the current flow into the IDT. Table 4.1 gives a list of the COM parameters and their meaning. It

should be noted that in some literature the parameter κ is referred to as the coupling between spatial harmonics propagating in the positive and negative x_1 directions. This notation will not be used here to avoid confusion with the electromechanical coupling.

Table 4.1: COM parameters

v	effective wave velocity in the grating
α	transduction between acoustic and electrical energy per unit length
κ	reflection per unit length
γ	propagation loss per unit length
C	capacitance per unit length

Normalised frequency deviation δ and normalised wavenumber $\hat{q}$ are usually used because they simplify the form of equations (4.53), and are defined as:

$$\delta = \frac{\omega}{v} - \frac{\pi}{p} - j\gamma. \tag{4.54a}$$

$$\hat{q} = \sqrt{\delta^2 - |\kappa|^2}\,. \tag{4.54b}$$

To be physically consistent, the branch of the square root is chosen to ensure that the imaginary part of q is zero. For unidirectional configurations of material or electrode geometry, the parameters α and κ can be complex. In this work they are assumed to be real, and this assumption can be verified by inspection of the harmonic admittance curves, which will exhibit multiple resonances for unidirectional configurations [40].

The algorithm used here was developed by Koskela et al. [97]. The COM parameters are extracted from $Y(Q/2, \omega)$ and $Y(Q/2 + \Delta\beta, \omega)$, where $\Delta\beta \ll Q/2$. Both of these curves are calculated at a sparse range of points over a frequency region which includes the resonance peak.

A numerical search is performed to find the resonant frequency f_r, the corresponding resonant peak $Y_r = \mathrm{Re}(Y(f_r))$, the half-maximum width of the resonance Δf and the anti-resonant frequency f_{ar}. The upper and lower stop-band edges f_u and f_l (see Figure 4.6) can also be determined without calculating the complete dispersion curve. From these parameters, it is possible to determine normalised versions of the COM

parameters. These are given as:

$$\kappa_p = \kappa\lambda_0. \tag{4.55a}$$

$$\alpha_n = \alpha\sqrt{\lambda_0/W}. \tag{4.55b}$$

$$\gamma_p = \gamma\lambda_0. \tag{4.55c}$$

$$C_n = C\lambda_0/W. \tag{4.55d}$$

The normalised capacitance C_n is obtained from imaginary part of admittance at low frequency, where the contribution of any acoustic resonance to the admittance will be negligible. From the relationships given in equation (4.55), these normalised parameters are then scaled for the device geometry of interest. This algorithm only gives the magnitude of κ_p, but it's sign is also important. If the resonant frequency f_r coincides with f_l, then κ_p will be negative, whereas if it coincides with f_u then κ_p will be positive.

For non-layered devices with infinitesimally thin electrodes, by scaling the COM parameters they can be used for any devices using the same substrate and having the same metallisation ratio l/p. For layered devices with infinitesimal electrode thickness, the COM parameters will depend on the ratio h/λ_0, as well as the metallisation ratio. Similarly, for non-layered devices with electrodes of finite thickness, there will be a dependency on h/h_e, the electrode cross-sectional shape (assumed rectangular in this work) and the electrode material. In the case of buried electrodes of finite thickness, the COM parameters will depend on all of these factors. As discussed in Section 3.2.2, for media such as viscous liquids there will be an explicit frequency dependance which cannot be normalised by scaling.

To check the accuracy of the COM fitting procedure, the admittance curve can be reconstructed from the extracted parameters. An example of this is given in Figure 4.7. It can be seen that overall the fit is very good, but that there is some discrepancy between the calculated (BEM) and fitted admittance (COM) curves. There is a non-zero real part of the admittance at high frequencies which is not included in the fitted curve. This corresponds to the launching of bulk waves into the substrate, which is excluded from this COM model. These effects could be included by the use of a more complicated version of the COM model, as discussed in Section 2.3. However, the behaviour of the device anti-resonance is only important for signal processing structures such as ladder filters, so it is not necessary to characterise this behaviour here.

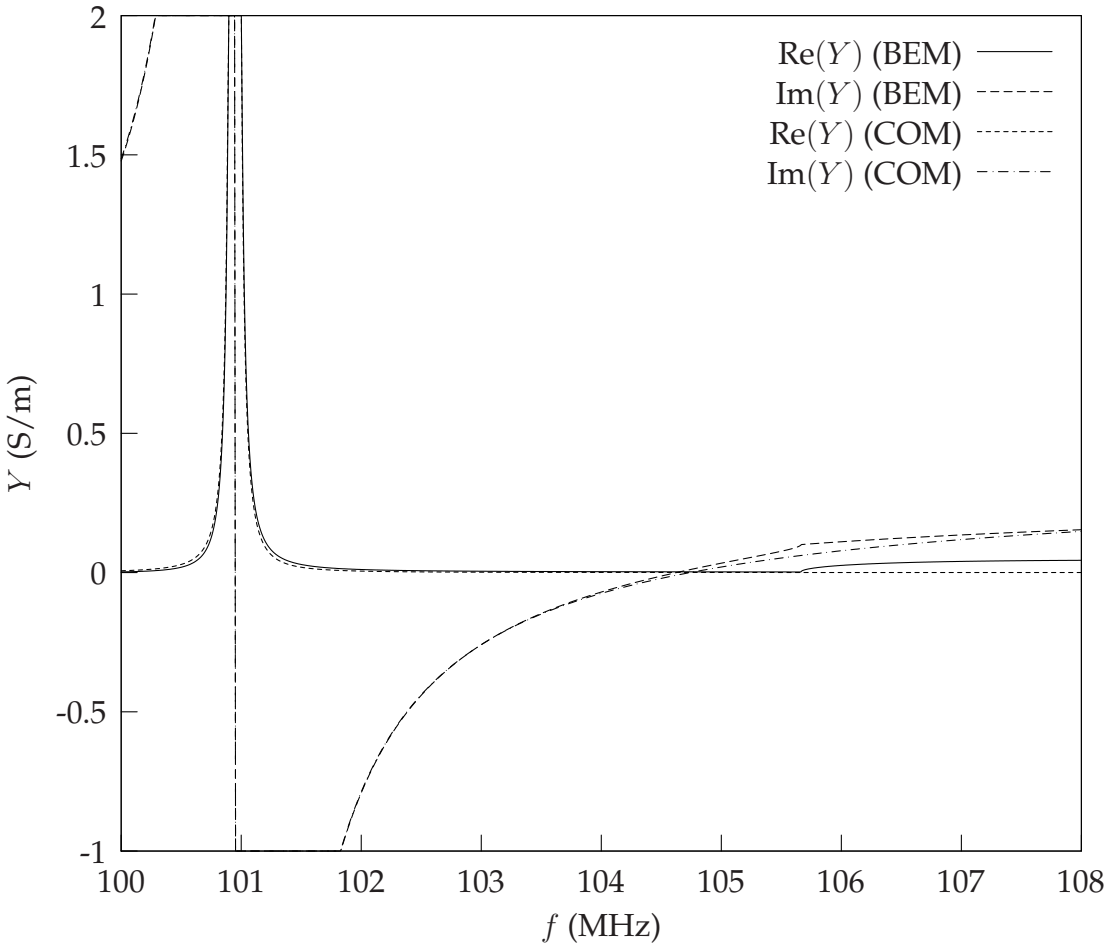

Figure 4.8: Harmonic admittance of SiO_2 on 36°-YX $LiTaO_3$ for $\beta = Q/2$, $p = 20$µm, $l = 10$µm, $h_e = 0$ and $h = 3$µm

In Figure 4.8 the admittance has been plotted for the same structure with a 3µm SiO_2 guiding layer above the electrodes. It can be seen that the resonant frequency is greatly reduced, which is consistent the results reported in Section 3.3.3. This means that the bulk wave generation is less problematic, since the mechanical loading has reduced the resonant and anti-resonant frequencies to be below the bulk wave cut-off frequency. A similar effect would also be observed where electrodes cause significant mechanical loading. It can be seen that the agreement around the resonant peak is slightly worse than in the non-layered case. This is because the layered device has some additional dispersion. To characterise this dispersion, it would be necessary to make the COM parameters (particularly v) dependent on frequency. However, since the agreement between the curves is still very good, it indicates that this dependency is very weak, and can be safely neglected.

In the paper by Koskela et al. describing this extraction technique [97], the capacitance was extracted in such a manner to give an accurate value for the anti-resonant frequency. However, it was found that this had the effect of degrading the match between the fitted and numerically calculated curves in the region of the admittance peak. For this reason the capacitance was calculated from the admittance at a very low frequency, where negligible acoustic wave generation will occur.

Having developed the rigourous periodic model and extracted the COM parameters, the next step is to use them for the analysis of SAW sensors. This will be undertaken in Section 4.3.

4.3 Device Analysis Using Periodic Model

The outcome of Section 4.2 was a set of COM parameters which are able to encapsulate much of the important behaviour of a SAW propagating in an electrode array. The question remains as to how these parameters can be utilised for sensors, and the answer will be presented here. In Section 4.3.1 the change in COM parameters with guiding layer thickness will be examined under mass-loading and liquid loading conditions. In Section 4.3.2 the COM parameters will be used to create a 2-port matrix representation of the SAW device, which gives the complete frequency response.

4.3.1 Sensitivity Analysis Using COM Model

The analysis presented in Section 3.3.3 showed that the spectral domain Green's function can be used for the characterisation of delay line SAW sensors. Whilst the results of this analysis may be applied to resonator structures, it does not take any account of the electrode interactions which are very important in determining the behaviour of these structures. In addition, the effects of liquid loading must be considered, as it is expected that these devices should be capable of operating in liquid media.

As discussed in Section 3.3.2, the perturbing mass is modelled by the addition of a thin layer, and the liquid is modelled as being in rigid contact with the sensor surface. Using the COM fitting model, the parameters were calculated as a function of layer thickness, both with and without liquid loading. The COM extraction technique given

in Section 4.2.3 is based on the admittance curve of an infinite length IDT. This means that the calculations presented in this section do not take into account the finite size of the device surface area. Such considerations will be deferred to Chapter 6.

The technique was applied to the configuration of a 36°-YX $LiTaO_3$ substrate with a SiO_2 guiding layer of varying thickness. The IDT period λ_0 was 40µm and metallisation ratio was 0.5, yielding a resonant frequency of 103.7MHz for the non-layered configuration. All configurations were analysed with both vacuum and water above the guiding layer. To understand the influence of finite electrode height, calculations were made using both the infinitely thin electrode approximation given in Section 4.2.1 and the novel mechanical model developed in Section 4.2.2. The electrode height was set to 0.1µm ($0.0025\lambda_0$) and the electrode material was gold for the full electrode model.

All calculations were performed with $N = 15$ expansion functions and $2L + 1 = 35$ harmonics. These values were determined empirically to provide sufficient convergence. By increasing these to 24 and 53 respectively, there was negligible change in the appearance of these graphs. Given the completeness property of the pulse expansion functions, it can be stated with confidence that the results presented here are sufficiently accurate.

Figure 4.9 gives the COM velocity parameter v as a function of guiding layer thickness. It can be seen that it is not perturbed greatly by the presence of a liquid, however the layer significantly reduces the propagation velocity. The mechanical influence of the thick electrodes reduces the velocity by an amount which shows weak dependence on guiding layer thickness.

Figure 4.10 shows the normalised electromechanical transduction coefficient α_n as a function of SiO_2 thickness. This curve follows the general trend reported in the literature for the device insertion loss as a function of layer thickness [19]. For low thickness the layer increases the degree of electromechanical coupling. However, for $h/\lambda_0 > 0.12$, the thicker layer is electrically isolating the IDT from the wave at the device surface, thus decreasing the coupling coefficient.

This can be understood by referring to Figure 4.11, which illustrates the degree of energy confinement as a function of layer thickness. It shows that as the guiding layer thickness increases, the degree of energy confinement towards the surface will

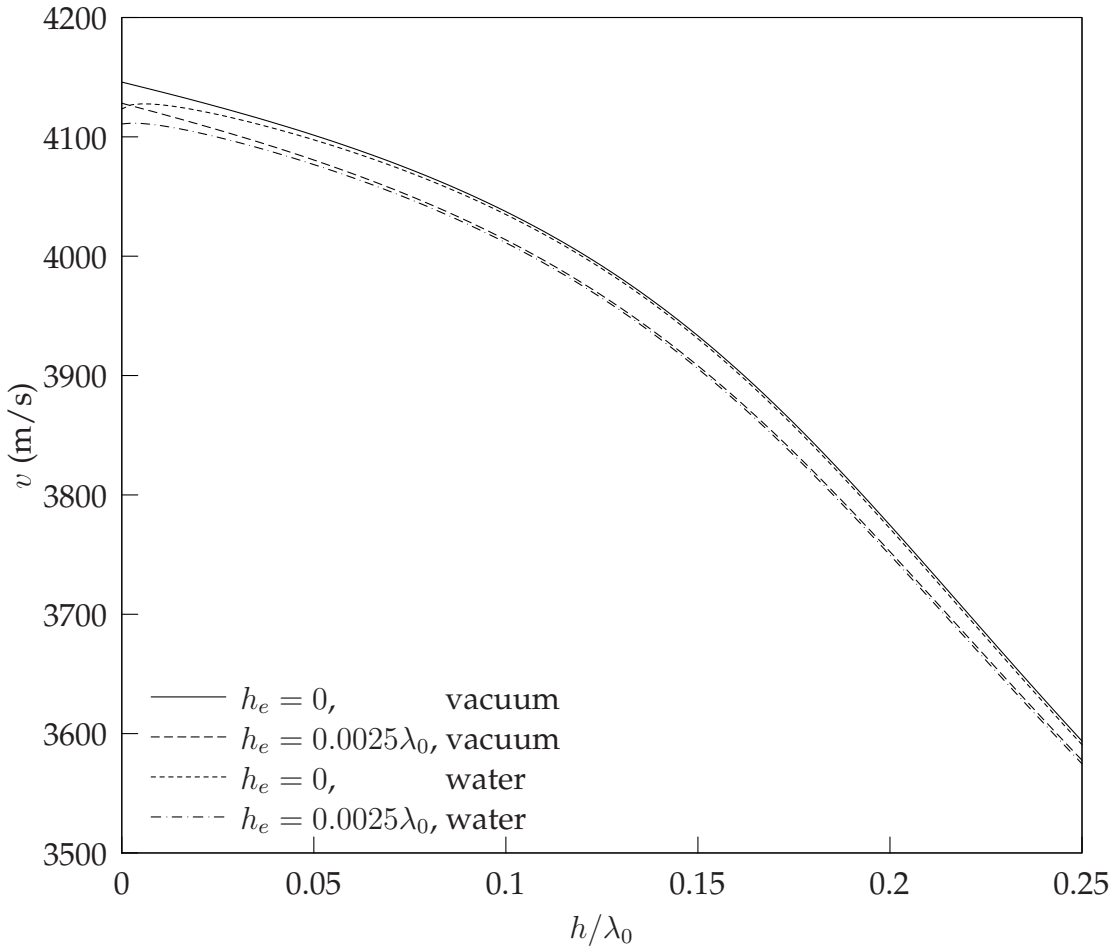

Figure 4.9: Variation of propagation velocity v with layer thickness

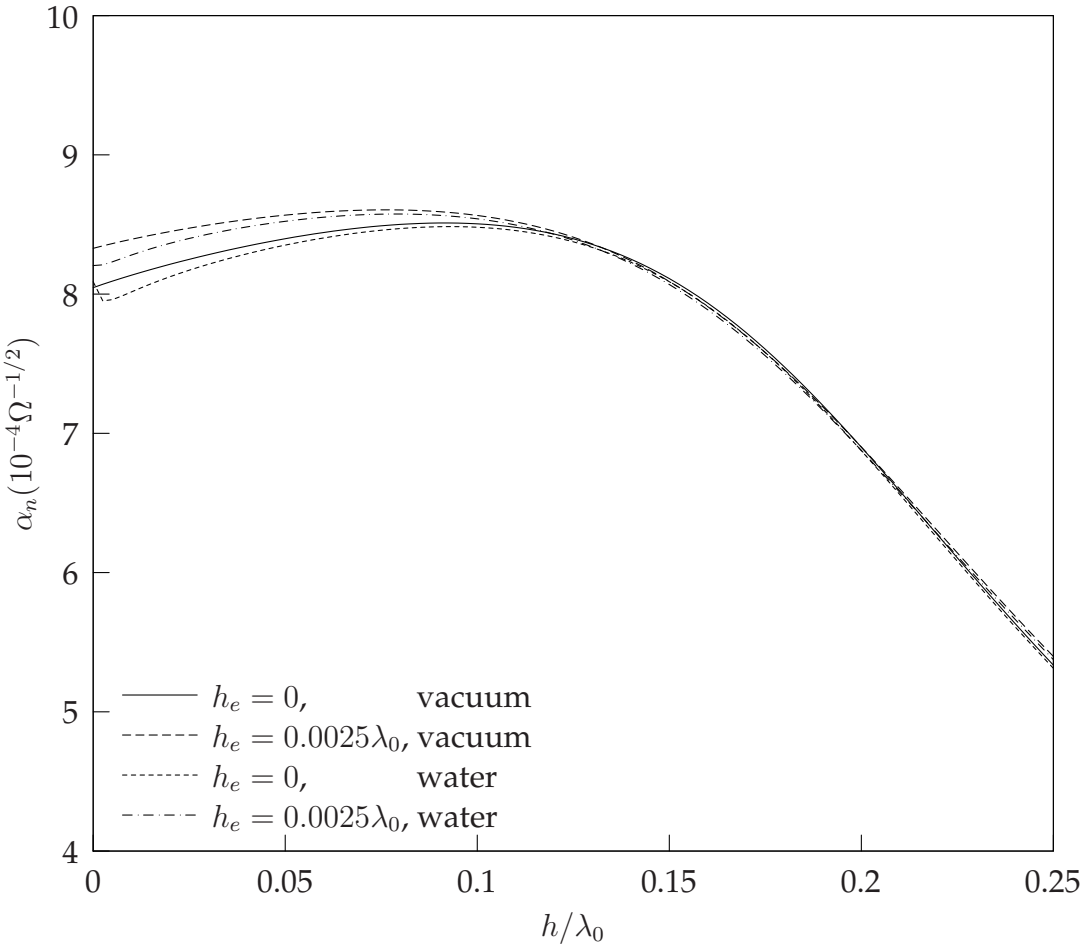

Figure 4.10: Variation of normalised electromechanical coupling parameter α_n with layer thickness

increase, which allows for greater interaction between the acoustic and electrical fields in the vicinity of the IDT. Eventually the device will reach a point where the energy is confined to the surface and away from the IDT. For this reason the effects of thick electrodes are greatly reduced at higher guiding layer thickness. The decreasing effect of liquid loading with increasing layer thickness can be explained by the electrical shielding effect of the guiding layer.

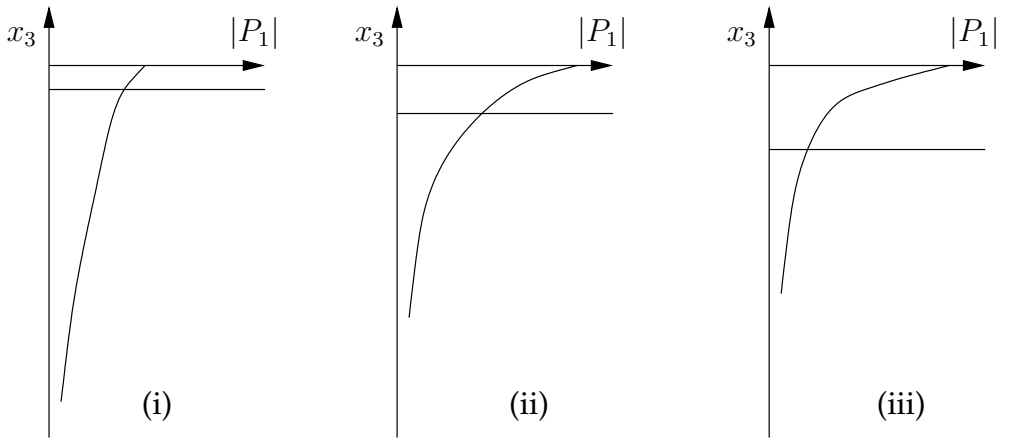

Figure 4.11: A sketch of the variation of surface energy confinement with layer thickness: (i) low thickness, moderate coupling (ii) optimal thickness, maximum coupling (iii) increased thickness, reducing coupling

Figure 4.12 shows the magnitude of the reflection per electrode κ_p. This indicates that the addition of a layer can increase the reflection coefficient, as well as reducing the sensitivity of the reflection coefficient to liquid loading. The increase in reflection due to the mechanical interactions with electrodes is dependant on the layer thickness, with the difference at $h/\lambda_0 = 0.25$ being about half that at $h/\lambda_0 = 0$. Again, this difference with layer thickness can be attributed to the wave being concentrated near the surface, which is further away from the electrodes for thicker layers. It can also be seen that liquid loading causes a dramatic reduction in the reflection coefficient, however this difference disappears at high layer thickness.

Figure 4.13 shows the normalised capacitance C_n as a function of guiding layer thickness. The capacitance in vacuum increases with layer thickness, due to additional dielectric material in the region near the electrodes. However, the change is very slight for this material combination, and asymptotically approaches a limit. The difference

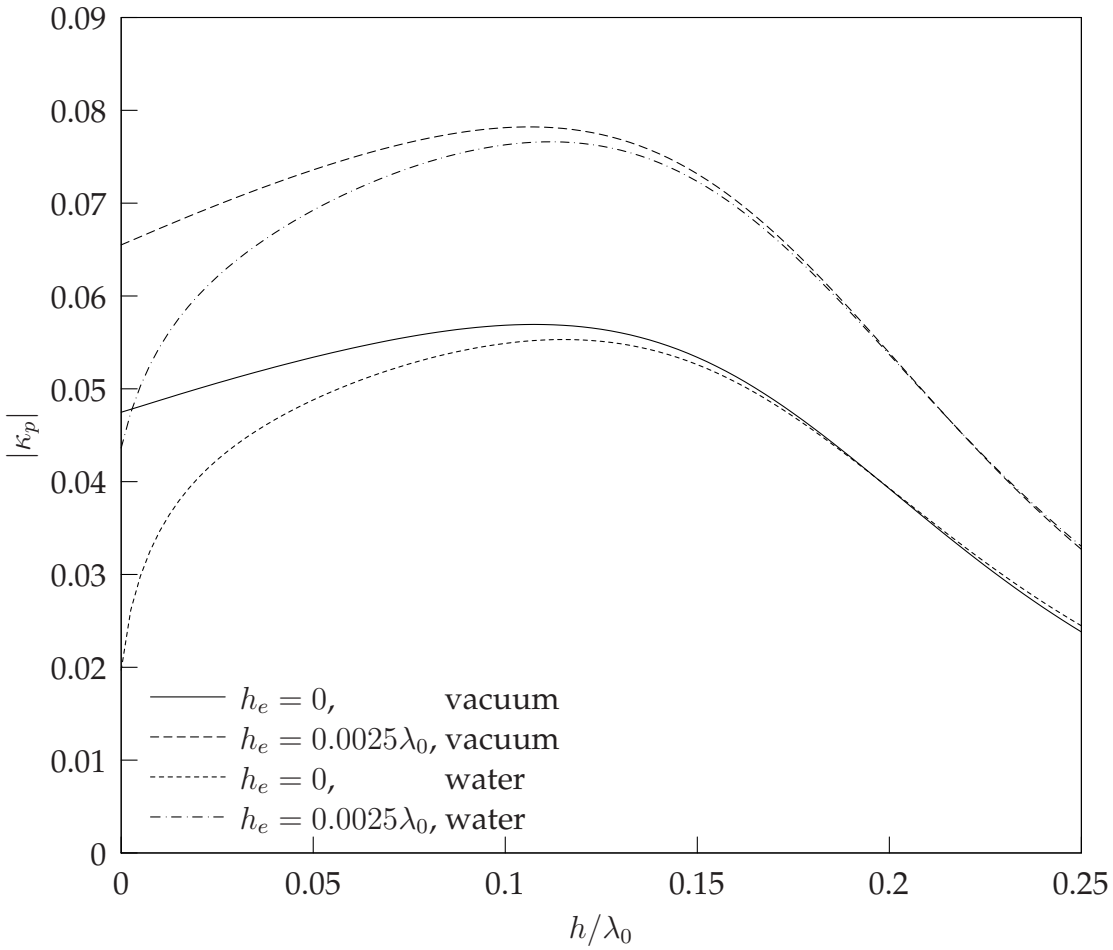

Figure 4.12: Variation of normalised reflection parameter κ_p with layer thickness

between the thick and thin electrode models is not significant, and can be attributed to the thick electrode model having effectively higher layer thickness. On the other hand, liquid loading can be seen to have an enormous impact on the capacitance of a non-layered device. As the layer thickness is increased a greater shielding effect is observed, and the capacitance approaches the same asymptotic limit as the case without liquid loading.

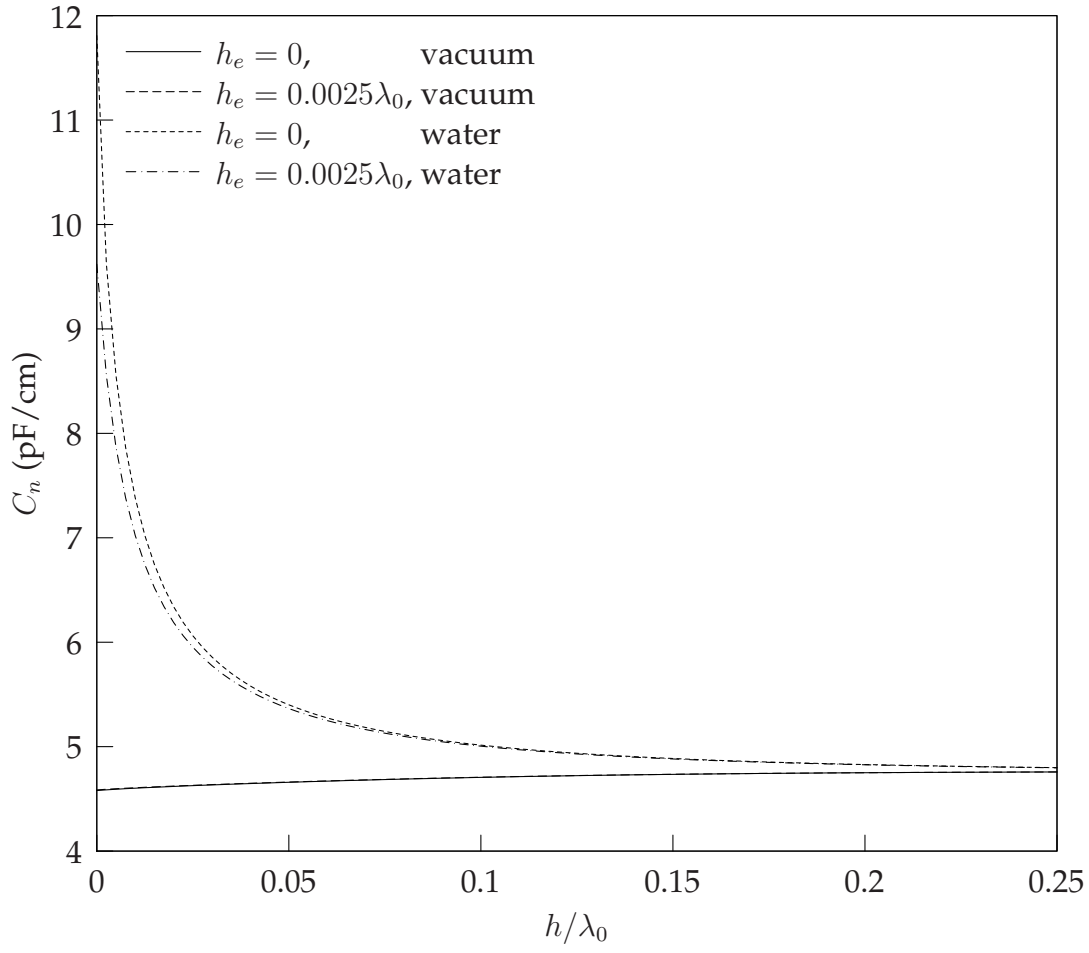

Figure 4.13: Variation of normalised capacitance C_n with layer thickness

Figure 4.14 shows attenuation parameter γ_p as a function of layer thickness. The calculations used to derive this figure include attenuation due to PSAW leakage and viscous losses in liquid, however attenuation due to scattering or absorption losses in the guiding layer is not included. Electrode resistivity is also neglected, however it can be calculated separately and included in an extended COM/P-matrix model (see Section 4.3.2), or approximated by a lumped resistance.

It can be seen from Figure 4.14 that a thicker guiding layer and thick electrodes both

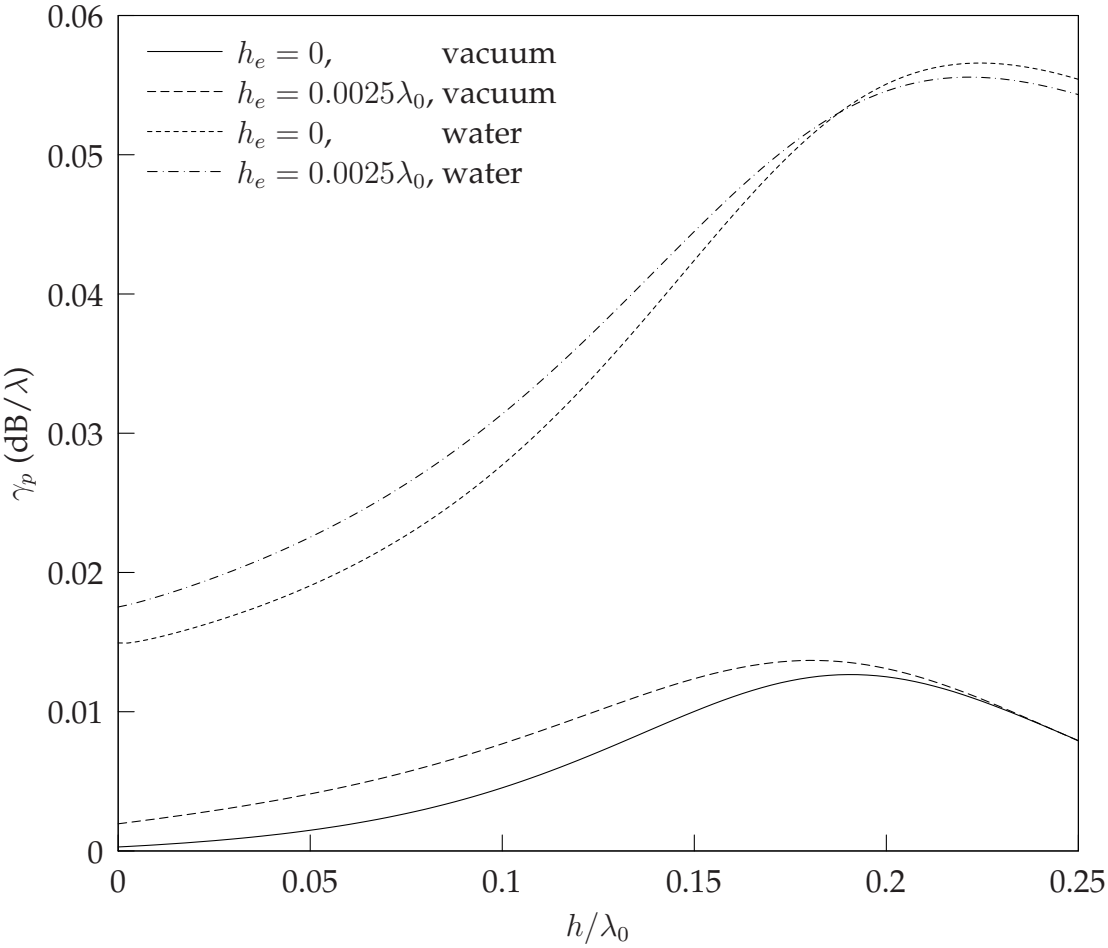

Figure 4.14: Variation of normalised propagation loss γ_p with layer thickness

increase attenuation, with a maximum around $h/\lambda_0 = 0.2$. This is due to the nature of the PSAW mode which propagates on $LiTaO_3$. The 36°-Y cut with X-axis propagation is commonly used because at this particular orientation the leakage of energy into the substrate is at a minimum. The guiding layer and electrodes disturb the boundary conditions, thus perturbing the structure from this minimum loss state. However, under liquid loading conditions there are much more significant attenuation mechanisms due to viscous losses. As the PSAW mode propagating has quasi-SH polarisation, some attenuation will also be due to radiation into the liquid. It can be seen that these losses also increase dramatically with increasing layer thickness. As was discussed in Section 2.7.3, higher mass sensitivity is strongly correlated with viscosity sensitivity. By comparison with the mass sensitivity shown in Figure 4.15, it can be seen that this correlation exists here.

Figure 4.15 shows the mass sensitivity as a function of guiding layer thickness. The sensitivity of the free and metallised surface velocities are calculated using the procedure given in Section 3.3.3. It can be seen that the mass sensitivity of the free and metallised surface velocities differ significantly. At low layer thickness the metallisation has a sensitivity enhancing effect, as it attracts the wave towards the top surface ($x_3 = h + h_e$). For large thicknesses the the wave is attracted towards the substrate-layer interface and away from the top surface, thus the sensitivity is higher in the free surface case.

The sensitivity of the resonant frequency is calculated from the change in f_r with mass loading, using the techniques developed in this chapter. Both the thin electrode approximation and the author's novel technique for dealing with mechanical electrode interactions are used in the calculations. These results show that the sensitivity of the metallised surface velocity to mass loading is an excellent measure of the sensitivity of the resonant frequency as calculated by the COM model. The result is that the mass sensitivity analysis which was performed in Section 3.3.3 for delay line devices is also applicable to resonator sensors.

The change in sensitivity between the thick electrode model and thin electrode model is not large for this electrode thickness. This might suggest that the periodic model developed in this chapter provides no extra information about the sensor per-

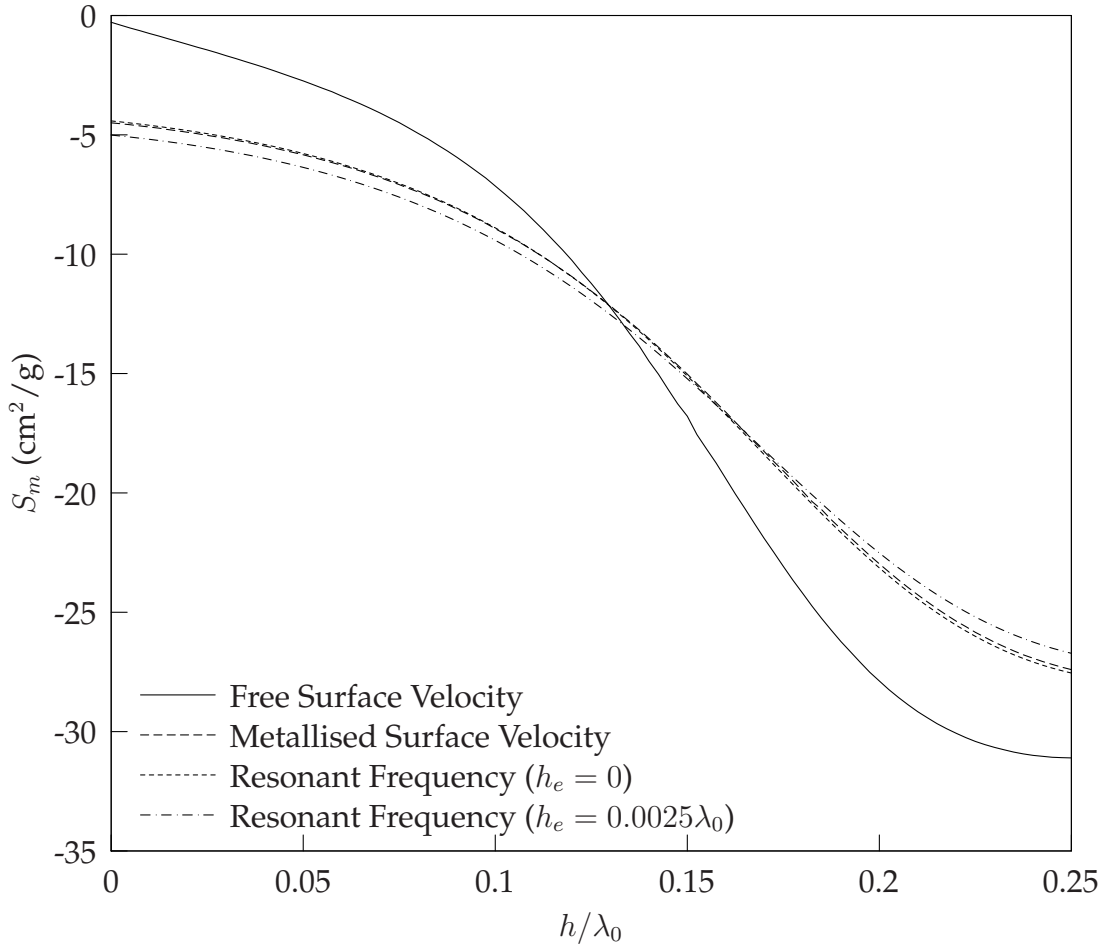

Figure 4.15: Variation of mass sensitivity in vacuum with layer thickness

formance. However, it will be shown in Section 4.3.2 that this periodic analysis is an excellent tool for calculating the device frequency response, which cannot be calculated via the techniques outlined in Chapter 3. In Chapter 6, when the question of inhomogeneous mass-loading of the device surface is considered, it will be shown that the periodic analysis developed here is an essential tool.

It was found that the mass sensitivity showed little variation with the number of pulse functions and harmonics used. However, the same number of functions needed to be used for the case with and without mass, otherwise quite spurious results were produced.

Figure 4.16 compares the mass sensitivity in liquid with the mass sensitivity in vacuum. The technique is identical to the case for vacuum, except that the dielectric constant of the mass loading layer is set to that of the liquid, to ensure that there is no dielectric contribution to the sensitivity. This analysis is conducted for both the free surface velocity and for the resonant frequency of the array using the full electrode model. It can be seen that the results are generally similar between vacuum and liquid media. The strongest difference is in the sensitivity of the free surface velocity at low thickness. This difference is not observed in the metallised surface velocity sensitivity (which has been omitted for clarity) or in the sensitivity of the resonant frequency.

As was discussed in Section 3.3.2, the parameters of the perturbing layer were carefully chosen in order to yield the same results as the analytical solution. However, the most important reason for taking this approach is because no analytical solution is available for the quasi-SH polarised PSAW mode. In the case of vacuum media, it was shown that if the additional layer has properties which differ from the idealised case, then the sensitivity will differ, and these considerations also apply to the liquid media case. In addition, there is a factor described in equation (2.25) which indicates that the properties of the guiding layer, mass loading layer and liquid media interact in a nonlinear fashion to influence mass sensitivity in liquid media.

Finally, the properties of the analyte itself need to be considered, since for many liquid media sensing applications large, complex molecules are being detected. These materials are not necessarily well represented by a continuum model as used here. In particular, viscous wave penetration depth into the surrounding liquid medium [136]

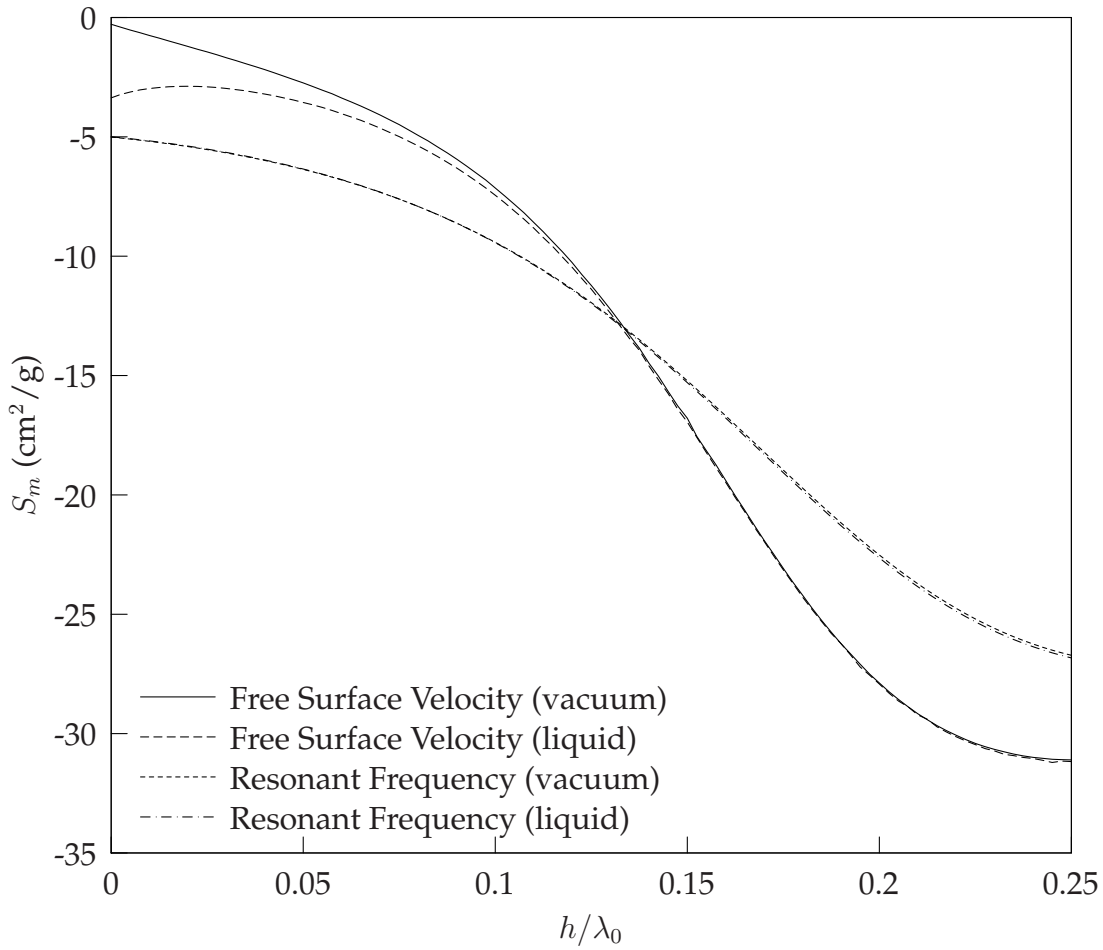

Figure 4.16: Variation of mass sensitivity in vacuum and liquid with layer thickness

means that the mass is not rigidly coupled to the device surface, as assumed here. The result of all these effects is that *mass sensitivity in liquid media should be understood as a purely qualitative tool for comparing between acoustic wave sensors, and yields only limited information regarding the response observed in a real experiment*. In light of this statement, and the observed similarity of the mass sensitivity curves for the vacuum and liquid media cases, it would be valid to consider the mass sensitivity calculated in vacuum media as being applicable to both gas and liquid media.

4.3.2 Frequency Response of SAW Sensors

In the previous sections, a COM model was developed for layered SAW resonator sensors, and the change in the COM parameters due to a guiding layer and liquid has been characterised. Once the parameters of the COM model are have been found, they can be used to calculate 2-port parameters of an acoustic wave device. The first step is to convert the COM parameters into a P-matrix form, since this allows device sections with differing properties (e.g. IDTs and reflective arrays) to be cascaded to form a complete device response. Referring to Figure 4.17, a P-matrix is a 3-port description relating voltage, current and acoustic wave amplitude:

$$\begin{bmatrix} w_{r1} \\ w_{r2} \\ I \end{bmatrix} = \begin{bmatrix} P_{11} & P_{12} & P_{13} \\ P_{21} & P_{22} & P_{23} \\ P_{31} & P_{32} & P_{33} \end{bmatrix} \begin{bmatrix} w_{i1} \\ w_{i2} \\ V \end{bmatrix}, \tag{4.56}$$

where w_i are the incident acoustic wave amplitudes at ports 1 and 2, V is the bus-bar voltage, w_r are the reflected acoustic wave amplitudes at each port and I is the bus-bar current. A P-matrix is created for each homogeneous section of the device, such as an IDT, short circuit grating or gap. For structures other than IDTs port 3 does not exist, thus the P-matrix will be 2×2 for reflective gratings and gaps.

For an IDT of length L (which must be an integer multiple of λ_0) the following

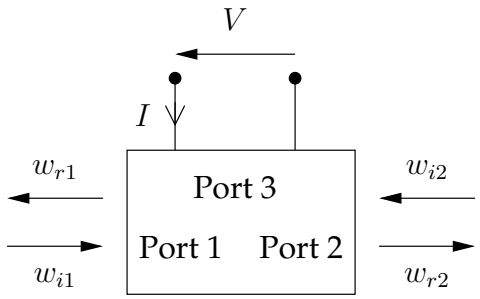

Figure 4.17: P-matrix basic block

equations are used to determine the elements of the P-matrix [40]:

$$P_{11} = \frac{j\kappa \sin(\hat{q}L)}{\hat{q}\cos(\hat{q}L) + j\delta \sin(\hat{q}L)}. \tag{4.57a}$$

$$P_{12} = \frac{(-1)^N \hat{q}}{\hat{q}\cos(\hat{q}L) + j\delta \sin(\hat{q}L)}. \tag{4.57b}$$

$$P_{13} = -\alpha L \frac{\sin(\hat{q}L/2)}{\hat{q}L/2} \frac{(\delta+\kappa)\sin(\hat{q}L/2) - j\alpha\hat{q}\cos(\hat{q}L/2)}{\hat{q}\cos(\hat{q}L) + j\delta\sin(\hat{q}L)}. \tag{4.57c}$$

$$P_{33} = -\frac{4\alpha^2(\delta+\kappa)}{\hat{q}^3} \frac{(\delta+\kappa)[1-\cos(\hat{q}L)] - j\hat{q}\sin(\hat{q}L)}{\hat{q}\cos(\hat{q}L) + j\delta\sin(\hat{q}L)} - j\frac{4\alpha^2}{\delta-\kappa}L + j\omega CL. \tag{4.57d}$$

The COM parameters used here are de-normalised, so they take into account the aperture width of the device. In addition, there are a number of simple relationships to determine the other elements:

$$P_{21} = P_{12}. \qquad P_{22} = P_{11}. \tag{4.58a}$$

$$P_{23} = (-1)^N P_{13}. \qquad P_{31} = -2P_{13}. \qquad P_{32} = -2P_{23}. \tag{4.58b}$$

A short circuit grating has identical elements, except only elements P_{11}, P_{12}, P_{21} and P_{22} are used. For an open circuit grating, the following parameters are used:

$$\delta_{oc} = \delta - \frac{2\alpha^2}{\omega C}. \tag{4.59a}$$

$$\kappa_{oc} = \kappa + \frac{2\alpha^2}{\omega C}. \tag{4.59b}$$

These are then substituted for δ and κ in equation (4.57), and the P-matrix parameters are calculated as for the short circuit grating. For a free surface or metallised surface gap of length L (which need not be a multiple of the electrode period), only the following elements of the P-matrix are non-zero:

$$P_{12} = P_{21} = \exp(j\omega s_{f,m} L). \tag{4.60}$$

Once all these P-matrix elements have been calculated, they can be combined to give the complete device response. Figure 4.18 shows a configuration which is general enough to include any device configuration of interest in this thesis, particularly 2-port resonators. Using techniques described in [137], the IDT and reflective grating can be

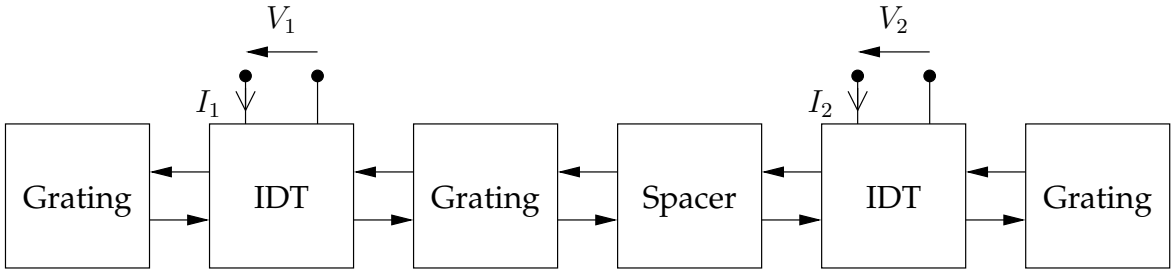

Figure 4.18: Combination of P-matrix elements to simulate complete device

combined into a single transmission matrix. All other elements can be converted into transmission matrix form, and cascaded analytically to yield transmission, admittance, impedance or scattering parameters of the structure as desired.

Since the periodic Green's function model does not include electromagnetic parasitic elements, these need to be included by some other model. The value of these elements can be calculated using electromagnetic packages based on methods such as FEM, FDTD or MOM. However, it is likely that there will be effects in the complete system such as the micro-fluidics and packaging which cannot be easily included. Thus for most purposes it is adequate to empirically add external circuit elements to match the observed response. This approach will be discussed further in Chapter 5. A noted exception is the case of electrode resistance, which can be calculated if the sheet resistance R_s of the electrode material is known. In this case the following substitutions can be made [40]:

$$r = \frac{2W}{3l} R_s \lambda_0. \tag{4.61a}$$

$$\alpha' = \frac{\alpha}{1 + j\omega C r}. \tag{4.61b}$$

$$\delta' = \delta - \frac{2jr|\alpha|^2}{1 + j\omega C r}. \tag{4.61c}$$

$$\kappa' = \kappa + \frac{2jr\alpha^2}{1 + j\omega C r}. \tag{4.61d}$$

$$C' = \frac{C}{1 + j\omega C r}. \tag{4.61e}$$

These values are then substituted into the P-matrix elements of equations (4.57) and (4.58). This COM/P-matrix based analysis will be applied in Chapter 5 to the resonator devices designed by the author. The frequency response of the designed devices will be calculated and compared with measured values.

4.4 Conclusion

In this chapter a model based on the periodic Green's function was presented for layered SAW resonators operating in liquid media. New developments were made by the author to account for the mechanical influence of electrodes buried within layered media, and results were compared with a simpler model assuming infinitesimally thin electrodes. The two approaches were shown to yield significantly different results for reflection, and to a lesser extent for other parameters. Much of this difference diminished for large layer thickness, however such large thicknesses are typically impractical for large scale fabrication. Thus, the technique developed by the author advances the understanding of layered SAW resonator structures in liquid media, and is important for achieving high accuracy.

It was shown that the spectral domain Green's function presented in Chapter 3 is an essential building block for this periodic Green's function. The admittance curve resulting from this periodic Green's function can be expressed in terms of a few analytical parameters from the COM model, using an extraction technique. It was shown how the COM parameters may be combined to yield a complete device response. In Chapter 5, these techniques will be applied to the design of a layered SAW resonator sensor, and the fabrication of this device will be described.

Chapter 5

Design and Fabrication of SAW Resonator Sensor

5.1 Introduction

In this chapter the processes used to design and fabricate the layered SAW resonator sensors are described. Firstly, in Section 5.2 it will be shown how the techniques developed in Chapter 4 can be applied to the design of a SAW device. This will be followed in Section 5.3 by a description of the processes used in fabrication of this device. This device will be utilised in Chapter 6 for experiments on the variation of mass sensitivity across the device surface.

5.2 Design of Resonator

The basic device layout is that presented by Avramov [7], however the analysis used in this thesis differs because of the need to take into account the layered media. The structure used is presented in Figure 5.1. The basic elements of this structure are the reflective gratings, which form the resonant cavity by reflecting acoustic waves, the IDTs, which are responsible for launching and detecting acoustic waves, and the trapping grating, which ensure that acoustic energy in the cavity is well confined to the surface. The trapping grating has a different period to the IDTs and reflectors to ensure that energy is not substantially reflected at centre frequency. Between the trapping grating

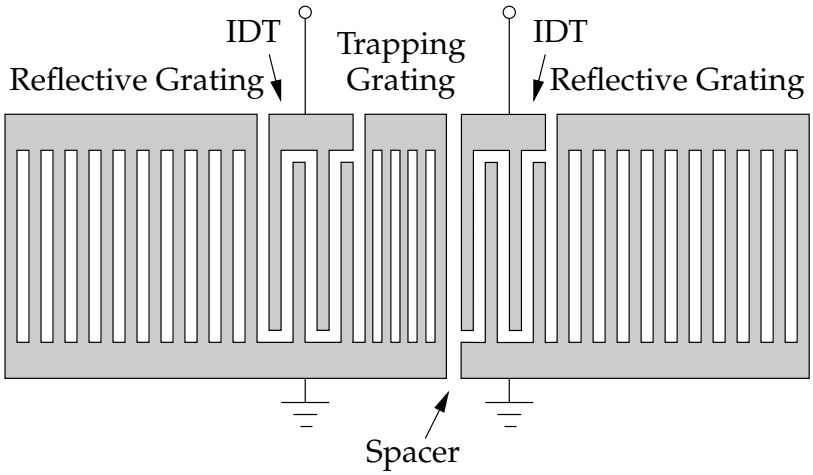

Figure 5.1: Layout of 2 port resonator

and one of the IDTs there is a small spacer (less than the period of the IDT), which is adjusted to give fine control over the location of the main resonant peak within the stop-band.

In selecting the design of the SAW resonator, the following criteria are used:

- There must be sufficient electrodes in the grating to reflect the majority of acoustic energy, thus ensuring that insertion loss is minimised and Q-factor is maximised.
- The total device size should be small enough to fit into the pre-existing liquid cell of approximately 5×13mm.
- There is a limit on the useful number of reflective electrodes, as acoustic losses in the array mean that the reflectivity cannot be made arbitrarily close to unity.
- There should be a single dominant resonant mode at which the device will oscillate, to prevent the possibility of mode-hopping causing random jumps in the frequency output signal
- The input admittance should be sufficient to ensure low insertion loss, without being too high so as to cause the loaded Q-factor of the device to be heavily reduced in circuit
- Device design should be applicable to a variety of layer thickness choices and layer materials

Table 5.1: Parameters of SAW resonator design

IDT electrodes	16
Reflector electrodes	120
Grating electrodes	20
Spacer Length	9.25µm
IDT Period	20µm
Grating Period	18.5µm
Metallisation Ratio	0.5
Aperture Width	350µm

Since all these criteria are inter-related, and a change in design parameters can affect any of them, it is not possible to define a specific procedure to design the device layout. Instead, engineering judgement has been used to find a compromise between all these requirements. Table 5.1 summarises the design parameters which were chosen for the device in order to meet the above criteria. Note that the periods quoted are for $\lambda_0 = 2p$, and that the number of electrodes is quoted, not the number of electrode pairs. The IDT period of 20µm was chosen to yield a centre frequency of approximately 200MHz, with 16 electrodes found to provide a good compromise between loaded Q-factor and insertion loss.

The S-parameters are calculated for the designed device in the non-layered case. Some care needs to be taken in applying the author's full electrode model to the case where the material between electrodes is a vacuum with $c = [0]$ and $\rho = 0$. Examining equation (4.33), it can be seen that in this case the elements of matrix $\mathcal{M}_{12}$ become infinite, and unlike the other $\mathcal{M}$ matrices this behaviour cannot be corrected by taking a limit as the elements of c approach zero.

However, by taking numerical values for the elements of c which are much less than those of the electrodes, it is expected that the results would be sufficiently accurate. To verify this, the variational electrode model presented by Biryukov (see reference [82] and Section 2.4.3) was also used. For comparison the response predicted by using the thin electrode approximation is also included. The magnitude of all three modelled

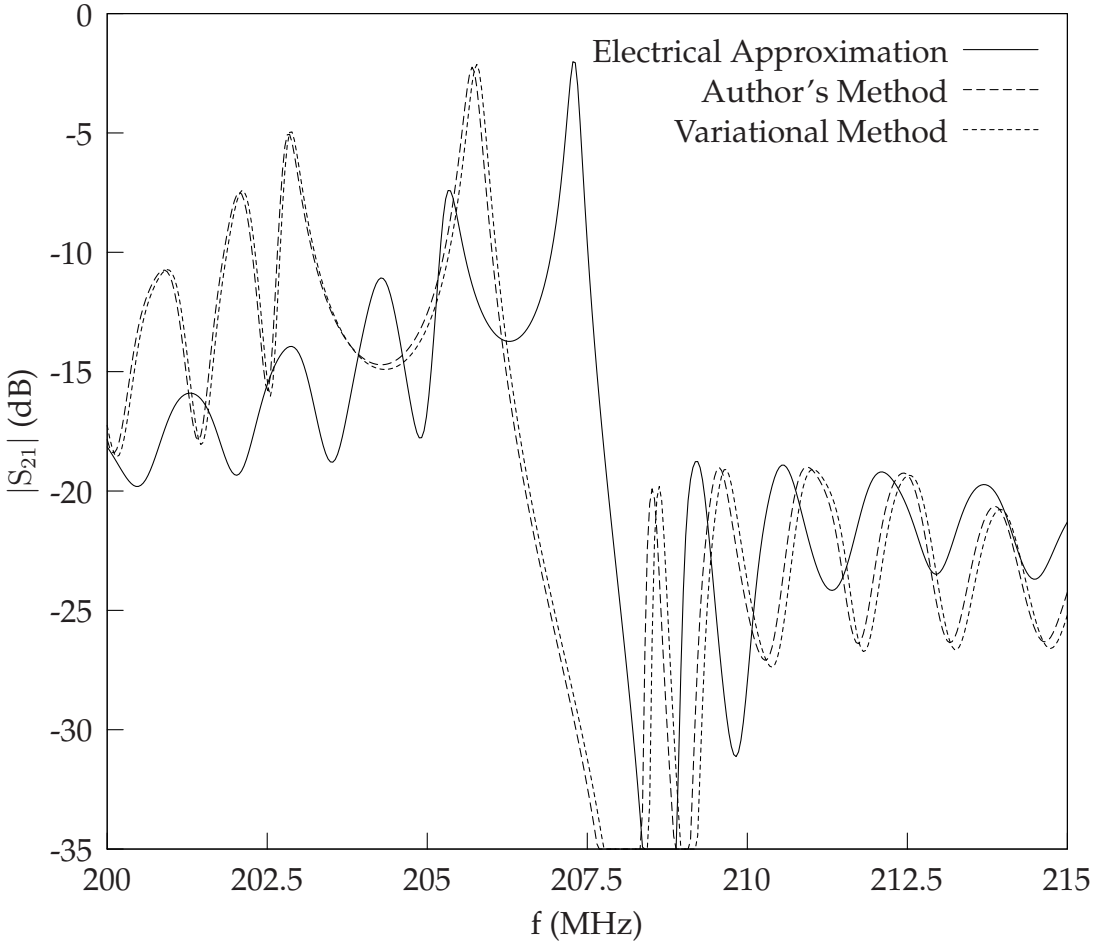

Figure 5.2: Transmission response of SAW resonator design

versions of S_{21} are given in Figure 5.2. It can be seen that the agreement between the author's approach and the variational model is very good, whilst the electrical approximation differs significantly in the location of the resonant frequency, and the relative position of the nearby peaks.

5.3 Fabrication of Devices

In this section the process used to fabricate the layered SAW resonator structures is described. The designs developed here were implemented using CAD layout tools, and the mask was fabricated by external contractors using electron beam lithography. The devices were fabricated in a dual configuration to allow viscosity, temperature and non-specific interactions with the sensor surface to be compensated for. The layout of the pads was designed for compatibility with an existing SAW measurement jig.

All fabrication performed by the author was undertaken within the Microelectronics and Materials Technology Centre (MMTC) clean-room and vacuum laboratory facilities at RMIT University. In this work, samples were diced before fabrication to allow the greatest flexibility in utilising the wafers. However, this has the disadvantage of increasing misalignment error, where the propagation direction of the fabricated device differs slightly from the desired crystal axis. Devices without a guiding layer were also fabricated in larger scale by an external contractor for use in the work of the Microtechnology CRC. These devices were used for the work in this and the next chapter, since the repeatability between devices was found to be better.

5.3.1 Deposition and Patterning of Electrodes

The gold electrodes were deposited by MMTC staff using electron beam evaporation, having thickness of 0.8µm. A 0.2µm Ti layer was deposited first in order to obtain good adhesion to the substrate. Gold was chosen as it is highly inert, which greatly enhances its usefulness in a sensing environment where the device cannot be isolated from potentially damaging liquids.

To pattern the electrodes, a layer of AZ1512 photo-resist was first spin-coated over the device surface, then baked at 100° C. A difficulty which occurs during this procedure is the pyroelectric charging which can occur when $LiTaO_3$ samples are raised to high temperature. This can cause a discharge, which can damage the electrodes. Although this is not usually sufficient to prevent the device from functioning, it can have a great impact on the repeatability of device performance.

The photo-resist coated devices were then exposed to ultra-violet radiation using a mask aligner, and developed in 1:4 AZ400K:H_2O solution for 15 seconds. After a 20 minute post-bake, the gold layer was etched using a 94:6 H_2O:"Technistrip" solution (17% Potassium Cyanide), followed by a thorough rinsing under water. The Ti adhesion layer was then etched using a 1.5:98.5 HF:H_2O solution. Photo-resist was then stripped by immersion in heated AZ100 for 20 minutes, followed by a rinse in de-ionised water.

5.3.2 Deposition of Guiding Layer

The guiding layer materials SiO_2 and ZnO were deposited by the author using RF magnetron sputtering. The sputtering parameters used for the ZnO layer are given in Table 5.2, and those for SiO_2 are given in Table 5.3.

Table 5.2: Sputtering parameters for ZnO layer

RF Power	140W
Sputtering Gas	40% O_2, Ar Balance
Sputtering Pressure	1×10^{-2} Torr
Base Pressure	$\sim 1 \times 10^{-5}$ Torr
Sample Distance	50mm
Substrate Temperature	270° C

Table 5.3: Sputtering parameters for SiO_2 layer

RF Power	140W
Sputtering Gas	10% O_2, Ar Balance
Sputtering Pressure	1×10^{-2} Torr
Base Pressure	$\sim 1 \times 10^{-5}$ Torr
Sample Distance	50mm
Substrate Temperature	180° C

Sputter deposition was performed by the author using parameters obtained from standard procedures used by other researchers working in the MMTC facilities. The temperature given in the tables is the temperature to which the sample was raised before sputtering commenced, and which the temperature controller was set to during sputtering. In the case of SiO_2 deposition the temperature increased due to the sputtering process. The system uses a ceramic target with diameter of 100mm.

Layers of ZnO were deposited on delay line structures for the analysis described in Section 3.3.3. For the verification of the author's model for resonator structures, it was

decided to use SiO_2 instead, as it's isotropic nature simplifies the analysis. In addition, it is a highly inert and well-studied material.

Following the deposition of guiding layer, it was necessary to pattern it in order to expose the electrical contact pads for connection to an external circuit. The photolithography process was performed in a similar manner to that used for the electrode patterning. To etch the ZnO layer, a solution of 1:10 HNO_3:H_2O was used, whereas for the SiO_2 layer a solution of 1:19 HF:H_2O was used.

5.4 Comparison of Measured and Calculated Frequency Response

Having fabricated the device, it is necessary to check whether its frequency response matches the predictions of the model. For the calculation of COM parameters, the periodic Green's function analysis was performed with $M = 15$ pulse function and $2L + 1 = 35$ harmonics. These numbers were determined by modifying them until no significant change was observable in the frequency response of the device.

5.4.1 Non-Layered Device

Since the guiding layer represents an additional source of uncertainty, the comparison is first made for a non-layered device. By examining the device under a microscope, it was found that the metallisation ratio of the fabricated was in fact 0.55, instead of the designed value of 0.5. As the device has both Ti and Au metal layers, their transmission matrices were cascaded, as discussed in Section 4.2.2.

The layout of the measurement jig resulted in some electromagnetic feed-through. A procedure was used during the measurements which calibrated the S-parameter measurements up to the SAW device, using custom-built open circuit, short circuit, matched 50Ω and through-line components. However, using such a calibration procedure it is not possible to eliminate the feed-through signal from the measurements. Instead, the S-parameters of the empty jig were measured after calibration, and converted into Y-parameters. These Y-parameters were added to the calculated Y-parameters

of the SAW resonator, thus placing the feed-through response in parallel with the SAW device's response.

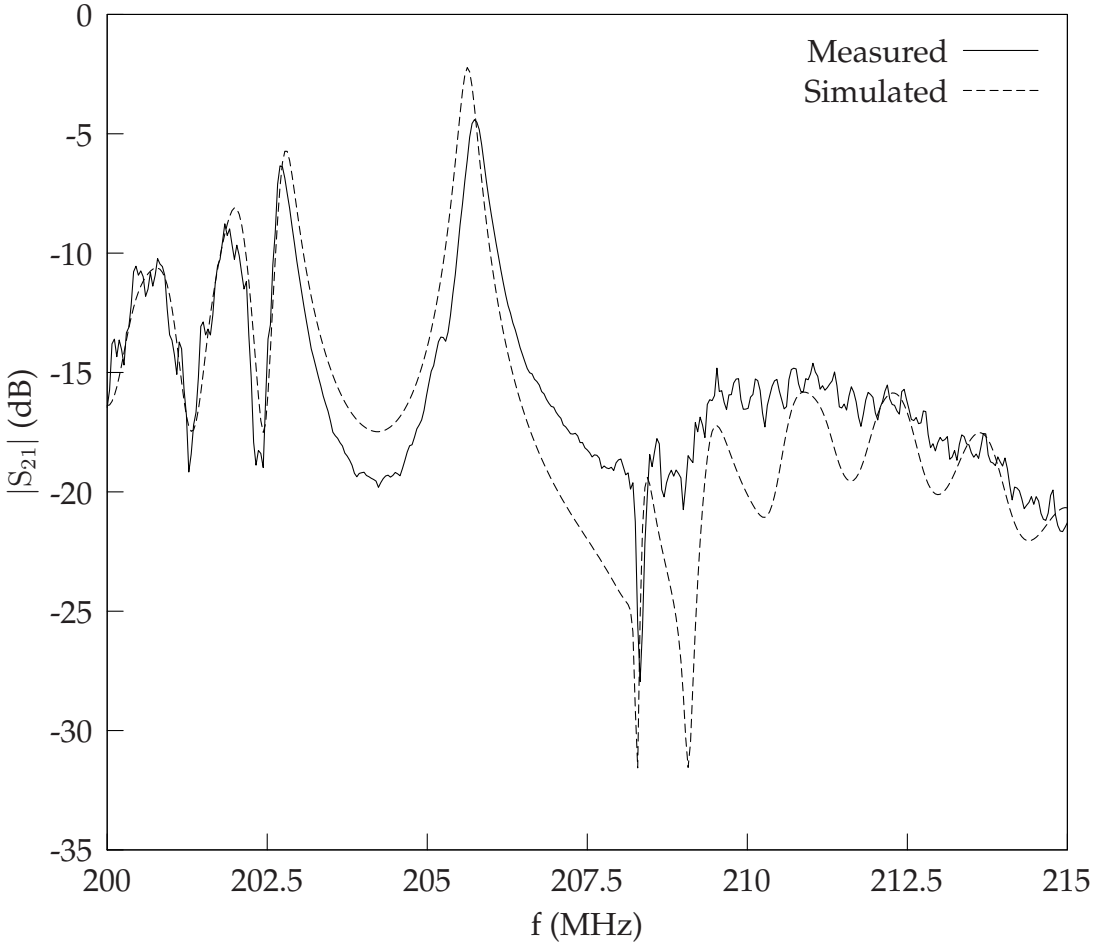

Figure 5.3: Transmission response of non-layered SAW resonator

Another parameter which was not included in the original design was the resistance of the electrodes. This can be included into the COM model using equation (4.61), however it requires that the value of the sheet resistance of the metal layer is known. Using 4-point probe measurements of thin film samples, the gold layer was found to have a sheet resistance of 0.45Ω. Incorporating all of these adjustments into the model, the S-parameters are compared with measured values in Figure 5.3. Similarly, the real part of the short circuit input admittance Y_{11} is plotted in Figure 5.4, and the imaginary part in Figure 5.5.

It can be seen that the agreement is generally good, but fails on a number of points. Firstly, the measured insertion loss at the resonant frequency is 2dB below the calculated value, and the real part of the measured input admittance at this frequency is

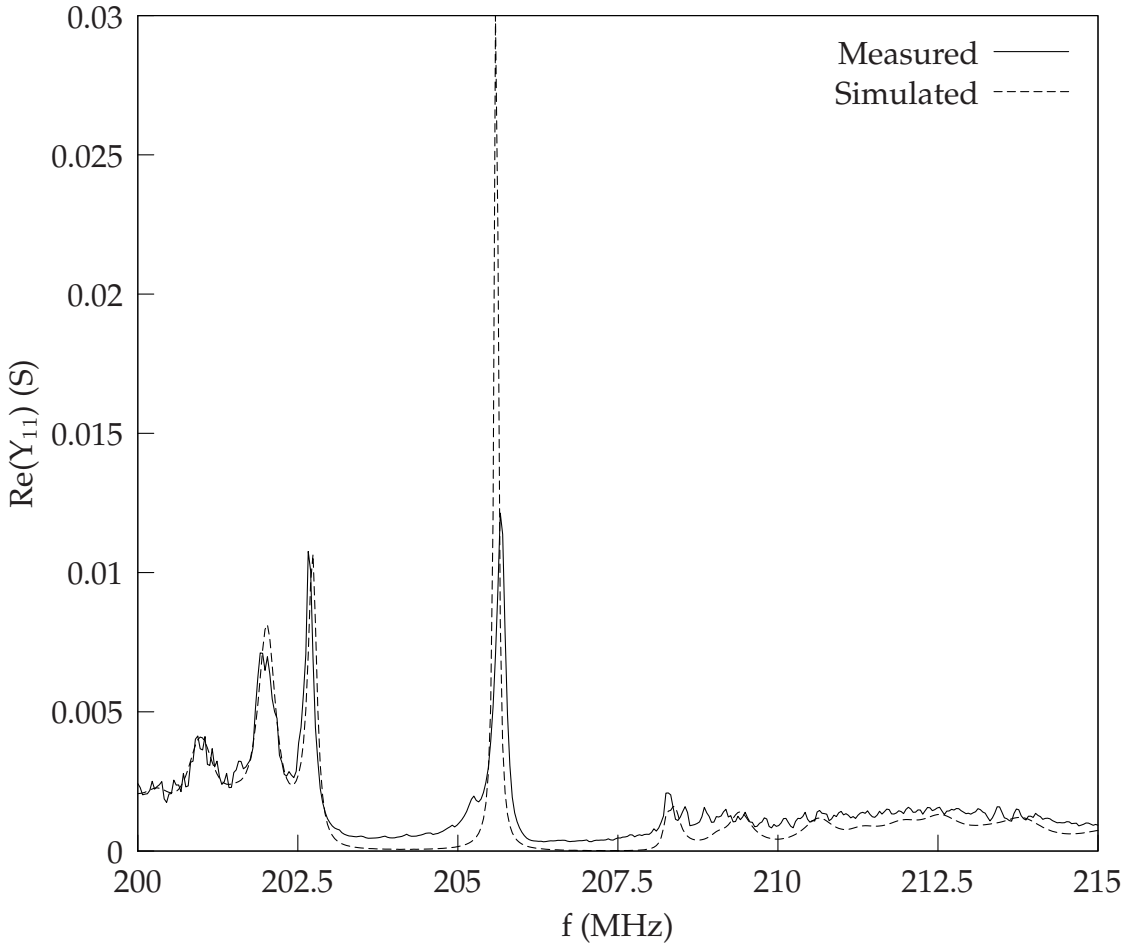

Figure 5.4: Real part of input admittance of non-layered SAW resonator

reduced by a factor of 2.5. This suggests that there are several loss mechanisms which have not been included in the model, as was discussed in Section 2.2.2. It is important to note that the excess attenuation observed experimentally cannot be modelled by simply increasing the COM attenuation parameter γ, since this reduces the agreement at all other frequencies. This suggests that acoustic losses in the gold layer are unlikely to be the cause, since this mechanism would not be so specific to a single resonant peak. A possible explanation is the conversion of surface trapped modes to SSBW, which is known to depend strongly on the location of the resonant peak within the stop-band [7]. It is possible that the lateral leakage of energy due to diffraction effects may have some influence, however with only a 2-dimensional model it is not possible to calculate the influence of this effect.

In addition, it can be seen that bulk-wave generation occurs at frequencies above 208MHz, which is not included in the COM model. However, since this is well above

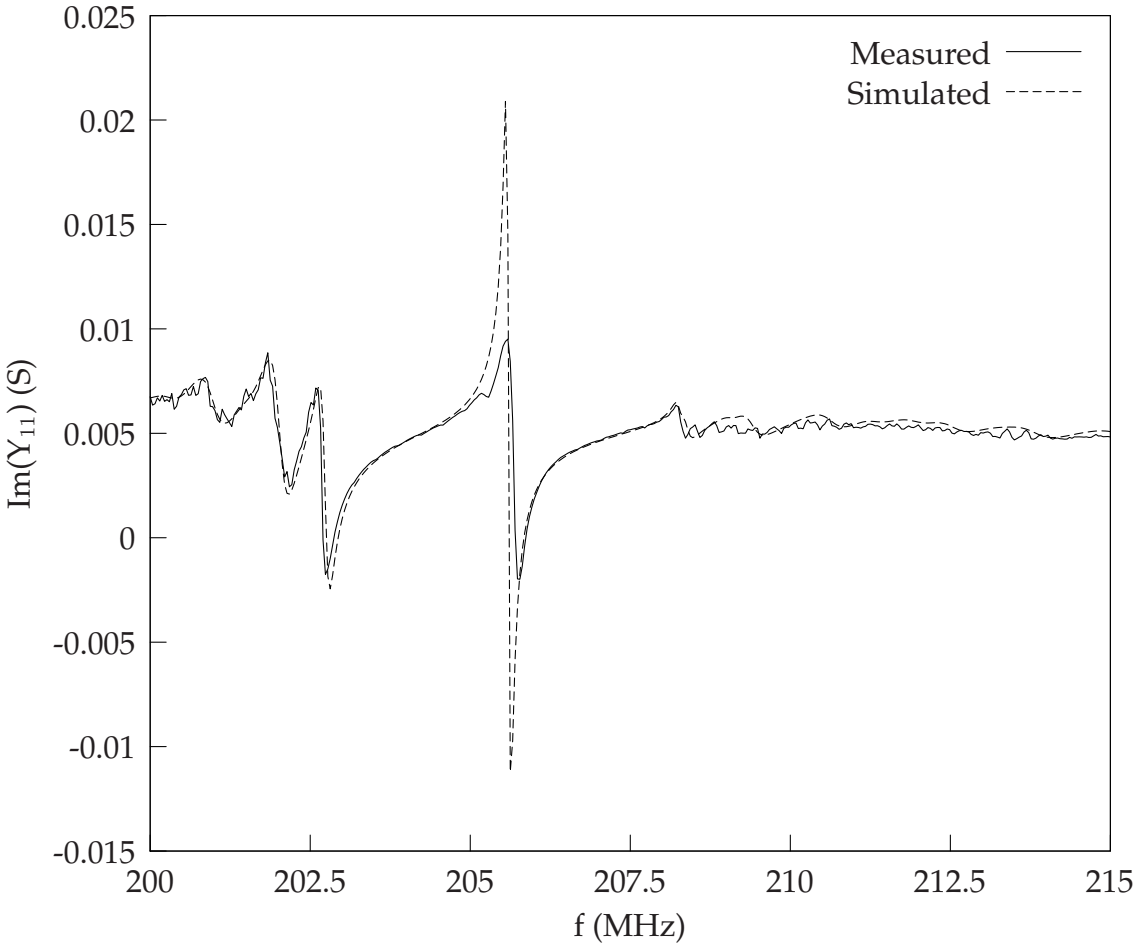

Figure 5.5: Imaginary part of input admittance of non-layered SAW resonator

the resonant frequency, the simplification of neglecting this bulk wave contribution is justified. At frequencies below resonance, some additional ripple is observed. This may be due to a combination of electromagnetic feed-through and reflections from the side and bottom of the SAW substrate. There is also disagreement in the region between the main resonance peak, and the next lowest peak, as well as between the resonant and anti-resonant frequencies. This is almost certainly due to the simple means of including the electromagnetic feed-through influence of the jig, since by comparison with Figure 5.2 it can be seen that these regions change the most when feed-through is included.

Finally, there was a disagreement in the imaginary component of Y_{11}, whereby it was lower than the measured value by an approximately constant factor across the whole measured bandwidth. This was rectified by adding an empirically determined capacitance of 2.2pF in parallel with the IDTs. This may be due to the influence of or

interaction between the measurement jig, tracks from the pads to the IDTs and the IDT bus-bars.

5.4.2 Layered Device

For the layered device, the agreement between theory and measurement was examined for a 0.4µm SiO_2 layer, since this is used for the measurements in chapter 6. For a layered device it is expected that the agreement would not be as good, because material constants for thin films tend to differ significantly from those of the bulk form. The values used for SiO_2 and ZnO are given in Appendix A and have been taken from other sources using similar deposition techniques. However this does not guarantee that identical results will be obtained, since the deposition conditions and apparatus are not identical.

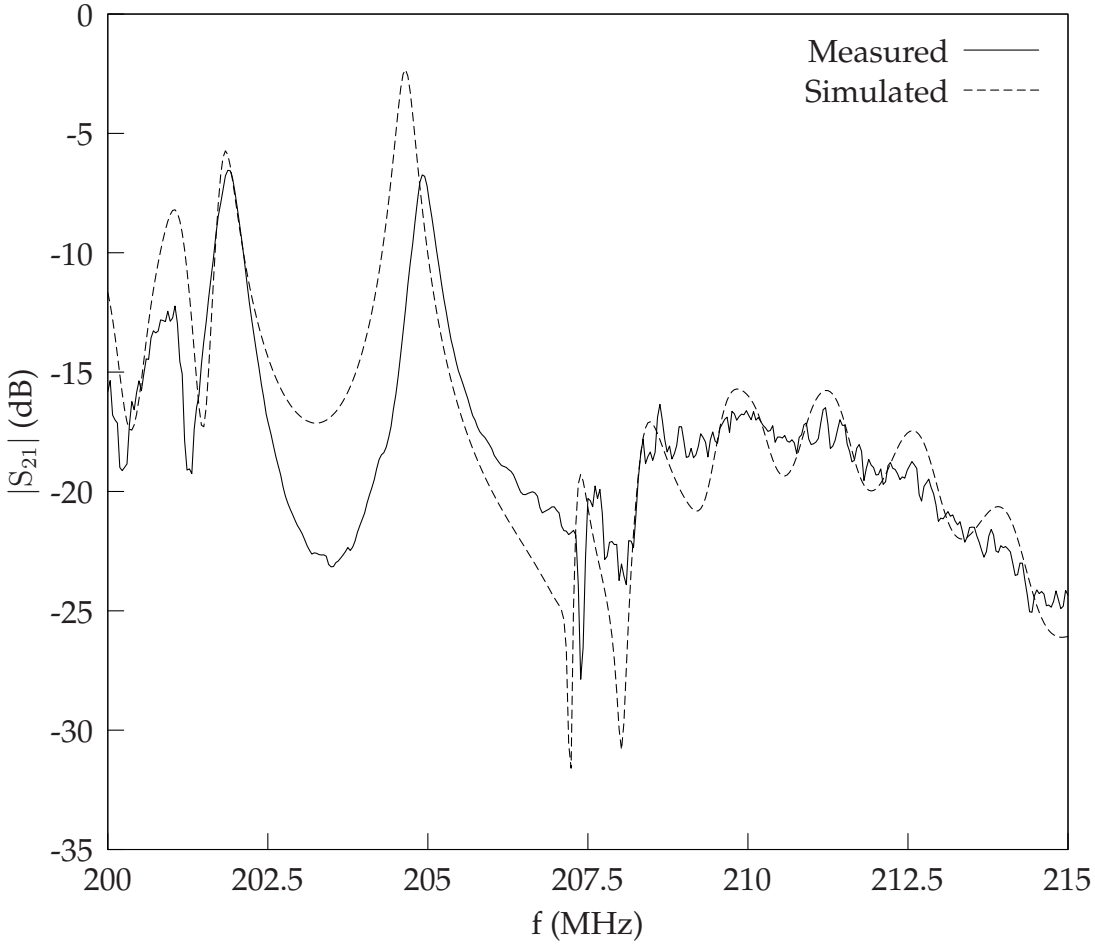

Figure 5.6: Transmission response of layered SAW resonator

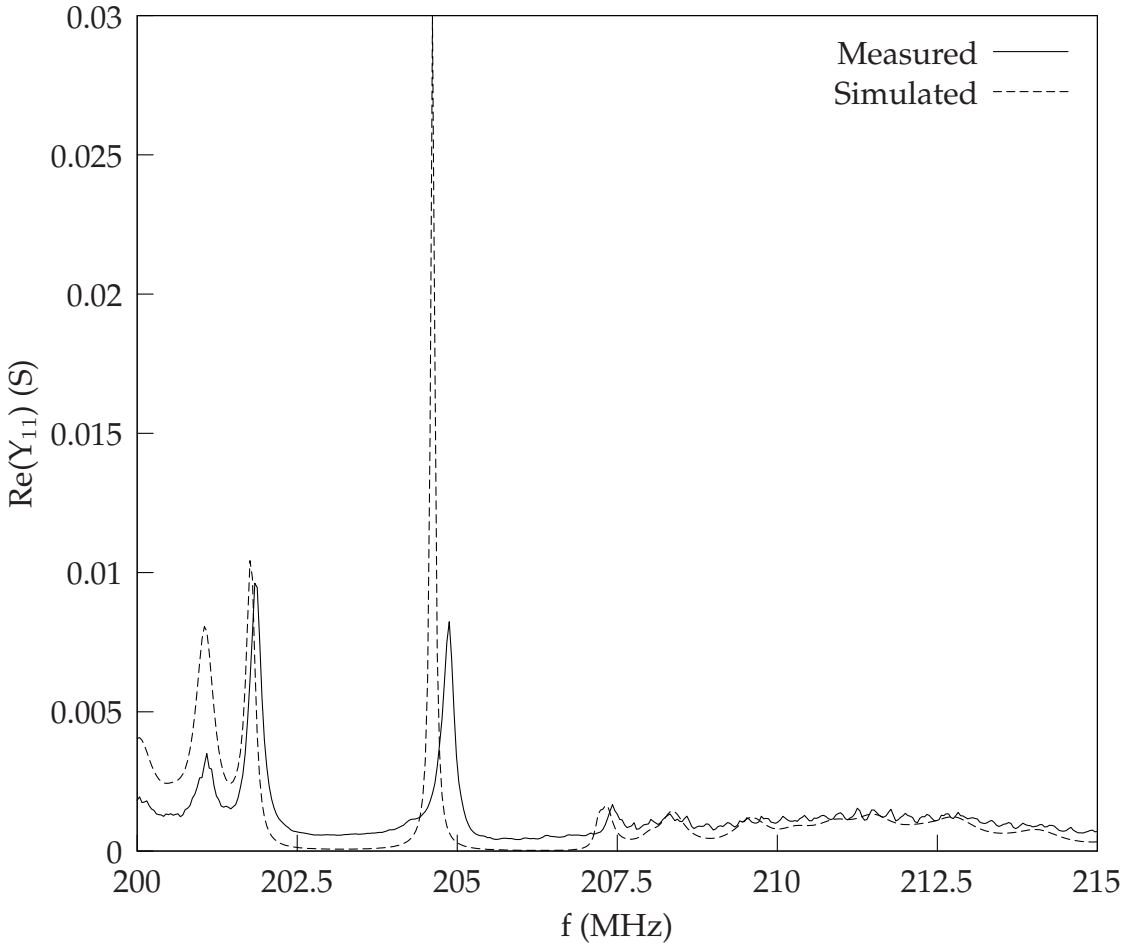

Figure 5.7: Real part of input admittance of layered SAW resonator

As with the non-layered devices, the influence of the measurement jig was included in the simulation, 2.2pF was added in parallel with each input IDT, the metallisation ratio was increased to 0.55 and the sheet resistance of the gold layer was included. The resulting S_{21} is plotted in Figure 5.6, while the real and imaginary parts of Y_{11} are plotted in Figures 5.7 and 5.8 respectively.

For the layered device it can be seen that the agreement is not as good as for the non-layered device. In particular, there is some error in the location of the main resonant peak, although the remaining features appear to be at the correct frequencies. The agreement of the height of the peaks is much poorer, as is the region between peaks. There is always some uncertainty of the parameters of thin film layer. However, this cannot explain the majority of the discrepancy, since changing the parameters of the layer changes the centre frequency, but has little effect on the shape and magnitude of the response. It should also be noted that in a layered device there is greater velocity

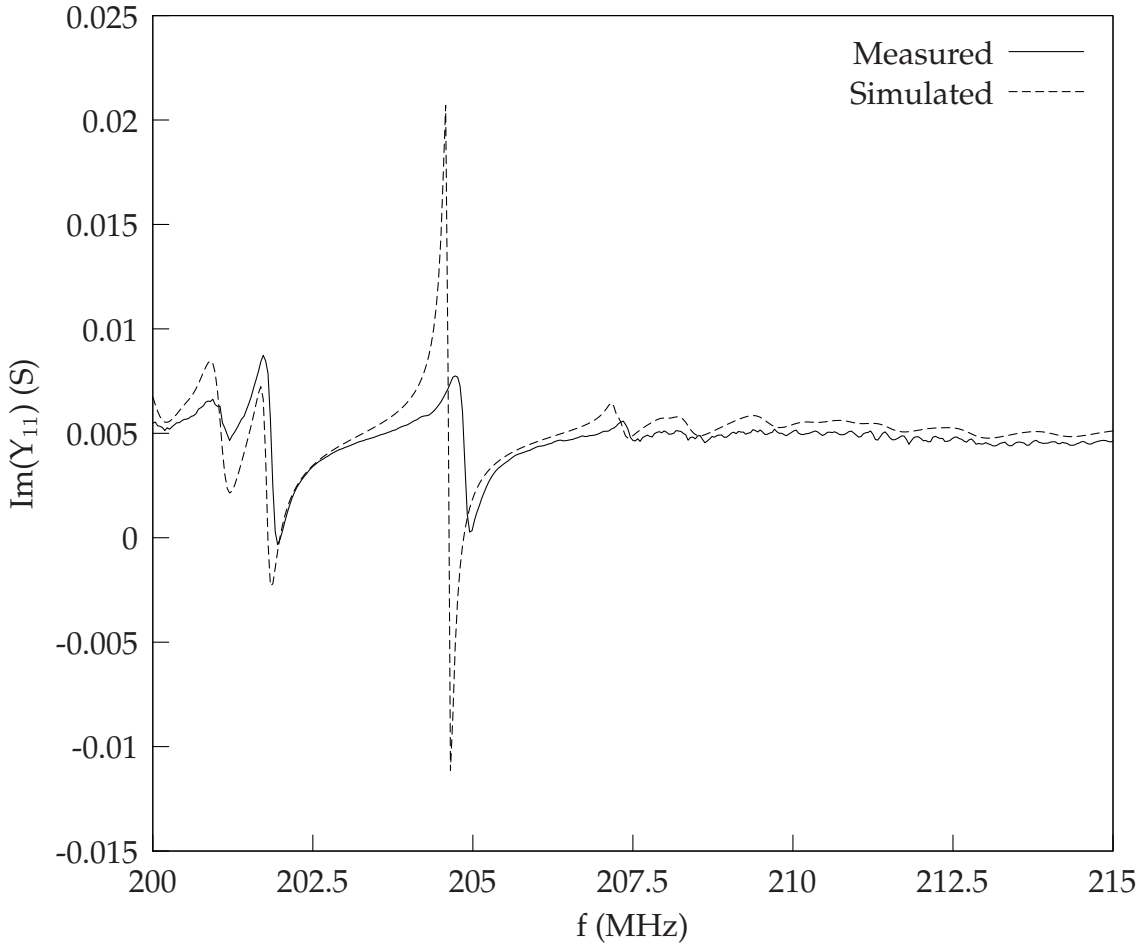

Figure 5.8: Imaginary part of input admittance of layered SAW resonator

dispersion, which is not included in the COM model used here. Finally, the possibility must be considered that some form of damage may be occurring to the layers during the fabrication process due to effects such as pyroelectric discharge.

5.5 Conclusion

In this chapter surface acoustic wave resonator sensors were designed using the tools developed in Chapters 3 and 4. The fabrication procedure used was described in detail. The scattering and admittance parameters of the devices were measured, and compared with the results of the author's modelling work. For non-layered devices the agreement was found to be good, with the sources of disagreement being understood. In the case of the layered devices there is less agreement between theory and measurement. The causes of this disagreement are less certain than in the non-layered

case. Possible causes include the influences of the measurement jig, errors in the material constants, the main resonant peak having some bulk wave characteristics and the influence of the tracks and pads.

However, despite the discrepancies, the technique is able to give a reasonable agreement as to the location of the resonant frequency. This is the most important factor in determining device sensitivity, thus it is expected to be sufficient for the analysis undertaken in Chapter 6. This analysis will be of the mass sensitivity of the fabricated devices, and how it varies across their surface.

Chapter 6

Sensitivity Distribution Across Device Surface

6.1 Introduction

As was shown in Chapter 2, existing models of the mass sensitivity of SAW sensors are based on the assumption that the response is due to the mass loading caused by a layer uniformly coating the device surface.

For delay line type SAW devices, there should be negligible reflections at points between input and output transducers, thus the delay is simply the accumulated phase change across the device surface due to the wave propagation. This means that the response should be independent of the location of mass loading. In [25] this was found to be true for mass loading in the region between the IDTs. However, in the same paper it was also shown that the mass sensitivity in the electrode regions can differ substantially from that in the region between electrodes. Since resonator structures are more complex than delay line structures, greater variation in mass sensitivity across the device surface would be expected. In particular, the acoustic energy is confined towards the centre of the device, thus it would be expected that mass loading at regions away from the device centre would have a reduced effect on the response.

It has been reported that most of the sensitivity of a SAW resonator can be attributed to a small region at the centre [138], and that a sample delivery system which concentrates the analyte on this small region in the centre can improve overall sensitivity of

the system [139]. However, no quantitative analysis was performed to characterise the sensitivity variation across the surface. The periodic techniques described in Chapter 4 will be employed to study this effect. The results of the author's novel model for mechanical electrode interactions in layered media will be compared with those from the simpler infinitesimal electrode approximation.

The implications of this surface sensitivity variation are particularly important in cases where only a small quantity of selective material is available, so that it can be placed on the most sensitive region of the SAW device. Similar considerations also apply when a limited amount of analyte is available. For example, in immuno-sensing applications expensive antibodies or antigens are immobilised onto the device surface. By the use of a resonator structure with carefully selected sensitive region, greater response could be observed in many practical sensing applications. In this chapter, the mass sensitivity variation over the surface of a resonator will be investigated, and the use in this task of the modelling techniques presented in previous chapters will be explained in detail.

6.2 Model

The model used to calculate the device's 2-port characteristics is described in Chapter 4. This needs to be modified to take into account the mass loading of specific regions of the device. Consider Figure 6.1, where the equivalent network of the IDT is replaced by 3 networks IDT_1, IDT_2 and IDT_3, with their acoustic ports cascaded, and their electrical ports in parallel. Network IDT_2 represents the region subject to mass loading. If this region extends to one of the edges of the IDT, then either network IDT_1 or IDT_3 will be absent.

To implement this model, the COM parameters are calculated separately for the case with and without mass loading, as discussed in Section 4.3.1. These COM parameters can be used to create P-matrices of the sub-elements of the IDT, using the techniques outlined in Section 4.3.2. However, it was discovered that direct implementation of this procedure can produce spurious results. If the operation described by Figure 6.1 is implemented with network IDT_2 having the COM parameters for the non mass-loaded case, then it would be expected that the combined network would

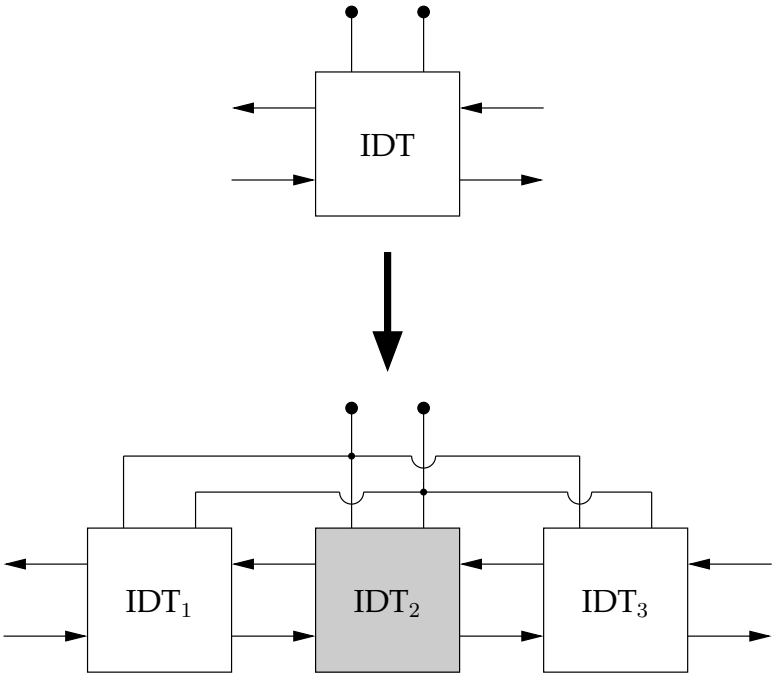

Figure 6.1: Partitioning of P-matrix elements to include inhomogeneous mass loading

be identical to the original network. In fact, it was found that some slight difference occurred. To eliminate these effects, the P-matrix was calculated for a single electrode pair, both with and without mass loading. These were then cascaded analytically using the expressions given in [140] to form the networks IDT_1, IDT_2, and IDT_3. Since the IDT is always split into the maximum number of P-matrices, no further error can occur due to the splitting of IDT networks into sub-networks.

Mass sensitivity is calculated along the length (x_1) of the device. Variation of the mass sensitivity across the width (x_2) of the device has been neglected in this model. This effect can be assumed to be insignificant since the device geometry is constant across its width, which is much greater than the acoustic wavelength.

Using the P-matrix model, the complete 2-port parameters of the SAW device can be calculated and the resonant frequency f_r determined. For the device with no mass loading, the resonant frequency was determined by finding the maximum amplitude of the transfer characteristic S_{21}. At this frequency the phase response will have a corresponding value of θ_r. When the device is subject to mass loading, the transfer response will change to S_{21}^m. The perturbed resonant frequency f_r^m is determined from the frequency where the phase response is θ_r, as illustrated in Figure 6.2. It should be

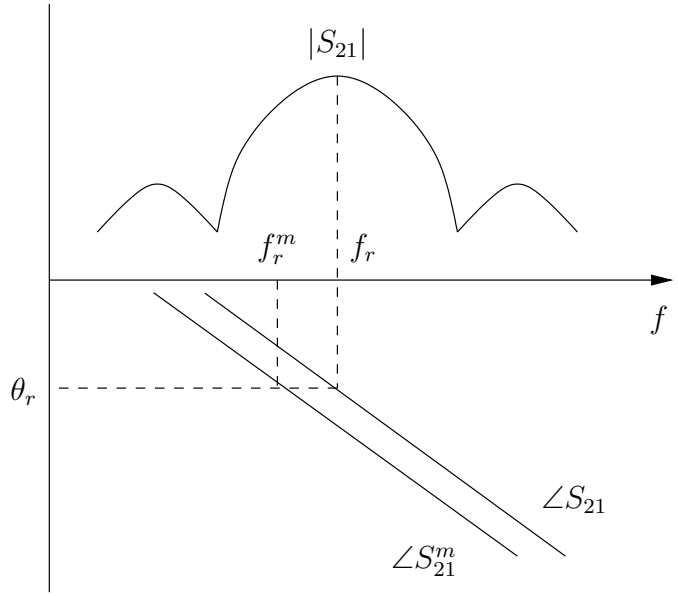

Figure 6.2: Determination of device response when modelling mass loading

noted that the perturbed resonant frequency f_r^m does not necessarily correspond to the maximum magnitude of the perturbed transmission response S_{21}^m. This model gives the response of a SAW sensor when placed in a feedback loop to create an oscillator circuit, neglecting the phase delay across other circuit elements.

For each region of the device, the mass sensitivity defined as:

$$S_m^f = \frac{f_r^m - f_r}{m}, \tag{6.1}$$

where m is the total mass of the perturbing material. This differs from the definition given in Section 2.17, since it is for a finite quantity of mass rather than mass loading per unit area and for absolute rather than relative frequency change. This is a more appropriate measure, since in this chapter calculations are being made of finite regions of a device, rather than for an idealised infinite case. This results in an expression with SI units of (Hz/kg), however it is more practical to express it in units of (Hz/ng).

6.3 Measurements

The 2-port resonator sensors were fabricated on a 36°-YX $LiTaO_3$ substrate, using the design outlined in Chapter 5. A 0.4µm layer of SiO_2 was deposited on the device surface by RF magnetron sputtering, in order to protect the electrodes. The resultant

devices had resonant frequencies in the range of 205-206MHz. It should be noted that for many sensing applications of these devices a thicker layer would be used, however a thinner layer was chosen because it results in less process variation between the devices.

Figure 6.3 shows a schematic representation of the 2-port resonator SAW structure (not to scale). Regions B-C and D-E represent the input and output interdigital transducers which are connected to the external circuit. Regions A-B and E-F are short circuited electrode gratings of the same period as the IDTs. Region C-D is a grating with a different period to that of the IDTs, and at point D there is a small spacer.

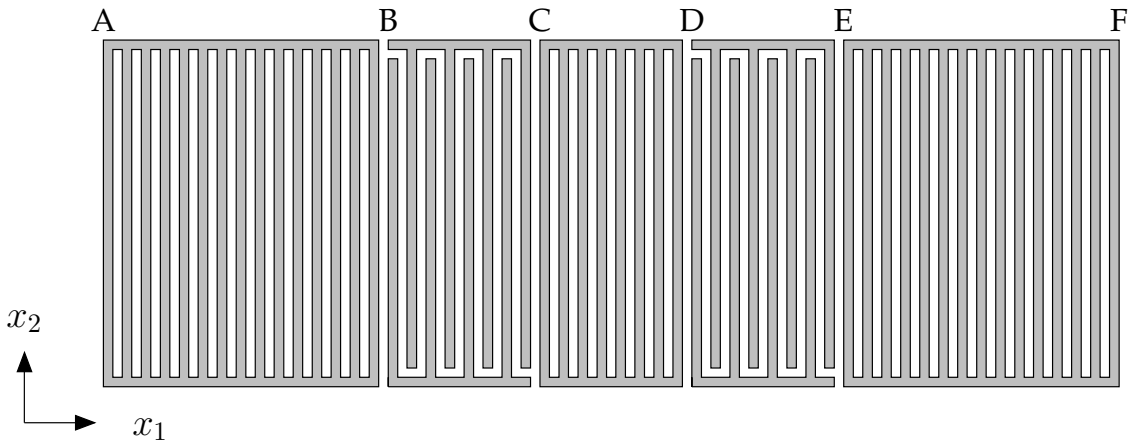

Figure 6.3: Layout of 2-port resonator SAW sensor in (x_1, x_2)-plane

Sensitivity measurements were performed by placing the SAW devices in the oscillator circuit before and after the addition of a perturbing mass, and measuring the change in oscillation frequency. The system was designed to ensure that the pressure placed on the SAW device by measurement probes was repeatable. The added mass was AZ5206E photo-resist, of thickness 0.6µm. This relatively thick layer was chosen to ensure that a strong response was observed. Because the photo-resist is a soft material the response should be mainly attributable to its mass, although some viscosity influence would also be expected. Each measurement was repeated simultaneously on 5 different devices, which were fabricated in the same batch.

Figure 6.4 shows the results of the measurement. The horizontal axis of the graph gives the location along the x_1-axis as shown in Figure 6.3, with the corresponding points A through F being marked out. Each horizontal line represents the region over

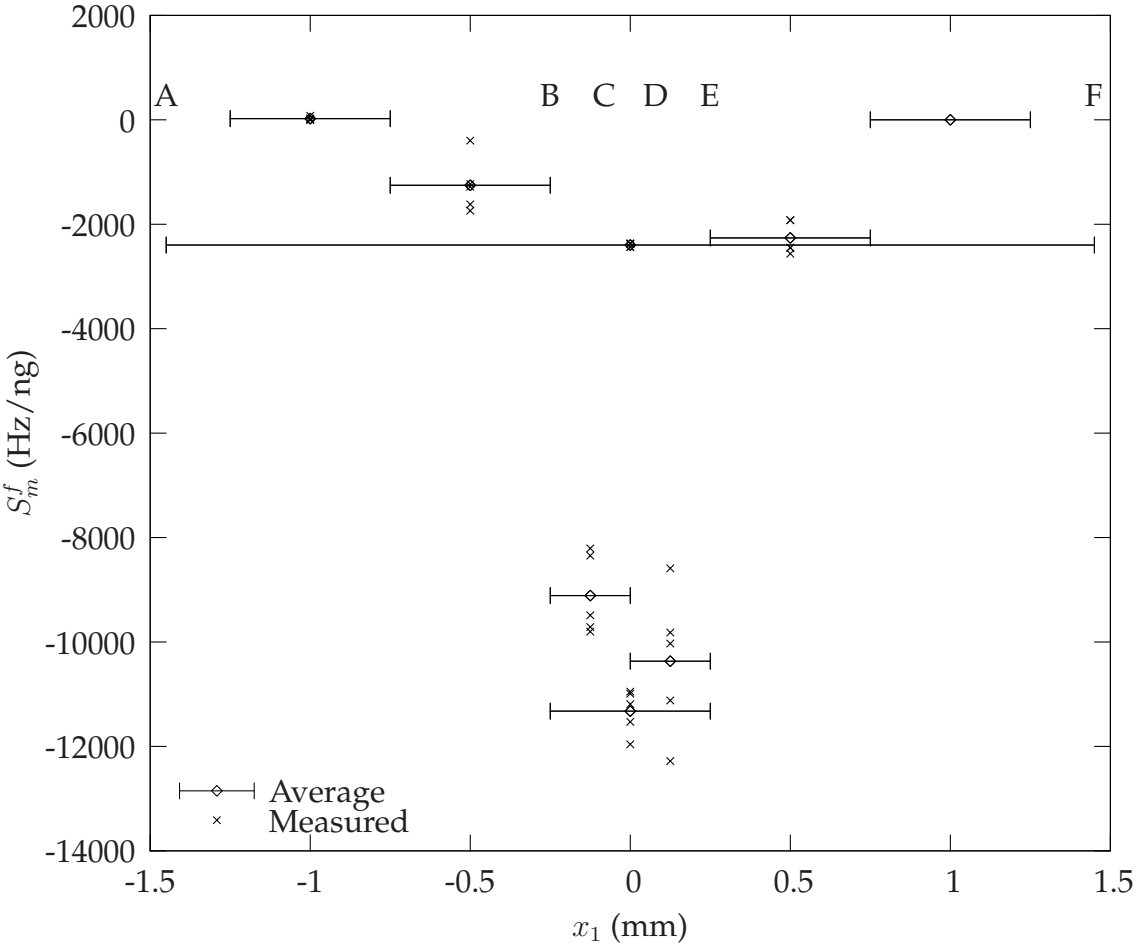

Figure 6.4: Measured sensitivity distribution

which the additional mass has been deposited. The nearby crosses represent the measured values of sensitivity. In all cases the mass has been deposited over the complete width of the device in the x_2-direction. These measurements shows how a local change in mass loading over a region on the device surface affects the resonant frequency of the device.

6.4 Comparison between Modelled and Measured Results

6.4.1 Infinitesimal Electrode Approximation

Provided that the electrodes are of negligible thickness compared with the acoustic wavelength, and are made from a light material, their mechanical properties do not need to be taken into account and they can be considered as being infinitely thin.

In Section 4.2 it was shown that this assumption greatly simplifies the analysis, and speeds up the computation. Figure 6.5 shows the measured and theoretical sensitivity distribution of the test device based on this assumption. The measured values are represented by crosses, whilst the theoretical values are represented by the circles at the centre of the horizontal bars. It can be seen that, as expected, the sensitivity is greatest at the centre of the device. The region B-E will be denoted the optimum region, although this region is arbitrarily selected, and may be chosen differently for another device geometry. This region accounts for the majority of the total device response.

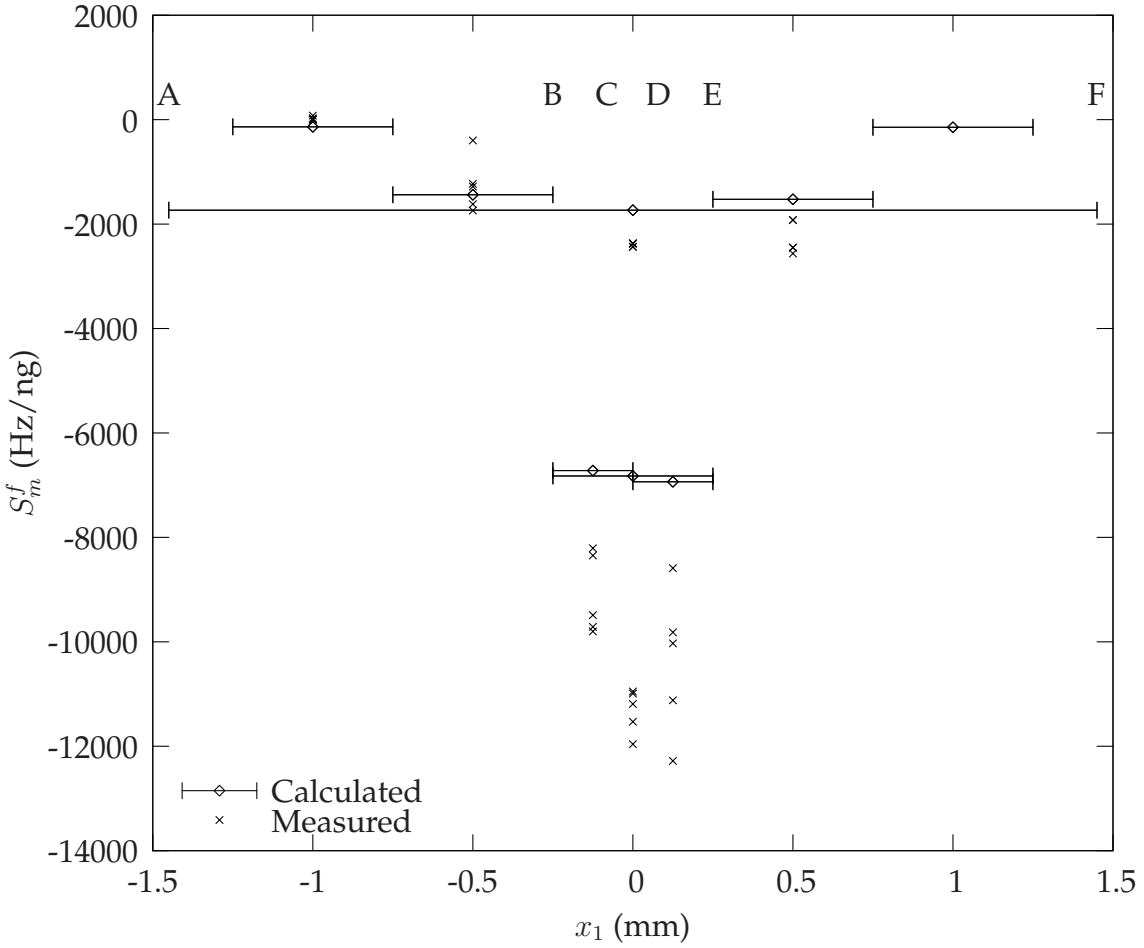

Figure 6.5: Sensitivity distribution with electrical approximation model

The qualitative agreement in shape is quite good, however the measured sensitivity is more confined to the centre than the model predicts, and the average sensitivity over the complete device is also greater. This disagreement can be attributed to the mechanical influence of the electrodes which was not included in the model. The heavy electrodes enhance the acoustic reflection, thus confining the acoustic energy to the

centre of the device. They also trap acoustic energy to the surface, thus further increasing the average mass sensitivity of the device.

6.4.2 Full Electrode Model

The results of Section 6.4.1 indicate that mechanical electrode interactions have a significant influence on the performance of the device. To improve the agreement between the calculated and experimental results, the novel model developed in Section 4.2.2 was applied to the problem.

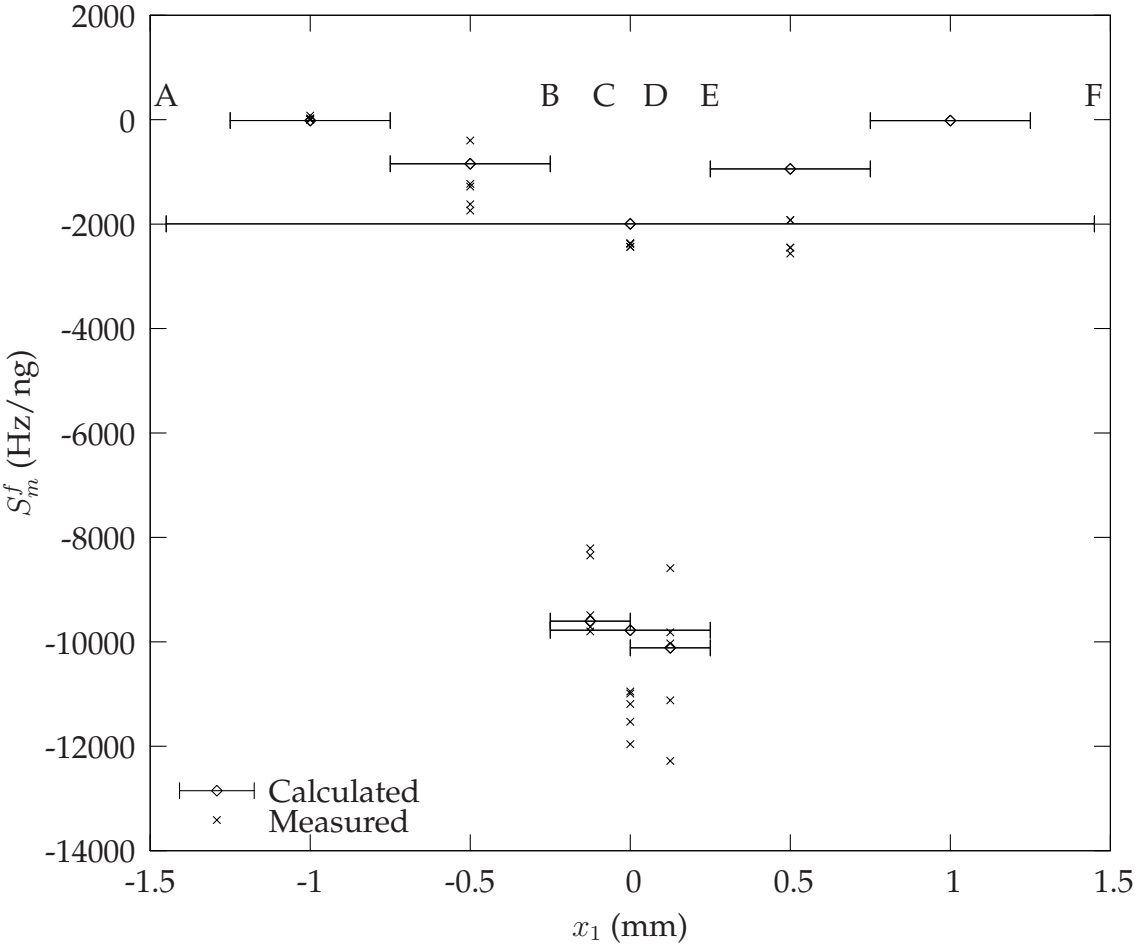

Figure 6.6: Sensitivity distribution with full electrode model

With the mechanical electrode model incorporated into the periodic Green's function analysis the sensitivity was calculated as before. The results are shown in Figure 6.6. The sensitivity shows better agreement with measurements in the case where complete device is mass loaded, as does the sensitivity in the optimum region. It is likely that the causes of inaccuracy cited in Section 5.4 would also come into play here as

well. These results are in contrast with those in Section 4.3.1, where it was found that there was a minimal difference in sensitivity for thin and thick electrode models.

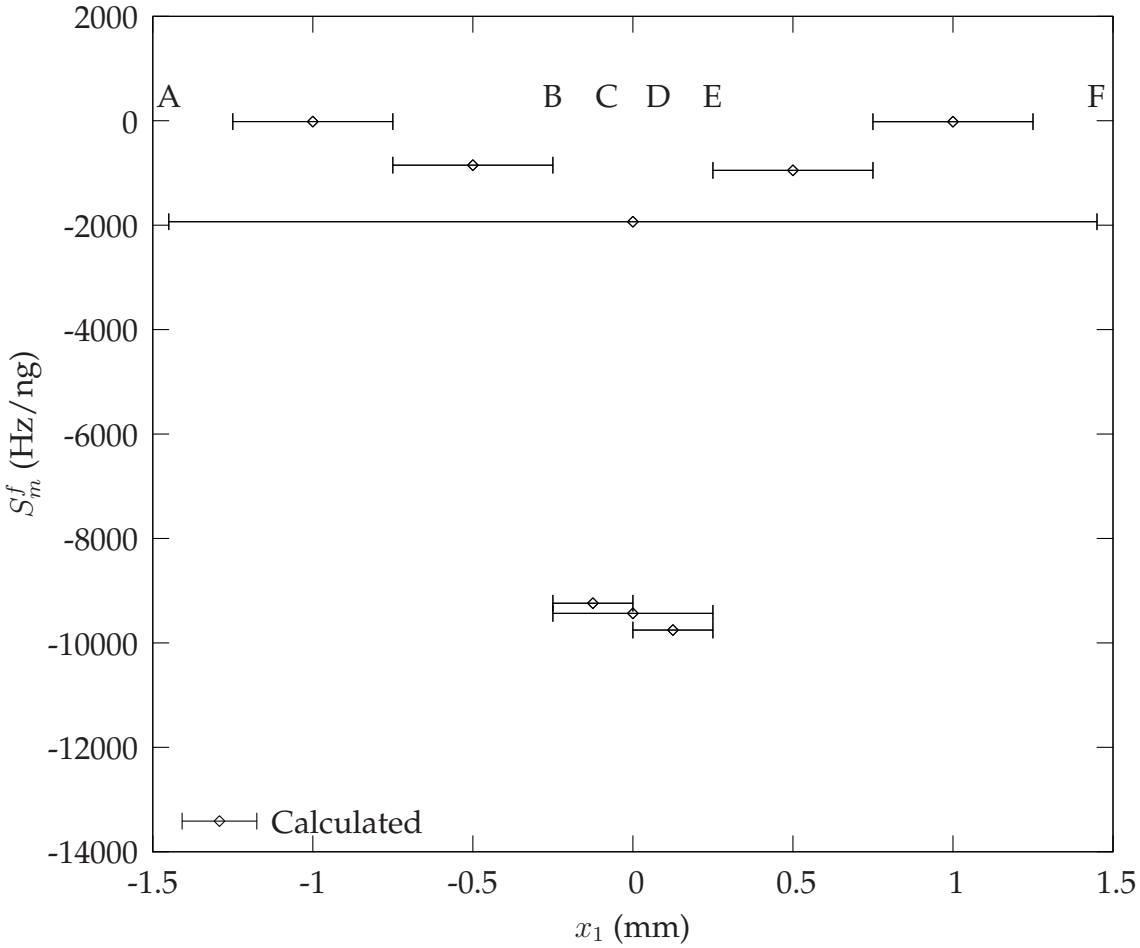

Figure 6.7: Sensitivity distribution considering only velocity change

As was discussed in Section 2.7.1, the change in velocity v is generally considered to be responsible for the device sensitivity to mass loading. However, since the COM parameters α, κ, C and γ influence the frequency response of the device, a change in these parameters may be contributing to the results presented in Figure 6.6. To determine the relative importance of velocity in determining sensitivity compared to these other parameters, all parameters except velocity have all been held constant during mass loading. The resulting sensitivity distribution is shown in Figure 6.7, being compared with the measured values. It can be seen that the results do not differ greatly from those in Figure 6.6, which indicates that in this case the velocity change is predominant.

6.4.3 Discussion

It is of interest to compare the sensitivity of the complete device (A-F), of the optimum region (B-E) and of an idealised infinite length IDT. Table 6.1 shows a comparison of these sensitivity calculations. To compare with the sensitivity of an infinite electrode array, mass loading per unit area must be considered. This shows that the optimum region accounts for 84% of the complete device response, despite the fact that it accounts for 34% of the active device area.

It can be seen that the response of the complete device is noticeably less than that of an ideal infinite length electrode array. A complicating feature of this design is that it has 2 different electrode periods, and the spacer, which moves the resonant frequency away from the resonant frequency of the infinite grating. Thus it is not surprising that the mass sensing behaviour of the complete structure differs from that of an infinite electrode array.

Table 6.1: Sensitivity comparison

Structure	Sensitivity cm^2/g
Infinite Electrode Array	-114.3
Complete Resonator	-99.3
Optimum Region	-83.5

The model suggests that for bio-sensing applications with a limited quantity of available selective material, to achieve maximum response this material should only be immobilised over the optimum region of the SAW device. It must be stressed that there are other factors which also need to be taken into account including mass transport, optimum receptor concentration and whether a flow-through or static cell has been used [136].

On the other hand, in situations such as environmental gas monitoring, it is more reasonable to assume that there is an unlimited quantity of analyte interacting with the complete device surface. A comparison of delay line and resonator structures has been made under these assumptions, resulting in quite different conclusions [8].

Although mass sensitivity is investigated here the mechanism for varying sensitiv-

ity across the device surface is not specific to mass loading. The principal is primarily the means by which the device structure translates a local velocity change $\Delta v/v$ to an overall change in the oscillation frequency of the device $\Delta f/f$. Thus similar results would be expected for sensors based on changes in other parameters such as viscosity or conductivity and for other types of SAW mode.

6.5 Conclusion

In this chapter, the layered SAW resonator structure has been subject to a new type of analysis devised by the author. The purpose of this analysis is to find the most sensitive region of the device's surface. This was undertaken by utilising the P-matrix resulting from the analysis performed in Chapter 4. It was found that the simplified model based on the thin electrode approximation was inadequate for describing the behaviour of the electrode grating, thus justifying the use of the author's novel technique.

A fixed quantity of analyte was shown to have a greater effect on the device response when immobilised or adsorbed onto a small region at the centre of the device. The sensitivity in this region was found to be around four times larger than the average sensitivity across the complete device. This could be of great importance for applications where maximum response is desired from a limited quantity of sensitive material.

[This page has intentionally been left blank.]

Chapter 7

Conclusion

In this thesis, novel techniques were developed for the modelling of layered surface acoustic wave resonator sensors operating in liquid media. The major achievements were:

- Development of a new model for the mechanical influence of electrodes buried within layered media
- Combination of the periodic Green's function and COM models applied to the study of layered SAW resonator sensors operating in liquid media
- Development of a model for the distribution of mass sensitivity across the surface of a SAW resonator sensor, showing that it is only necessary for the sensitive material to be placed in a small region of the device
- Design, fabrication and testing of a SAW resonator which confirmed the results of the author's theoretical developments

In Section 7.1 an overview of these achievements will be given, following the sequence used in the main thesis body. Section 7.2 will list the author's publications, some of which were not included in the body of this thesis. The author's suggestions for future research directions are detailed in Section 7.3.

7.1 Thesis Overview

In the critical literature review undertaken in Chapter 2 it was shown that the most accurate and universally applicable techniques for SAW device modelling are those based on the boundary element method, which requires the development of a Green's function. It was also shown that the combination of the periodic Green's function and the coupling of modes models gives excellent accuracy and computation speed.

Although models for the mechanical interaction between acoustic waves and electrodes are abundant in the literature, almost all of these models assume that the electrodes are placed on the device surface, whereas in many sensing applications they are placed between the substrate and guiding layer. This means that in order to avoid making unwarranted simplifications to the device model, there is a requirement for an approach which describes the mechanical interaction with electrodes buried within layered media.

Existing models to calculate the sensitivity of SAW devices towards mass loading were also evaluated. A significant inadequacy of these models is that they assume that mass loading occurs evenly over the surface. Thus, they are unable to yield information on the variation of sensitivity across the surface of the device. The variation of mass sensitivity across the surface of a SAW resonator is an important problem to study because it dictates where the sensitive material should be placed. In immunosensing applications, this sensitive material is usually antibodies or antigens, which may only be available in limited quantities and should thus be placed optimally on the surface of the device. If they are placed on a region of very low sensitivity then they may be detrimental to the response, since they would immobilise analyte and prevent it from interacting with the more sensitive regions.

The mathematical foundations for the Green's function based analysis were presented in Chapter 3. It was shown that as well as forming the basis for the boundary element method, the spectral domain Green's function also serves as an excellent analytical tool in its own right. It can be used to calculate the phase velocity, electromechanical coupling factor and mass sensitivity of SAW structures in the absence of electrode interactions. Examples were presented comparing these theoretical predictions with measurements made on delay line structures fabricated on lithium tantalate

with a zinc oxide guiding layer, and were shown to be in good agreement.

The periodic Green's function analysis was presented in Chapter 4, including the author's novel modifications. By considering an infinite length array, only a single period of the electrodes needs to be modelled, greatly reducing the computational cost. A technique was developed which accounts for the mechanical influence of electrodes buried within layered media. This model is based on the formulation of a matrix-eigen operator for periodic media, and is much less cumbersome than existing solutions for this problem based on the finite element method. It was also compared with the simpler and faster technique based on and electrical Green's function approximation.

It was then shown how the COM parameters could be extracted from this periodic Green's function model, and used to calculate the frequency response of the SAW resonator. COM parameters were studied as a function of guiding layer thickness for the SiO_2 on 36°-YX $LiTaO_3$ layered structure. It was shown that particularly for the reflection of acoustic waves, the electrical Green's function approximation is inadequate, and the author's novel approach is required to fully account for the electrode interactions.

This was followed in Chapter 5 by the author's design of a 2-port resonator structure. The frequency response of this device was analysed using the author's method, which was found to yield almost identical results as other methods in the literature for the case with no layer above the electrodes. This serves as a convincing verification of the author's technique. The fabrication procedure was described and the frequency response of the fabricated device was compared with the theoretical response. For the non-layered case this agreement was found to be good, with only a minimal number of adjustments required to achieve this agreement. For the non-layered case agreement was poorer, but most importantly, the model is able to give quite accurate predictions of resonant frequency. This implies accurate modelling of the propagation velocity, which is the most important part of the sensor response. The result is that this new tool can confidently be used to model acoustic interactions with electrodes buried within layered media.

In Chapter 6 the sensitivity of the designed device was analysed, with particular regard to the variation of mass sensitivity across its surface. This analysis was under-

taken using the previously developed modelling techniques and was compared with experimental measurements. It was shown experimentally that sensitivity is greatest towards the centre of the device, and decreases strongly with increasing distance away from the centre. The electrical Green's function approximation was found to give very poor agreement with measurements, since it does not take full account of the increased reflection and surface trapping effects of heavy electrodes. The model developed by the author for electrodes buried within layered media was found to yield much better agreement, since it accounts for these effects.

The result of this analysis is that SAW resonator sensors are able to achieve almost complete sensitivity by having a selective layer only in the centre of the device. This is expected to be highly beneficial in cases where the selective material is expensive, so that it's use must be minimised. This allows an extra degree of design freedom for SAW resonator sensors, where the benefits of large Q-factor available from large device length can be achieved without having to coat the complete device in selective material.

7.2 Author's Publication Record

The following papers have been published based on the work undertaken in this thesis, in the proceedings of international conferences and in refereed international journals:

- D. A. Powell, K. Kalantar-zadeh, W. Wlodarski, and S. J. Ippolito, "Layered surface acoustic wave chemical and bio-sensors," in *Encyclopedia of Sensors*, C. Grimes, E. Dickey, and M. V. Pishko, Eds. American Scientific, 2006, vol. 5, pp. 245–262.

- D. A. Powell, K. Kalantar-zadeh, and W. Wlodarski, "Spatial sensitivity distribution of surface acoustic wave resonator chemical and bio-sensors," *IEEE Sensors J.*, 2006, (accepted for publication).

- D. A. Powell, K. Kalantar-zadeh, and W. Wlodarski, "Numerical calculation of SAW sensitivity: Application to ZnO/$LiTaO_3$ transducers," *Sens. Act. A: Phys.*, vol. 115, pp. 456–461, 2004.

- D. A. Powell, K. Kalantar-zadeh, and W. Wlodarski, "Comprehensive analysis of SAW sensor performance in liquid media by Green's function method," in *Proc. IEEE Ultrason. Symp.*, Oct. 2003, pp. 146–149.

- D. A. Powell, K. Kalantar-zadeh, S. Ippolito, and W. Wlodarski, "A layered SAW device based on ZnO/$LiTaO_3$ for liquid media sensing applications," in *Proc. IEEE Ultrason. Symp.*, 2002, pp. 493–496.

In addition, the following research publications were carried out, during the course of study whilst collaborating with other researchers from the Sensor Technology Group at RMIT University, and from the materials science group at University of Perugia. Although not directly relevant to the objectives of this thesis, the work in these publications makes use of some of the concepts and modelling techniques which were presented:

- D. A. Powell, L. Valentini, I. Armentano, W. Wlodarski, K. Kalantar-zadeh, and J. M. Kenny, "Langasite SAW gas sensor with self-assembled carbon nanotube functional layer," in *Proc. Eurosensors XIX*, 2005.

- D. A. Powell, K. Kalantar-zadeh, S. Ippolito, and W. Wlodarski, "Comparison of conductometric gas sensitivity of surface acoustic wave modes in layered structures," *Sensor Letters*, vol. 3, no. 1, pp. 66–70, Mar. 2005.

- K. Kalantar-zadeh, D. A. Powell, S. Ippolito, and W. Wlodarski, "Study of layered SAW devices operating at different modes for gas sensing applications," in *Proc. IEEE Ultrason. Symp.*, 2004, pp. 191–194.

7.3 Directions for Further Work

This thesis has presented advancements in the field of modelling SAW resonator sensors. In this section some proposals will be made and possible future developments will be considered. Firstly, improvements to the modelling technique will be suggested, then suggestions will be made regarding the most promising future directions of acoustic wave sensor research.

7.3.1 Modelling

Although the work undertaken in this thesis is specific to the area of acoustic wave devices, the periodic matrix eigen-operator technique applied here has previously been applied to electromagnetic problems [141], and in combination with finite difference techniques to photonic crystals [142]. This is possible because both the electromagnetic and acoustic wave equations are partial differential equations which can be diagonalised to form a matrix eigen-operator. It would thus be expected that the technique could find further useful application in the study of optical fibre gratings, photonic and phononic crystals, microwave and optical meta-materials and lasers.

Whilst modelling techniques developed in this thesis are adequate for the task, they involve a number of approximations, particularly that the field distribution can be well approximated as being Floquet-periodic in the propagation direction x_1, with infinite extent in the lateral dimension x_2. For improved accuracy, or as a final check for a design optimised using these techniques, it is desirable to have a model which does not use these approximations. For this work it would have been desirable to have such a model to verify that the use of the 2-dimensional approximation was fully justified.

The problem of a 3-dimensional Green's function based SAW analysis has been studied (e.g. [143]), and 3-dimensional analysis has also been undertaken using the finite element method (e.g. [144], in which the author had some involvement). However, to the best of the author's knowledge a full 3-dimensional simulation of wave propagation on an anisotropic piezoelectric substrate has not been presented in the literature for a device of realistic size.

Perhaps the greatest problem in performing a full 3-dimensional BEM analysis is the extremely high computational expense which would be involved. Since the BEM relates each discretised region to every other, its computational cost increases as N^3, where N is the number basis functions used to model the device. The result is that solving the 3-dimensional BEM equations for practical sized devices is cannot be performed without the utilisation of enormous computational resources. It is unlikely that such an enterprise would produce sufficient benefits to justify the required time and expense. However, by utilising a more advanced approach to the BEM, this situation may be remedied.

The Fast Multi-pole Method (FMM) and it's variants are a group of powerful techniques which greatly reduce the computational burden of large scale linear partial differential equations. These techniques have typically been applied to problems having a Green's function of the form $1/|\mathbf{r}|$ [145] or $\exp(jk|\mathbf{r}|)/|\mathbf{r}|$ [146], where $\mathbf{r}$ is the vector between source and observation points, and k is the wave number of a propagating wave. However, in the analysis of piezoelectric devices Green's functions having such simple forms do not occur, due to the anisotropic nature of piezoelectric materials.

Recent theoretical developments [147] indicate that these techniques can be applied to Green's functions of any form, including those which arise in the study of anisotropic media. Thus it should be possible to combine these techniques with the established Green's function based methods for SAW devices to enable highly accurate simulations to be performed within a practically useful computation time. It should be noted that such a technique would be equally applicable to any linear piezoelectric device, including SAW and BAW devices for sensing and signal processing applications.

7.3.2 Acoustic Wave Sensors

SAW resonator sensors are only one class of device amongst the variety of piezoelectric and acoustic resonant sensors. This area of sensors is strongly influenced by developments in devices for signal processing and communications applications, although as discussed in Section 2.2 there are specific requirements for sensors. SAW and QCM technology are both quite mature, so it is the author's opinion that only incremental changes are likely to occur in these areas. Thus, when considering new developments which may have a significant impact in the sensor field, it is most likely that other structures will provide the greatest impetus for significant new advances.

Recent developments in the field of acoustic wave devices are film bulk acoustic resonator (FBAR) and solidly mounted resonator (SMR) structures [148]. These devices are similar in principal to the QCM, but offer much higher operational frequency, which may be in the GHz range. They consist of a thin film which resonates in its thickness dimension. They are either free standing films (FBAR) or fabricated on top of a Bragg mirror (SMR) in order to minimise acoustic losses into the surrounding medium. Originally developed for RF frequency stabilisation and filtering applications, these

structures have been successfully applied as gas sensors [149].

As they operate in a longitudinally polarised mode, these devices suffer from significant attenuation when operated in liquid media. More recently, shear-horizontally polarised variants have been developed which are suitable for operation in liquid media [150, 151]. It is not entirely clear that such devices offer any performance advantage over a QCM, since acoustic losses, are much higher at the GHz frequency range than the MHz range in which QCM sensors typically operate, thus reducing the device Q and the signal to noise ratio. However, there are other advantages regarding the device size and ease of integration with other components that make these devices appealing. It also unclear to what extent these devices will be seen as replacing, rather than complementing SAW sensor technology. SAW devices have a much simpler planar structure, and unlike FBARs do not require bulk micro-machining techniques. However thin film resonators can be much more readily fabricated on commonly used substrates such as silicon.

Appendix A

Material Constants

To enable work such as that presented in this thesis to be reproduced, it is essential that the material constants used are consistent. For this reason, Table A.1 lists the material constants used in this thesis, and the sources from which they were obtained. Only independent constants are listed, the others are obtained according to the relationships given in [36], which depend on the material's symmetry class. The value "-" indicates that the constant is not independent, which does not mean that it is zero. For piezoelectric materials, the stiffness at constant electric field c^E and dielectric constant at constant strain ε^S are given, since these are the values required for the analysis used in this thesis. For non-piezoelectric materials, this distinction does not need to be made. The permittivity is normalised to the permittivity of free space $\varepsilon_0 = 8.854 \times 10^{-12}$F/M. The full dielectric properties of a metal are not well represented by a single constant, and are not used in this thesis.

Table A.1: Material constants

Material	Source	Symmetry Class	Density (kg/m^3)	Stiffness (10^{10} N/m^2)					
				c_{11}^E	c_{12}^E	c_{13}^E	c_{14}^E	c_{33}^E	c_{44}^E
$LiTaO_3$	[152]	3m	7454	23.28	4.65	8.36	-1.05	27.59	9.49
ZnO	[153]	6mm	5720	15.7	8.9	8.3	-	20.8	3.8
SiO_2	[16]	Isotropic	2200	7.85	-	-	-	-	1.74
Au	[36]	Isotropic	19300	20.7	-	-	-	-	2.85
Ti	[36]	Isotropic	4500	16.59	-	-	-	-	4.4
Water	[119]	Isotropic	997	$\kappa = 2.24\times10^9 N/m^2$, $\eta = 8.9\times10^{-4} Ns/m^2$					

Material	Piezoelectric Constants (C/m^2)				Permittivity	
	e_{15}	e_{22}	e_{31}	e_{33}	$\varepsilon_{11}^S/\varepsilon_0$	$\varepsilon_{33}^S/\varepsilon_0$
$LiTaO_3$	2.64	1.86	-0.22	1.71	40.9	42.5
ZnO	-0.48	-	-0.573	1.32	8.55	10.2
SiO_2	0				3.75	-
Au	0				-	-
Ti	0				-	-
Water	0				80	-

Bibliography

[1] G. Sauerbrey, "The use of quartz oscillators for weighting thin layers and for microweighting," *Z. Phys.*, vol. 155, p. 206, 1959.

[2] M. V. Voinova, M. Jonson, and B. Kasemo, "'Missing mass' effect in biosensor's QCM applications," *Biosensors and Bioelectronics*, vol. 17, no. 10, pp. 835–841, Oct. 2002.

[3] R. M. White and F. W. Voltmer, "Direct piezoelectric coupling to surface elastic waves," *Appl. Phys. Lett.*, vol. 7, no. 12, pp. 314–316, 1965.

[4] D. P. Morgan, *Surface-Wave Devices for Signal Processing*. Amsterdam: Elsevier, 1991.

[5] H. Wohltjen and R. Dessy, "Surface acoustic wave probe for chemical analysis. I. introduction and instrument description," *Analytical Chemistry*, vol. 51, no. 9, pp. 1458–1464, Aug. 1979.

[6] A. E. H. Love, *A Treatise on the Mathematical Theory of Elasticitiy*. Cambridge: Dover, 1967.

[7] I. D. Avramov, *High-Performance Surface Transverse Wave Resonators in the Lower GHz Frequency Range*. Singapore: World Scientific Publishing, 2000, vol. 1, pp. 735–792.

[8] A. Mauder, "SAW gas sensors: comparison between delay line and two port resonator," *Sens. Act. B: Chem.*, vol. 26-27, pp. 187–90, 1995.

[9] I. D. Avramov, M. Rapp, S. Kurosawa, P. Krawczak, and E. Radeva, "Gas sensi-

tivity comparison of polymer coated SAW and STW resonators operating at the same acoustic wavelength," in *Proc. IEEE Freq. Cont. Symp.*, 2001, pp. 465–473.

[10] M. Penza and G. Cassano, "Relative humidity sensing by PVA-coated dual resonator SAW oscillator," *Sens. Act. B: Chem.*, vol. 68, pp. 300–306, 2000.

[11] N. Wakatsuki and M. Bannai, "Study of $LiTaO_3$ shear wave resonator for viscosity sensor of polymer liquid in MHz range," in *Proc. IEEE Ultrason. Symp.*, 2003, pp. 1334–1337.

[12] T. Nomura, M. Takebayashi, and S. Furukawa, "One-port surface acoustic wave resonators for sensing in liquids," in *Proc. IEEE Ultrason. Symp.*, 1992, pp. 299–302.

[13] ——, "Chemical sensor based on surface acoustic wave resonator incorporating Langmuir-Blodgett films," in *Proc. IEEE Ultrason. Symp.*, 1996, pp. 395–398.

[14] E. Gizeli, N. J. Goddard, C. R. Lowe, and A. C. Stevenson, "A Love plate biosensor utilising a polymer layer," *Sens. Act. B: Chem.*, vol. 6, pp. 131–137, 1992.

[15] E. Gizeli, A. C. Stevenson, N. J. Goddard, and C. R. Lowe, "A novel Love-plate acoustic sensor utilizing polymer overlayers," *IEEE Trans. Ultrason., Ferroelect., Freq. Contr.*, vol. 39, no. 5, pp. 657–659, Sept. 1992.

[16] G. Kovacs, G. W. Lubking, M. J. Vellekoop, and A. Venema, "Love waves for (bio)chemical sensing in liquids," in *Proc. IEEE Ultrason. Symp.*, 1992, pp. 281–285.

[17] G. Kovacs, M. J. Vellekoop, R. Haueis, G. W. Lubking, and A. Venema, "A Love wave sensor for (bio)chemical sensing in liquids," *Sens. Act. A: Phys.*, vol. 43, no. 1-3, pp. 38–43, May 1994.

[18] J. A. Ogilvy, "The mass-loading sensitivity of acoustic Love wave biosensors in air," *J. Phys. D: Appl. Phys.*, vol. 30, pp. 2497–2501, 1997.

[19] J. Du, G. L. Harding, J. A. Ogilvy, P. R. Dencher, and M. Lake, "A study of Love-wave acoustic sensors," *Sens. Act. A: Phys.*, vol. 56, pp. 211–219, 1996.

[20] J. Du, G. L. Harding, A. F. Collings, and P. R. Dencher, "An experimental study of Love-wave acoustic sensors operating in liquids," *Sens. Act. A: Phys.*, vol. 60, pp. 54–61, 1997.

[21] B. Jakoby and M. J. Vellekoop, "Analysis and optimization of Love wave liquid sensors," *IEEE Trans. Ultrason., Ferroelect., Freq. Contr.*, vol. 45, no. 5, pp. 1293–1302, Sept. 1998.

[22] B. Jakoby, G. M. Ismail, M. P. Byfield, and M. Vellekoop, "A novel molecularly imprinted thin film applied to a Love wave gas sensor," *Sens. Act. A: Phys.*, vol. 76, no. 1–3, pp. 93–97, Aug. 1999.

[23] F. Herrmann, M. Weihnacht, and S. Büttgenbach, "Properties of shear-horizontal surface acoustic waves in different layered quartz-SiO_2 structures," *Ultrasonics*, vol. 37, pp. 335–341, 1999.

[24] J. Du and G. L. Harding, "A multilayer structure for Love-mode acoustic sensors," *Sens. Act. A: Phys.*, vol. 65, pp. 152–159, 1998.

[25] G. L. Harding, "Mass sensitivity of Love-mode acoustic sensors incorporating silicon dioxide and silicon-oxy-fluoride guiding layers," *Sens. Act. A: Phys.*, vol. 88, pp. 20–28, 2001.

[26] K. Kalantar-zadeh, A. Trinchi, W. Wlodarski, and A. Holland, "A novel Love-mode device based on a ZnO/ST-cut quartz crystal structure for sensing applications," *Sens. Act. A: Phys.*, vol. 100, pp. 135–143, 2002.

[27] K. Kalantar-zadeh, W. Wlodarski, Y. Y. Chen, B. N. Fry, and K. Galatsis, "Novel Love mode surface acoustic wave based immunosensors," *Sens. Act. B: Chem.*, vol. 91, no. 1–3, pp. 143–147, June 2003.

[28] K. Kalantar-zadeh, "Investigation of a Love mode acoustic wave transducer for bio-sensing applications," Ph.D. dissertation, RMIT University, Nov. 2001.

[29] S.-Y. Chu, W. Water, and J.-T. Liaw, "An investigation of the dependence of ZnO film on the sensitivity of Love mode sensor in ZnO/quartz structure," *Ultrasonics*, vol. 41, pp. 133–139, 2003.

[30] E. Gizeli, F. Bender, A. Rasmusson, K. Saha, F. Josse, and R. Cernosek, "Sensitivity of the acoustic waveguide biosensor to protein binding as a function of the waveguide properties," *Biosensors and Bioelectronics*, vol. 18, pp. 1399–1406, 2003.

[31] F. Herrmann, D. Hahn, and S. Büttgenbach, "Separate determination of liquid density and viscosity with sagitally corrugated Love-mode sensors," *Sens. Act. A: Phys.*, vol. 78, pp. 99–107, 1999.

[32] C. Zimmermann, D. Rebière, C. Déjous, J. Pistré, E. Chastaing, and R. Planade, "A Love-wave gas sensor coated with functionalized polysiloxane for sensing organophosphorus compounds," *Sens. Act. B: Chem.*, vol. 76, no. 1–3, pp. 86–94, June 2001.

[33] M. Penza, F. Antolini, and M. Vittori Antisari, "Carbon nanotubes as SAW chemical sensors materials," *Sens. Act. B: Chem.*, vol. 100, pp. 47–59, 2004.

[34] A. J. Ricco, S. J. Martin, and T. E. Zipperian, "Surface acoustic wave gas sensor based on film conductivity changes," *Sens. Act.*, vol. 8, no. 4, pp. 319–333, Dec. 1985.

[35] D. P. Morgan, "A history of surface acoustic wave devices," in *Advances in Surface Acoustic Wave Technology, Systems and Applications*, C. C. W. Ruppel and T. A. Fjeldly, Eds. Singapore: World Scientific Publishing, 2000, vol. 1, pp. 1–50.

[36] B. A. Auld, *Acoustic Fields and Waves in Solids*, 2nd ed. Florida: Krieger, 1990, vol. 1.

[37] ——, *Acoustic Fields and Waves in Solids*, 2nd ed. Florida: Krieger, 1990, vol. 2.

[38] F. Schmidt and G. Scholl, "Wireless SAW identification and sensor systems," in *Advances in Surface Acoustic Wave Technology, Systems and Applications*, C. C. W. Ruppel and T. A. Fjeldly, Eds. Singapore: World Scientific Publishing, 2001, vol. 2, pp. 277–325.

[39] J. J. Campbell and W. R. Jones, "A method for estimating optimal crystal cuts and propagation directions for excitation of piezoelectric surface waves," *IEEE Trans. Sonics Ultrason.*, vol. 15, no. 4, pp. 209–217, Oct. 1968.

[40] V. Plessky and J. Koskela, "Coupling-of-modes analysis of SAW devices," in *Advances in Surface Acoustic Wave Technology, Systems and Applications*, C. C. W. Ruppel and T. A. Fjeldly, Eds. Singapore: World Scientific Publishing, 2001, vol. 2, pp. 1–83.

[41] A. J. Slobodnik, Jr, "Materials and their influence on performance," in *Acoustic Surface Waves*, A. A. Oliner, Ed. Berlin: Springer-Verlag, 1978, ch. 6, pp. 225–304.

[42] P. C. Painter and M. M. Coleman, *Fundamentals of Polymer Science*, 2nd ed. Pennsylvania: Technomic, 1997.

[43] M. I. Newton, F. Martin, K. Melzak, E. Gizeli, and G. McHale, "Harmonic Love wave devices for biosensing applications," *Electronics Letters*, vol. 37, no. 6, pp. 340–341, Mar. 2001.

[44] R. S. Wagers, "Analysis of finite-width interdigital transducer excitation profiles," *IEEE Trans. Sonics Ultrason.*, vol. 26, no. 2, pp. 105–111, Mar. 1979.

[45] H. P. Zidek, A.-R. Baghai-Wadji, and O. Männer, "Full-wave 3D analysis of wave scattering on SAW-structures with finite aperture," in *Proc. IEEE Ultrason. Symp.*, 1993, pp. 149–152.

[46] G. I. Stegeman, "Optical probing of surface waves and surface wave devices," *IEEE Trans. Sonics Ultrason.*, vol. 23, no. 1, pp. 33–63, Jan. 1976.

[47] R. H. Tancrell and M. G. Holland, "Acoustic surface wave filters," *Proc. IEEE*, vol. 59, no. 3, pp. 393–409, Mar. 1971.

[48] W. R. Smith, H. M. Gerard, J. H. Collins, T. M. Reeder, and H. J. Shaw, "Analysis of interdigital surface wave transducers by use of an equivalent circuit model," *IEEE Trans. Microwave Theory Tech.*, vol. 17, no. 11, pp. 856–864, Nov. 1969.

[49] R. W. Rhea, *Oscillator design and computer simulation*, 2nd ed. Atlanta: Noble, 1995.

[50] R. L. Rosenberg and L. A. Coldren, "Scattering analysis and design of SAW resonator filters," *IEEE Trans. Sonics Ultrason.*, vol. 26, no. 3, pp. 205–230, May 1979.

[51] G. Tobolka, "Mixed matrix representation of SAW transducers," *IEEE Trans. Sonics Ultrason.*, vol. 26, no. 6, pp. 426–428, Nov. 1979.

[52] C. Elachi, "Wave in active and passive periodic structures: A review," *Proc. IEEE*, vol. 64, no. 12, pp. 1666–1698, Dec. 1976.

[53] D.-P. Chen and H. A. Haus, "Analysis of metal-strip SAW gratings and transducers," *IEEE Trans. Sonics Ultrason.*, vol. 32, no. 3, pp. 395–408, May 1985.

[54] T. Thorvaldsson, "Analysis of the natural single phase unidirectional SAW transducer," in *Proc. IEEE Ultrason. Symp.*, 1989, pp. 91–96.

[55] V. P. Plessky, "A two parameter coupling-of-modes model for shear horizontal type SAW propagation in periodic gratings," in *Proc. IEEE Ultrason. Symp.*, 1993, pp. 195–200.

[56] B. P. Abbot and K. Hashimoto, "A coupling-of-modes formalism for surface transverse wave devices," in *Proc. IEEE Ultrason. Symp.*, 1995, pp. 239–245.

[57] J. Koskela, V. P. Plessky, and M. M. Salomaa, "Theory of shear horizontal surface acoustic waves in finite synchronous resonators," *IEEE Trans. Ultrason., Ferroelect., Freq. Contr.*, vol. 47, no. 6, pp. 1550–1560, Nov. 2000.

[58] A. H. Fahmy and E. L. Adler, "Multilayer acoustic-surface-wave program," *Proceedings of the IEE*, vol. 122, no. 5, pp. 470–472, May 1975.

[59] G. S. Kino, *Acoustic Waves: Devices, Imaging and Analog Signal Processing*. New Jersey: Prentice-Hall, 2000.

[60] J. D. N. Cheeke, *Fundamentals and Applications of Ultrasonics Waves*. Boca Raton, Florida: CRC Press, 2001.

[61] F. Chagla, C. Cabini, and P. Smith, "Perfectly matched layer for FDTD computations in piezoelectric crystals," in *Proc. IEEE Ultrason. Symp.*, 2004, pp. 517–520.

[62] P. M. Smith and W. Ren, "Finite-difference time-domain techniques for SAW device analysis," in *Proc. IEEE Ultrason. Symp.*, 2002, pp. 325–328.

[63] E. L. Adler, "SAW and pseudo-SAW properties using matrix methods," *IEEE Trans. Ultrason., Ferroelect., Freq. Contr.*, vol. 41, no. 5, pp. 699–705, Sept. 1994.

[64] S. V. Biryukov and M. Weihnacht, "Real-space field of surface source and the problem of fast leaky wave generation in a piezoelectric half space," *J. Appl. Phys.*, vol. 83, no. 6, pp. 3276–3287, Mar. 1998.

[65] K.-Y. Hashimoto, T. Omori, and M. Yamaguchi, "SAW excitation and propagation under periodic metallic grating structures," in *Advances in Surface Acoustic Wave Technology, Systems and Applications*, C. C. W. Ruppel and T. A. Fjeldly, Eds. Singapore: World Scientific Publishing, 2000, vol. 1, pp. 133–182.

[66] V. Y. Zhang, J.-E. Lefebvre, C. Bruneel, and T. Gryba, "A unified formalism using effective surface permittivity to study acoustic waves in various anisotropic and piezoelectric multilayers," *IEEE Trans. Ultrason., Ferroelect., Freq. Contr.*, vol. 48, no. 5, pp. 1449–1461, Sept. 2001.

[67] K. Bløtekjær, K. A. Ingebrigtsen, and H. Skeie, "Acoustic surface waves in piezoelectric materials with periodic metal strips on the surface," *IEEE Trans. Electron Devices*, vol. 20, no. 12, pp. 1139–1146, Dec. 1973.

[68] R. F. Milsom, N. H. C. Reilly, and M. Redwood, "Analysis of generation and detection of surface and bulk acoustic waves by interdigital transducers," *IEEE Trans. Sonics Ultrason.*, vol. 24, no. 3, pp. 147–166, May 1977.

[69] K. A. Ingebrigtsen, "Surface waves in piezoelectrics," *J. Appl. Phys.*, vol. 40, no. 7, pp. 2681–2686, June 1969.

[70] L. Boyer, J. Desbois, Y. Zhang, and J. M. Hodé, "Theoretical determination of the pseduo surface acoustic wave characteristic parmaeters," in *Proc. IEEE Ultrason. Symp.*, 1991, pp. 353–358.

[71] C. S. Hartmann, S. Jen, M. A. Domalewski, and J. C. Andle, "Improved accuracy for determining SAW transducer capacitance and K^2," in *Proc. IEEE Ultrason. Symp.*, 1987, pp. 161–167.

[72] R. C. Peach, "A general Green function analysis for SAW devices," in *Proc. IEEE Ultrason. Symp.*, 1995, pp. 221–225.

[73] V. P. Plessky and T. Thorvaldsson, "Periodic Green's function analysis of SAW and leaky SAW propagation in a periodic system of electrodes on a piezoelectric crystal," *IEEE Trans. Ultrason., Ferroelect., Freq. Contr.*, vol. 4, no. 2, pp. 280–293, Mar. 1995.

[74] A.-R. Baghai-Wadji and D. Penunuri, "Coordinate-free, frequency indepedent universal function for BAW analysis in SAW devices," in *Proc. IEEE Ultrason. Symp.*, 1995, pp. 287–290.

[75] D. P. Morgan, "Quasi-static analysis of generalized SAW transducers using the Green's function method," *IEEE Trans. Sonics Ultrason.*, vol. 27, no. 3, pp. 111–123, May 1980.

[76] K.-Y. Hashimoto, Y. Watanabe, M. Akahane, and M. Yamaguchi, "Analysis of acoustic properties of multi-layered structures by means of effective acoustic impedance matrix," in *Proc. IEEE Ultrason. Symp.*, 1990, pp. 937–942.

[77] D. Qiao, W. Liu, and P. M. Smith, "General Green's functions for SAW device analysis," *IEEE Trans. Ultrason., Ferroelect., Freq. Contr.*, vol. 46, no. 5, pp. 1242–1253, Sept. 1999.

[78] H. P. Reichinger and A.-R. Baghai-Wadji, "Dynamic 2D analysis of SAW-devices including massloading," in *Proc. IEEE Ultrason. Symp.*, 1992, pp. 7–10.

[79] R. C. Peach, "Green function anysis for SAW devices with arbitrary electrode structures," in *Proc. IEEE Ultrason. Symp.*, 1997, pp. 99–103.

[80] P. Ventura, J. M. Hodé, and B. Lopes, "Rigorous analysis of finite SAW devices with arbitrary electrode geometries," in *Proc. IEEE Ultrason. Symp.*, 1995, pp. 257–262.

[81] K.-Y. Hashimoto and M. Yamaguchi, "Derivation of coupling-of-modes parameters for SAW device analysis by means of boundary element method," in *Proc. IEEE Ultrason. Symp.*, 1991, pp. 21–26.

[82] S. V. Biryukov, "Fast variation method for elastic strip calculation," *IEEE Trans. Ultrason., Ferroelect., Freq. Contr.*, vol. 49, no. 5, pp. 635–642, Mar. 2002.

[83] S. V. Biryukov and M. Weihnacht, "Elastic electrode polarization in a spatial harmonic field and the natural boundary element method," in *Proc. IEEE Ultrason. Symp.*, 2001, pp. 111–114.

[84] K. J. Gamble and D. C. Malocha, "Simulation of short LSAW transducers including electrode mass loading and finite finger resistance," *IEEE Trans. Ultrason., Ferroelect., Freq. Contr.*, vol. 49, no. 1, pp. 47–56, Jan. 2002.

[85] O. A. Peverini, R. Orta, and R. Tascone, "A fast Green's function method for the analysis of IDT's for acousto-optical devices," *IEEE Trans. Ultrason., Ferroelect., Freq. Contr.*, vol. 49, no. 3, pp. 365–373, Mar. 2002.

[86] Y. Zhang, J. Desbois, and L. Boyer, "Characteristic parameters of surface acoustic waves in a periodic metal grating on a piezoelectric substrate," *IEEE Trans. Ultrason., Ferroelect., Freq. Contr.*, vol. 40, no. 3, pp. 183–192, May 1993.

[87] A.-R. Baghai-Wadji, C. Mecklenbrauker, and F. Seifert, "Convenient method for noise-free elastodynamic field calculatlons in general periodic SAW structures," *Electron. Lett.*, vol. 28, no. 15, pp. 1466–1468, July 1992.

[88] P. Ventura, J. M. Hodé, and M. Solal, "A new effecient combined FEM and periodic Green's function formalism for the analysis of periodic SAW structures," in *Proc. IEEE Ultrason. Symp.*, 1995, pp. 263–268.

[89] V. Laude, A. Reinhardt, M. Wilm, A. Khelif, and S. Ballandras, "Fast FEM/BEM simulation of SAW devices via asympototic waveform evaluation," *IEEE Trans. Ultrason., Ferroelect., Freq. Contr.*, vol. 51, no. 3, pp. 359–363, Mar. 2004.

[90] V. Laude, A. Reinhardt, S. Ballandras, A. Khelif, and M. Solal, "Fast FEM/BEM computation of SAW harmonic admittance and slowness curves," in *Proc. IEEE Ultrason. Symp.*, 2004, pp. 445–448.

[91] S. Ballandras, V. Laude, T. Pastureaud, W. Wilm, W. Daniau, A. Reinhardt, and W. Steichen, "A FEA/BEM approach to simulate complex electrode structures

devoted to guided elastic wave periodic transducers," in *Proc. IEEE Ultrason. Symp.*, 2002, pp. 309–312.

[92] S. Clatot, V. Laude, A. Reinhardt, M. Wilm, W. Daniau, S. Ballandras, R. Lardat, and M. Solal, "Sensitivity of interface acoustic wave to the nature of the interface," in *Proc. IEEE Ultrason. Symp.*, 2003, pp. 2126–2129.

[93] B. Jakoby and M. J. Vellekoop, "FFT-based analysis of periodic structures in microacoustic devices," *IEEE Trans. Ultrason., Ferroelect., Freq. Contr.*, vol. 47, no. 3, pp. 651–656, May 2000.

[94] N. Finger, G. Kovacs, J. Schöberl, and U. Langer, "Accurate FEM/BEM-simulation of surface acoustic wave filters," in *Proc. IEEE Ultrason. Symp.*, 2003, pp. 1680–1685.

[95] V. P. Plessky, S. V. Biryukov, and J. Koskela, "Harmonic admittance and dispersion equations–the theorem," *IEEE Trans. Ultrason., Ferroelect., Freq. Contr.*, vol. 49, no. 4, pp. 528–534, Apr. 2002.

[96] P. Ventura, J. M. Hodé, J. Desbois, and M. Solal, "Combined FEM and Green's function analysis of periodic SAW structure, application to the calculation of reflection and scattering parameters," *IEEE Trans. Ultrason., Ferroelect., Freq. Contr.*, vol. 48, no. 5, pp. 1259–1274, 2001.

[97] J. Koskela, V. P. Plessky, and M. M. Salomaa, "SAW/LSAW COM parameter extraction from computer experiments with harmonic admittance of a periodic array of electrodes," *IEEE Trans. Ultrason., Ferroelect., Freq. Contr.*, vol. 46, no. 4, pp. 806–816, 1999.

[98] K.-Y. Hashimoto, T. Omori, and M. Tamaguchi, "Modelling of shear-horizontal-type surface acoustic waves and its application to COM-based device simulation," in *Proc. IEEE Ultrason. Symp.*, 2001, pp. 127–132.

[99] B. V. Sveshnikov and A. P. Shitvov, "Evaluation of dispersion in COM-parameters," in *Proc. IEEE Ultrason. Symp.*, 2003, pp. 715–719.

[100] W. T. Thomson, "Transmission of elastic waves through a stratified solid medium," *J. Appl. Phys.*, vol. 21, pp. 89–93, Feb. 1950.

[101] A. H. Fahmy and E. L. Adler, "Propagation of acoustic surface waves in multilayers: A matrix description," *Appl. Phys. Lett.*, vol. 22, no. 10, pp. 495–497, May 1973.

[102] E. L. Adler, "Matrix methods applied to acoustic waves in multilayers," *IEEE Trans. Ultrason., Ferroelect., Freq. Contr.*, vol. 37, no. 6, pp. 485–490, Nov. 1990.

[103] E. L. Adler, J. K. Slaboszewicz, G. W. Farnell, and C. K. Jen, "PC software for SAW propagation in anisotropic multilayers," *IEEE Trans. Ultrason., Ferroelect., Freq. Contr.*, vol. 37, no. 2, pp. 215–223, May 1990.

[104] P. M. Smith, "Dyadic Green's functions for multi-layer SAW substrates," *IEEE Trans. Ultrason., Ferroelect., Freq. Contr.*, vol. 48, no. 1, pp. 171–179, Jan. 2001.

[105] T. Pastureaud, V. Laude, A. Soufyane, and S. Ballandras, "Stabilization of the simulation of SAW devices on stratified structures: Application to transverse plate mode resonators," in *Proc. IEEE Ultrason. Symp.*, 2001, pp. 629–634.

[106] T. Pasturead, V. Laude, and S. Ballandras, "Stable scattering-matrix method for surface acoustic waves in piezoelectric multilayers," *Appl. Phys. Lett.*, vol. 80, no. 14, pp. 2544–2546, Apr. 2002.

[107] E. L. Tan, "A robust formulation of SAW Green's functions for arbitrarily thick multilayers at high frequencies," *IEEE Trans. Ultrason., Ferroelect., Freq. Contr.*, vol. 49, no. 7, pp. 929–936, July 2002.

[108] L. Wang and S. I. Rokhlin, "A compliance/stiffness matrix formulation of general Green's function and effective permittivity for piezoelectric multilayers," *IEEE Trans. Ultrason., Ferroelect., Freq. Contr.*, vol. 51, no. 4, pp. 453–463, Apr. 2004.

[109] B. Collet, "Recursive surface impedance matrix method for ultrasonic wave propagation in piezoelectric multilayers," *Ultrasonics*, vol. 42, pp. 189–197, 2004.

[110] A. Reinhardt, T. Pastureaud, S. Ballandras, and V. Laude, "Scattering matrix method for modeling acoustic waves in piezoelectric, fluid, and metallic multilayers," *J. Appl. Phys.*, vol. 94, no. 10, pp. 6923–6931, Nov. 2003.

[111] L. Wang and S. I. Rokhlin, "Modeling of wave propagation in layered piezoelectric media by a recursive asymptotic method," *IEEE Trans. Ultrason., Ferroelect., Freq. Contr.*, vol. 51, no. 9, pp. 1060–1071, Sept. 2004.

[112] Z. Wang, J. D. N. Cheeke, and C. K. Jen, "Perturbation method for analyzing mass sensitivity of planar multilayer acoustic sensors," *IEEE Trans. Ultrason., Ferroelect., Freq. Contr.*, vol. 43, no. 5, pp. 844–851, Sept. 1996.

[113] G. Kovacs and A. Venema, "Theoretical comparison of sensitivities of acoustic shear wave modes for (bio)chemical sensing in liquids," *Appl. Phys. Lett.*, vol. 61, no. 6, pp. 639–641, Aug. 1992.

[114] T. M. Niemczyk, S. J. Martin, G. C. Frye, and A. J. Ricco, "Acoustoelectric interaction of plate modes with solutions," *J. Appl. Phys.*, vol. 64, no. 10, pp. 5002–5008, 1988.

[115] F. Josse and Z. A. Shana, "Acoustoionic interaction of SH surface waves with dilute ionic solutions," *IEEE Trans. Ultrason., Ferroelect., Freq. Contr.*, vol. 38, no. 3, pp. 297–304, May 1991.

[116] J. Kondoh, K. Saito, S. Shiokawa, and H. Suzuki, "Simultaneous measurements of liquid properties using multichannel shear horizontal surface acoustic wave microsensor," *Jpn. J. Appl. Phys., Part 1*, vol. 35, no. 5B, pp. 3093–3096, May 1996.

[117] O. Tamarin, C. Déjous, D. Rebière, and J. Pistré, "Simple analytical method to estimate the influence of liquids viscosity on Love wave chemical sensors," in *Proc. IEEE Ultrason. Symp.*, 2001, pp. 343–346.

[118] G. McHale, M. I. Newton, and F. Martin, "Theoretical mass, liquid and polymer sensitivity of acoustic wave sensors with viscoelastic guiding layers," *J. Appl. Phys.*, vol. 93, no. 1, pp. 675–690, Jan. 2003.

[119] S. Furukawa, T. Nomura, and T. Yasuda, "Theoretical study of leaky surface acoustic wave propagating on water/ZnO/glass structures," *J. Phys. D: Appl. Phys.*, vol. 21, pp. 216–218, 1988.

[120] S. Ballandras, A. Reinhardt, A. Khelif, M. Wilm, V. Laude, W. Daniau, V. Blondeau-Pâtissier, and W. Boireau, "Theoretical analysis of damping effects of SAW at solid/fluid interfaces," in *Proc. IEEE Freq. Cont. Symp.*, 2003, pp. 907–910.

[121] B. D. Zaitsev, I. E. Kuznetsova, S. G. Joshi, and I. A. Borodina, "Shear-horizontal acoustic waves in piezoelectric plates bordered with conductive liquid," *IEEE Trans. Ultrason., Ferroelect., Freq. Contr.*, vol. 48, no. 2, pp. 627–631, Mar. 2001.

[122] J. B. Briot, S. Ballandras, E. Bigler, and G. Martin, "Gravimetric sensitivity of transverse waves trapped by metal grating on thin quartz plates," in *IEEE Symp. Freq. Cont.*, 1997, pp. 207–212.

[123] F. M. Pitschi, J. E. Kiwitt, C. C. W. Ruppel, and K. C. Wagner, "Accurate modelling and simulation of SAW RF filters," in *IEEE MTT-S Digest*, 2003, pp. 2009–2012.

[124] A.-R. Baghai-Wadji, "Theory and applications of Green's functions," in *Advances in Surface Acoustic Wave Technology, Systems and Applications*, C. C. W. Ruppel and T. A. Fjeldly, Eds. Singapore: World Scientific Publishing, 2001, vol. 2, pp. 83–149.

[125] A. B. Bhatia, *Ultrasonic Absorption*. Oxford: Oxford University Press, 1967.

[126] R. Peach, "On the existence of surface acoustic waves on piezoelectric substrates," *IEEE Trans. Ultrason., Ferroelect., Freq. Contr.*, vol. 48, no. 5, pp. 1308–1320, Sept. 2001.

[127] D. A. Powell, K. Kalantar-zadeh, and W. Wlodarski, "Numerical calculation of SAW sensitivity: Application to ZnO/$LiTaO_3$ transducers," *Sens. Act. A: Phys.*, vol. 115, pp. 456–461, 2004.

[128] K. Nakamura, T. Shoji, and H.-B. Kang, "Growth of ZnO films on (012)$LiTaO_3$ by ECR-MBE and determination of their polarity," in *Int. Symp. App. Ferroelec.*, 2000, pp. 467–470.

[129] T. Shoji, K. Nakamura, and D. Yamazaki, "Propagation characteristics of the SH-SAW on (110)ZnO/(012)$LiTaO_3$," in *Proc. IEEE Ultrason. Symp.*, 2001, pp. 215–219.

[130] C. K. Campbell, *Surface Acoustic Wave Devices for Mobile and Wireless Communications*. San Diego: Academic Press, 1998.

[131] F. Herrmann, M. Weihnacht, and S. Büttgenbach, "Properties of sensors based on shear-horizontal surface acoustic waves in $LiTaO_3/SiO_2$ and quartz/SiO_2 structures," *IEEE Trans. Ultrason., Ferroelect., Freq. Contr.*, vol. 48, no. 1, pp. 268–273, Jan. 2001.

[132] L. Tessier, F. Patat, N. Schmitt, M. Lethiecq, and Y. F. D. Guilloteau, "Significance of mass and viscous loads discrimination for an AT-quartz blood group immunosensor," *Sens. Act. B: Chem.*, vol. 18, pp. 698–703, 1994.

[133] R. F. Harrington, *Field Computation by Moment Methods*. New York: MacMillan, 1968.

[134] A.-R. Baghai-Wadji, *A Unified Approach for Construction of Green's Functions: Theory and Applications (Habilitation manuscript)*. Vienna: Vienna University of Technology, 1994.

[135] W. H. Press, S. A. Teukolsky, W. T. Vetterling, and B. P. Flannery, *Numerical Recipes in C++*. Cambridge University Press, 2002.

[136] E. Gizeli and C. R. Lowe, Eds., *Biomolecular Sensors*. London: Taylor & Francis, 2002.

[137] R. B. Brown, B. H. Horine, and J. H. Hines, "Practical implementation of coupling-of-modes theory for SAW device modeling," in *Proc. IEEE Ultrason. Symp.*, 1989, pp. 153–158.

[138] G. Watson and E. Staples, "SAW resonators as vapor sensors," in *Proc. IEEE Ultrason. Symp.*, 1990, pp. 311–314.

[139] G. Watson, W. Horton, and E. Staples, "Gas chromatography utilizing SAW sensors," in *Proc. IEEE Ultrason. Symp.*, 1991, pp. 305–309.

[140] D. P. Morgan, "Cascading formulas for identical transducer P-matrices," *IEEE Trans. Ultrason., Ferroelect., Freq. Contr.*, vol. 43, no. 5, pp. 985–987, Sept. 1996.

[141] B. Jakoby and A.-R. Baghai-Wadji, "Analysis of bianisotropic layered structures with laterally periodic inhomogeneities-an eigenoperator formulation," *IEEE Trans. Antennas Propagat.*, no. 5, pp. 615–626, May 1996.

[142] K. Varis and A.-R. Baghai-Wadji, "Hybrid planewave/finite-difference transfer method for solving photonic crystals in finite thickness slabs," in *Proc. IEEE Int. Symp. Electron Devices for Micro. Optoelec. App.*, 2001, pp. 161–166.

[143] V. Laude, C. F. Jerez-Hanckes, and S. Ballandras, "Surface Green's function of a piezoelectric half-space," *IEEE Trans. Ultrason., Ferroelect., Freq. Contr.*, vol. 53, no. 2, pp. 420–428, Feb. 2006.

[144] S. Ippolito, K. Kalantar-Zadeh, D. Powell, and W. Wlodarski, "A 3-dimensional finite element approach for simulating acoustic wave propagation in layered SAW devices," in *Proc. IEEE Ultrason. Symp.*, 2003, pp. 303–306.

[145] H. Cheng, L. Greengard, and V. Rokhlin, "A fast adaptive multipole alogirhm in three dimensions," *Journal of Computational Physics*, vol. 155, pp. 468–498, 1999.

[146] E. Darve and P. Havé, "Effecient fast multipole method for low-frequency scattering," *Journal of Computational Physics*, vol. 197, pp. 341–363, 2004.

[147] A.-R. Baghai-Wadji and E. Li, "Factorization of potential and field distributions without utilizing the addition theorem," in *Computational Methods in Large Scale Simulation*, K.-Y. Lam and H.-P. Lee, Eds. Singapore: World Scientific, 2005.

[148] K. M. Lakin, "Thin film resonator technology," *IEEE Trans. Ultrason., Ferroelect., Freq. Contr.*, vol. 52, no. 5, pp. 707–716, May 2005.

[149] M. Benetti, D. Cannata, A. D'Amico, F. Di Pietrantonio, V. Foglietti, and E. Verona, "Thin film bulk acoustic wave resonator (TFBAR) gas sensor," in *Proc. IEEE Ultrason. Symp.*, 2004, pp. 1581–1584.

[150] M. Link, M. Schmidt, J. Weber, R. Primig, D. Pitzer, R. Gabl, and M. Schreiter, "Film bulk acoustic resonators for sensing applications in liquid environments," in *Eurosensors XIX*, 2005.

[151] J. Bjurström, G. Wingqvist, I. Katardjiev, and A. L. Spetz, "Shear mode AlN thin film electroacoustic reonsator for biosensor applications," in *Proc. IEEE Sensors Conference*, 2005, pp. 492–495.

[152] G. Kovacs, M. Anhorn, H. E. Engan, G. Visintini, and C. C. W. Ruppel, "Improved material constants for $LiNbO_3$ and $LiTaO_3$," in *Proc. IEEE Ultrason. Symp.*, 1990, pp. 435–438.

[153] G. Carlotti, G. Socino, A. Petri, and E. Verona, "Elastic constants of sputtered ZnO films," in *Proc. IEEE Ultrason. Symp.*, 1987, pp. 295–299.

[154] C. C. W. Ruppel and T. A. Fjeldly, Eds., *Advances in Surface Acoustic Wave Technology, Systems and Applications*. Singapore: World Scientific Publishing, 2000, vol. 1.

[155] ——, *Advances in Surface Acoustic Wave Technology, Systems and Applications*. Singapore: World Scientific Publishing, 2001, vol. 2.